



**FLOW SIMULATION OF AMMONIA REACTANT
GASES VIA MICROMIXER**

AHMAD SHAHIR MOHD RADZANI

**CHEMICAL ENGINEERING
UNIVERSITI TEKNOLOGI PETRONAS
SEPTEMBER 2014**

Flow Simulation Of Ammonia Reactant Gases Via Micromixer

By:

AHMAD SHAHIR MOHD RADZANI

15539

Dissertation submitted in partial fulfilment of
the requirements for the
Bachelor of Engineering (Hons)
(Chemical)

SEPTEMBER 2014

Universiti Teknologi PETRONAS
Bandar Seri Iskandar
31750 Tronoh
Perak Darul Ridzuan

CERTIFICATION OF APPROVAL

Flow Simulation of Ammonia Reactant Gases Via Micromixer

By

Ahmad Shahir Mohd Radzani
15539

A project dissertation submitted to the
Chemical Engineering Programme
Universiti Teknologi PETRONAS
in partial fulfilment of the requirement for the
BACHELOR OF ENGINEERING (HONS)
(CHEMICAL)

Approved by,

Mohd Zamri B. Abdullah

UNIVERSITI TEKNOLOGI PETRONAS
TRONOH, PERAK

September 2014

CERTIFICATION OF ORIGINALITY

This is to certify that I am responsible for the work submitted in this project, that the original work is my own except as specified in the references and acknowledgements, and that the original work contained herein have not been undertaken or done by unspecified sources or persons.

AHMAD SHAHIR MOHD RADZANI

ABSTRACT

The conventional method to produce ammonia employs the Haber–Bosch process at extremely high temperature and pressure. These working conditions not only consumes tremendous amount of energy, it has higher safety risk and yields very low conversion. Prior to study on microreactor, it is essential to understand the hydrodynamics of flow in microchannel. The results will serve as a stepping point to design a microreactor for the ammonia synthesis in a very economical, energy saving, safer and achieving higher conversion and yield than the conventional Haber–Bosch process. At low gas flowrates, mixing of nitrogen and hydrogen gases are less effective as the flow regime within a microchannel is largely laminar. This work aims to enhance mixing of flow as well as shortening the residence time for reaction to occur by investigating the hydrodynamics of the mixing of nitrogen and hydrogen gases in different geometry configurations of a microchannel in order. Three geometry configurations were developed and tested via Computational Fluid Dynamics simulation. Velocity and Pressure distribution of the microsystem was analysed extensively contributed to approximating the mixing efficiency for ammonia reactant gases. The study had found that in all models, the pressure in micromixers ranged from approximately minimum 100 kPa abs. to 102.5 kPa abs. maximum and mostly working pressure is established at 101.3 kPa which conformed to desired atmospheric pressure. The flow of Nitrogen gas was found to be uniform across the micromixer gaining maximum speed at most intersections as it had less volume fraction. Velocity distribution for Hydrogen has wider spectrum which reflected good mixing strategies in many sections of the micromixer as well as center of mixing chambers

ACKNOWLEDGEMENTS

In the name of Allah, the most gracious, most merciful.

I would like to express my gratitude to my supervisor, Mr. Mohd. Zamri bin Abdullah for giving me the opportunity to carry out my bachelor thesis under his supervision. His invaluable guidance and advice throughout my Final Year Project period has tremendously contribute to the completion of this project. Besides that he always spend time through his busy working schedule to meet and discuss and explain to me the theory and procedure to carry out this project study. Without his kind encouragement, I believe I would not have been able to complete this project smoothly. It was indeed a pleasure working with him throughout this project study. Appreciations also extends to Post-Graduate Mr. Basit and Mr. Tanh whom are part of the ONEBaja research project.

I wish to express highest gratitude towards my beloved mother, Che Fuzlina Bt. Mohd Fuad, father, Mohd Radzani Bin Abdul Razak, sisters and Huurun Eiin Bt. Che Hashim. These are special individuals whom are my inspirations to becoming a better son and chemical engineer. They have cherished me with their warmth, comfort and love through the course and are my refuge during the troubled times. They have provided me with endless support, motivation and encouragement. I dedicate this work to them. Special appreciations also extends to close friends such as Mohd Farhan Alias as well as others in UTP for their assistance. Close friends have made UTP a haven and home away from home. Their valuable friendship and support is highly obliged.

Lastly, an honorable mention to all individuals whose name are not mentioned but have contributed directly and indirectly to this project.

Thank you.

All thanks and praises belong to Allah.

TABLE OF CONTENTS

CERTIFICATION OF APPROVAL.....	i
CERTIFICATION OF ORIGINALITY.....	ii
ABSTRACT.....	iii
ACKNOWLEDGEMENTS.....	iv
LIST OF FIGURES.....	vii
LIST OF TABLES.....	x
CHAPTER 1 INTRODUCTION	1
1.1 Background	2
1.2 Problem Statement	2
1.3 Objectives of Study	3
1.4 Scope of Study	3
CHAPTER 2 LITERATURE REVIEW	4
2.1 Ammonia Synthesis By Haber - Bosch Process	4
2.2 Microreactor	5
2.3 Micromixer Design Configurations	6
2.4 Flow Characteristics	8
2.5 Flow of Gas	9
CHAPTER 3 METHODOLOGY AND PROJECT WORK.....	11
3.1 Development of Geometry	12
3.1.4 Geometry Technical Drawing	12
3.4.1.1 Model A	13
3.4.1.2 Model B.....	14

3.4.1.3 Model C.....	15
3.2 Mesh Generation	16
3.2.1 Mesh Data.....	16
3.3 Flow Parameter Setup and Governing Equations	18
CHAPTER 4 RESULTS AND DISCUSSION.....	20
4.1 Pressure Contours	20
4.1.1 Pressure Contours for 1.67 m/s Inlet Velocity	21
4.1.2 Pressure Contours for 3.33 m/s Inlet Velocity	23
4.1.3 Pressure Contours for 10.99 m/s Inlet Velocity	25
4.2 Nitrogen Velocity Contours	27
4.2.1 Axial Contours for 1.67 m/s inlet velocity	27
4.2.2 Radial Contours for 1.67 m/s inlet velocity	30
4.2.3 Axial Contours for 3.33 m/s velocity	31
4.2.4 Radial Contours for 3.33 m/s inlet velocity	33
4.2.5 Axial Contours for 10.99 m/s velocity	34
4.2.6 Radial Contours for 10.99 m/s inlet velocity	36
4.3 Hydrogen Velocity Contours	37
4.3.1 Axial Contours for 1.67 m/s inlet velocity	37
4.3.2 Radial Contours for 1.67 m/s inlet velocity	40
4.3.3 Axial Contours for 3.33 m/s velocity	41
4.3.4 Radial Contours for 3.33 m/s inlet velocity	43
4.3.5 Axial Contours for 10.99 m/s velocity	44
4.3.6 Radial Contours for 10.99 m/s inlet velocity	46
CHAPTER 5 CONCLUSIONS AND RECOMMENDATIONS	48
5.1 Conclusions	48
5.2 Recommendations	51
REFERENCES.....	53
APPENDIX I: Velocity Contours For Hydrogen Component.....	55
APPENDIX II: Velocity Contours For Nitrogen Component.....	73
APPENDIX III: Gantt Chart Of Project Work And Milestones	91

LIST OF FIGURES

Figure 1.1: Molecular structure of Urea.....	1
Figure 2.1: Sample of a micromixer developed.....	5
Figure 2.2: A micromixer schematic diagram.....	5
Figure 2.3: Serpentine geometrical design.....	6
Figure 2.4: A zigzag geometry of microchannel.....	7
Figure 2.5: Complex flow microchannel design by Amadin.....	7
Figure 3.1: Flow Chart of work scope.....	12
Figure 3.2: Microchannel dimension.....	13
Figure 3.3: Technical drawing of the Model A system.....	14
Figure 3.4: Technical drawing of the Model B system.....	15
Figure 3.5: Technical drawing of the Model C system.....	16
Figure 4.2: Pressure Contour of Model A.....	21
Figure 4.3: Pressure Contour of Model B	21
Figure 4.4: Pressure Contour of Model C	22
Figure 4.5: Pressure Contour of Model A.....	23
Figure 4.6: Pressure Contour of Model B	23
Figure 4.7: Pressure Contour of Model C	24

Figure 4.8: Pressure Contour of Model A.....	25
Figure 4.9: Pressure Contour of Model B	25
Figure 4.10: Pressure Contour of Model C	26
Figure 4.11: Location of Radial Contour Plots sample.....	27
Figure 4.12: Axial Velocity Contour of Model A.....	28
Figure 4.13: Axial Velocity Contour for Model B.....	28
Figure 4.14: Axial Velocity Contour of Model C	29
Figure 4.15: Series of Radial Contours for Model B	30
Figure 4.16: Series of Radial Contours for Model C	30
Figure 4.17: Axial Velocity Contour for Model A	31
Figure 4.18: Axial Velocity Contour for Model B.....	31
Figure 4.19: Axial Velocity Contour for Model C.....	32
Figure 4.20: Radial Velocity Contour for Model B	33
Figure 4.21: Radial Velocity Contour for Model C	33
Figure 4.22: Axial Velocity Contour for Model A	34
Figure 4.23: Axial Velocity Contour for Model B.....	34
Figure 4.24: Axial Velocity Contour for Model C.....	35
Figure 4.25: Radial Velocity Contour for Model B	36
Figure 4.26: Radial Velocity Contour for Model C	36
Figure 4.27: Location of Radial Contour Plots sample.....	37
Figure 4.28: Axial Velocity Contour of Model A.....	38

Figure 4.29: Axial Velocity Contour of Model B	38
Figure 4.30: Axial Velocity Contour of Model C	39
Figure 4.31: Radial Velocity Contours for Model B	40
Figure 4.32: Radial Velocity Contours for Model C	40
Figure 4.33: Axial Velocity Contour of Model A.....	41
Figure 4.34: Axial Velocity Contour of Model B	41
Figure 4.35: Axial Velocity Contour of Model C	42
Figure 4.36: Axial Velocity Contour for Model B.....	43
Figure 4.37: Axial Velocity Contours for Model C	43
Figure 4.38: Axial Velocity Contour of Model A.....	44
Figure 4.39: Axial Velocity Contour of Model B	44
Figure 4.40: Axial Velocity Contour of Model C	45
Figure 4.41: Radial Velocity Contours for Model B	46
Figure 4.42: Radial Velocity Contours for Model C	46
Figure 5.1: Proposed Catalyst location at 1.67 m/s operation	52
Figure 5.2: Proposed Catalyst location at 3.33 m/s operation	52
Figure 5.3: Proposed Catalyst location for Model C design	52

LIST OF TABLES

<i>Table 1.1: Table showing general differences between two mixers</i>	<i>6</i>
<i>Table 3.2 Fluid Properties</i>	<i>18</i>
<i>Table 5.1 Best Micromixer selection based on speed</i>	<i>18</i>

CHAPTER 1

INTRODUCTION

Synthetic urea is produced from synthetic ammonia and carbon dioxide, which can be either in liquid or solid form. Ammonia was first commercially synthesized in 1870 through Haber-Bosch process, by which at present the process is used to produce more than 500 million tons of artificial fertilizer per year; roughly 1% of the world's energy is used for it, and it sustains about 40% of our planetary population (Fryzuk, 2004). Carbamide (urea) is currently widely used in the fertilizer industry.

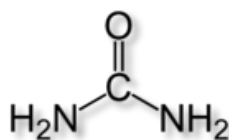


Figure 1.1: Molecular structure of Urea

In a typical ammonia synthesis, two reactant gases i.e. nitrogen and hydrogen are reacted with the aid of a catalyst in an extremely high temperature, high pressure reactor. Despite the lower conversion and yield, the Haber–Bosch process imposes a costly method to produce ammonia, in addition to the higher safety and control regulation that have to be looked upon.

1.1 Background

The ammonia and urea industry is changing significantly as a new market for bio-fuels and NO_x abatement emerges. A key driver of this fluctuation activity has been the cost of feedstock which is the natural gas that inflicts some production curtailments for major plant in North America and Western Europe. Access to low cost gas and processing technology has become a major priority for the plant to have upper hand on economic capability in order to produce low cost ammonia and urea.

The usage of microscale devices such as micromixer and microreactor in industries is crucial in order to save space, cost and energy. Baldyga and Bourne (1990) stated that the objective of the mixing process is to distribute the components evenly and obtain homogenization of components in one another. The homogenization of components enables uniform properties of the mixture to be attained. Subsequently, fluid mixing in channels with a sub-millimeter dimension is a fundamental operation in microfluidic devices. The flow in such microfluidic devices is laminar, making it difficult to mix the fluids especially in a smooth simple microchannel.

1.2 Problem Statement

The flow of nitrogen and ammonia in a microchannel requires the gases to mix in order for reaction to occur. Due to the laminar flow regime that is anticipated in a microsystem at the given gases inlet velocities, mixing is hardly observed for a straight-line microchannel. Hence, this study will look into predicting the possible modification of the microchannel geometry where pseudo-turbulence would occur for mixing to be created at low gases flow rate. The alteration of the geometry will lead to the analysis of flow dynamics for the gases flow, which will later provide vital information on the optimized location where the catalyst for the reaction would be decided to be placed inside the microsystem.

1.3 Objectives of Study

This research aim to study the flow dynamics in between two different microchannel designs with the variables such as velocity and pressure distribution as functions of space and time that contribute to the analysis. The objective of the study is to enhance mixing of hydrogen and nitrogen gas flow thus better mixing characteristics can be observed.

1.4 Scope of Study

This new method involved the design of a new reactor and a new product that could enhance the process and performance, respectively. This project utilizes computational fluid dynamic (CFD) approach to predict and design these new concepts. CFD is the science of predicting fluid flow, heat transfer, chemical reaction and other related phenomena by solving numerical set of Navier-Stokes equations. The results of CFD analysis are relevant for conceptual studies of new design, detail product development, troubleshooting and redesign. In this project, ANSYS CFX software was used as a platform to predict the dynamic behaviour of the nitrogen and hydrogen gases flow in a microchannel.

CHAPTER 2

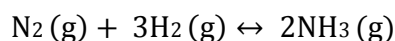
LITERATURE REVIEW

Ammonia or Azane is a compound of nitrogen and hydrogen with the formula NH_3 . It is a color-less gas with a strong smell. It serves as intermediate product for urea production and use primarily in fertilizers, chemicals, explosives, fiber and plastics among others.

2.1 Ammonia Synthesis By Haber - Bosch Process

Ammonia synthesis was developed by the German scientist called Fritz Haber at the start of the 20th century. Jointly, Robert le Ressignol developed high pressure devices for the Haber process. It was until middle of 1909, they demonstrated the process producing Ammonia in droplets from air at the rate of 125 ml/hr. It was chemical engineer named Carl Bosch that expanded the process into industrial-level production (Harrison, 2013).

It is synthesised by the exothermic reaction of 3 molecule of Hydrogen gas (H_2) and 1 molecule of Nitrogen gas (N_2) at high temperature (400°C- 500°C) and pressure (150 bars – 300 bars) in the presence of the porous iron as a catalyst.



Currently, Ammonia plants utilizes raw materials from natural gas for producing hydrogen by processes including; catalytic reforming of natural gas, purification of synthesis gas and compression of synthesis gas prior to Ammonia conversion process. Harrison (2013) explained that large release of ammonia due to

accidents and vessel failures etc. has decreased considerably in the last three decades. However, problems and failures do occur frequently in the ammonia plant even after following the inherently safer design philosophy and risk assessment. Major areas of concern failures are reforming and synthesis loop causing fires and shutdowns. In a typical Ammonia synthesis, Hydrogen and Nitrogen particles are reacted in the presence of an iron catalyst in high temperature and pressure reactor. Apart from the low conversion and yield, the Haber-Bosch process imposes a costly method to produce ammonia as well as its more complex safety and regulation control strategies. In spite of the high operating costs, this conventional method remains widely used in today's industry as the best method for ammonia synthesis.

2.2 Microreactor

In recent years, there has been a sharp increase in the study of chemical reactors far smaller than those commonly used in industry today (Claus, 2001; Ajmera, 2002). The promise of meso and microreactors rests upon the many possible advantages that small scale reactors possess compared to their larger, conventional counterparts. These advantages include improved heat and mass transfer due to smaller characteristic lengths, improved reaction efficiency due to higher surface-to-volume ratios, and ease of use in portable applications due to reduced volume.

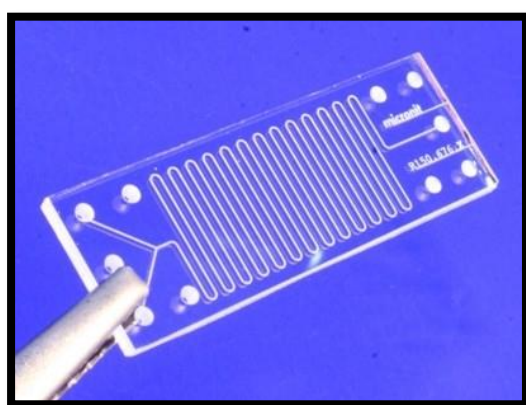


Figure 2.1: Sample of a micromixer developed

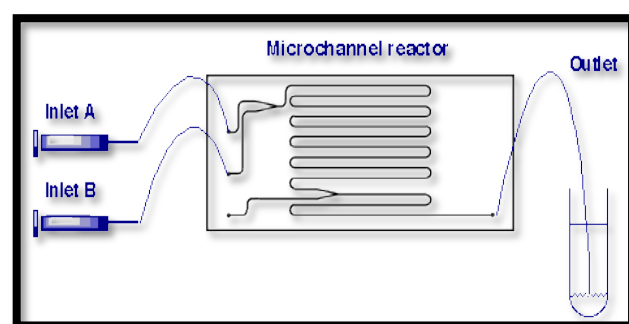


Figure 2.2: A micromixer schematic diagram

Micromixers can be classified into two major categories which are active mixers and passive mixers. Active mixers generate disturbances with external field or energy sources, whereas passive mixers use the flow energy to create multilamination structures, which are stretched and combined to promote mixing by molecular diffusion.

Table 1.1: Table showing general differences between two mixers

Active Mixers	Passive Mixers
Pressure field disturbance	T- or Ymicromixers
Electro-hydrodynamic disturbance	Multilamination micromixers
Dielectrophoretic disturbance	Chaotic advection
Electro-kinetic disturbance	Micronozzle injection
Micropump	Hydrodynamics focusing

In this study, a passive micromixer was applied for the study of flow behavioral dynamics of ammonia synthesis process considering it's less complex structure and low cost operation as compared to an active micromixer.

Flow characteristics (laminar, turbulent and laminar-to-turbulent flow regimes) and pressure drop correlations are the huge aspect to determine the accuracy and optimization of the design of microreactors and micromixers. Previous studies by Su, Chen and Yuan (2010) in this field has shown, micro-mixing has been ineffective due to laminar flow of fluid in micro fluid devices.

2.3 Micromixer Design Configurations

Typical micromixer geometrical dimensions influence the performance of the micromixer. Liaw (2013) Azeman (2012) had performed computational fluid dynamics study for serpentine geometrical structure as shown in Figure 2.3 which reported fair mixing but largely uniform throughout their microchannel.

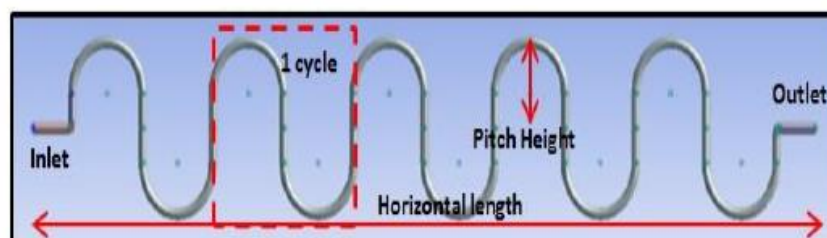


Figure 2.3: Serpentine geometrical design

Whereas, study made by Ren and Leung (2012) had concentrated their design on a zigzag microchannel with the objectives of improving mixing. A similar design can be seen in figure 2.4, achieving Re numbers of 127 as well as reduced residence time. Similar approach taken by Mengeaudet *al.* (2002) had also concluded with rapid homogeneous mixing effect as compared to straight flow channel. Nevertheless, MohdAmadin (2013) had experimented with his own design shown in Figure 2.5 in effort to obtain mixing and residence time.

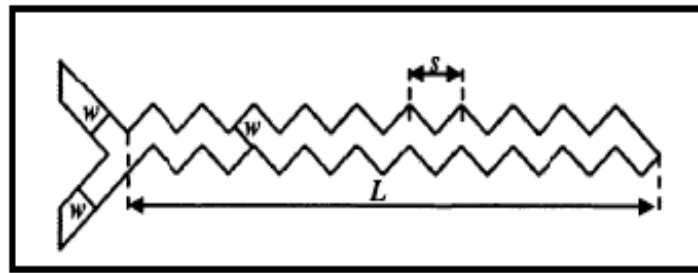


Figure 2.4: A zigzag geometry of microchannel

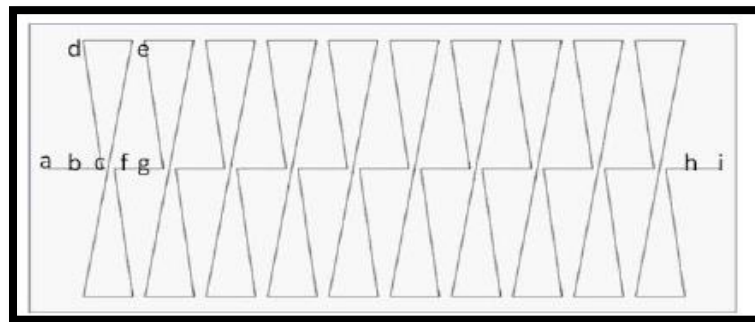


Figure 2.5: Complex flow microchannel design by Amadin

Studies by Amadin, Liaw and Azeman had focused on microchannels with cylindrical dimensions. Apart from geometric design, the shape and dimensions of a microchannel also impacts its mixing performance. Many researchers has obtained better results with reduced channel dimensions, the shape itself can also influence bending angles in complex flow system. In contrast to their models, an attempt was

made to study designs for a rectangular microchannel with dimensions of 100 μm (height) x 100 μm (width).

2.4 Flow Characteristics

Mixing is the central process of most microfluidic devices for medical diagnostics, genetic sequencing, chemistry production, drug discovery and proteomics. Mixing is a transport process for species, temperature, and phases to reduce in homogeneity. It leads to secondary effects such as reaction and change in properties. Micromixing is the smallest scale of fluid motion and molecular motion.

Turbulent flow is generally preferred in a channel if intimate mixing is desired between two streams. Mixing in microfluidic devices is generally achieved by taking advantage of the relevant small length, which dramatically increases the effect of diffusion and advection. Liaw (2013) had stated that Reynolds number above a critical value of around 2300 indicates a turbulent flow however for microscale cases, a low Reynolds number (for example < 100) or a laminar flow is expected.

$$Re = \frac{\rho v D_H}{\mu} \quad (1)$$

Nguyen (2005) also stated the Strouhal number is an important factor in micromixer designs. The Strouhal number is a function of the Reynolds number in cylindrical systems which represents the ration between residence time of a species and the time period of its disturbance.

$$St = \frac{f D_H}{U} \quad (2)$$

Microfluidic devices are not merely a miniature version of their macroscale counterpart because of many physical characteristics, such as surface area-to-volume ratio, surface tension and diffusion aren't linearly proportional from large to small

devices. Microfluidic mixer should be designed in such ways that leverage the physical characteristic of the mixing in a confined space.

2.5 Flow of Gas

It is well documented that differences in between gas flow and liquid flow in a microchannel are influenced by several factors as stated beforehand. Researches have concluded that the density effect and the difference in molecular weight would affect the mixing performance. Apart from density and molecular weight differences, the Knudsen number is also part and parcel of theoretical data in governing microfluidic flow. Knudsen number is a dimensionless factor defined as the ratio of molecular mean free path to a representative physical length scale, given by the relationship below;

$$K_n = \frac{\lambda}{L} \quad (3)$$

Where;

K_n = Knudsen Number

λ = mean free path; the average distance travelled by a moving particle between successive collisions.

L = physical length; such as the radius of the body in a fluid.

For a Boltzmann gas (assumption), the mean free path may be readily calculated so that,

$$Kn = \frac{k_B T}{\sqrt{2} \pi d^2 p L} \quad (4)$$

k_B is the Boltzmann constant = $1.3806504(24) \times 10^{-23}$ J/K (in SI units)

T is the thermodynamic temperature,

d is the particle hard shell diameter

P is the total pressure

In gas system, mixing in microchannels can be a challenge as the flow is often laminar even though velocity is increased. As the value of Knudsen number increases, thus pressure drop, shear stress, heat flux, and corresponding mass flow rate cannot be predicted from flow and heat transfer based on the continuum hypothesis. On the other hand, the gas acceleration occurs due to density variations, which results in a higher friction and pressure drop.

Wang and Li (2005) has studied the inherent factors affecting micro-gas mixing. From the research, mixing of two component gas streams were investigated using the direct simulation monte carlo's method (DSMC). As the continuum assumption may not apply, the Boltzmann and molecular dynamics based methods are the last choices for analyzing high Knudsen number gas flow. For a 50 - 200 m/s velocity, their simulation results show that the wall characteristics have little effect on the mixing length when the main gas flow velocities for different wall characteristics were the same. Gas mixing in microchannels is mainly due to the relationship between the flow characteristics and the gas properties. However, their study has eliminated the effect of density as they selected two different gas with the same molar mass.

CHAPTER 3

METHODOLOGY AND PROJECT WORK

The hydrodynamics behaviour of ammonia synthesis was studied by using ANSYS CFX to determine optimum geometry design for the process. Computational Flow Dynamics (CFD) is a branch of study which employs numerical method and algorithm that investigates fluid flow.

In this study, a passive micro-channel was applied for the study of flow behavioural dynamics of ammonia synthesis process because it is more stable and less complex in its geometry design and operation as compared to an active micromixer. This selection is based on continuation of the previous studies by Liaw S.Y (2013) by employing cyclic configurations.

Simulations was performed for this project. As stated earlier, the hydrodynamics can be observed with ANSYS CFX software. Typical methodology in CFD applies i.e.:

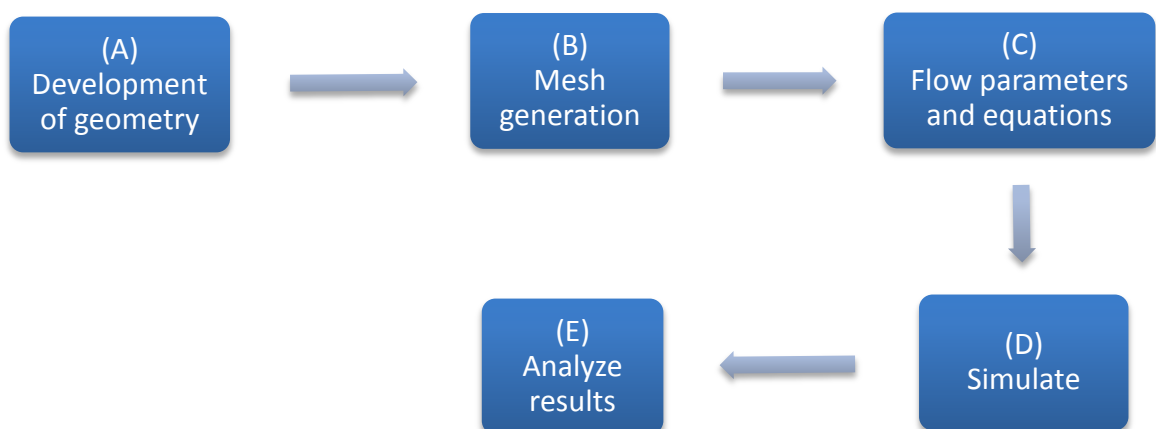


Figure 3.1: Flow Chart of work scope

3.1 Development of Geometry

Creation of geometry is done by using built-in Design Modeller within Workbench Module in the ANSYS CFX 14.5 software. In this study, a microchannel design was performed with three different geometries. Previously, Amadin (2013) and Liaw (2013) had completed their design for total length of 10 cm by 3 cm microreactor whilst 100 μm for channel width, hence identical variables is used for this concept.

3.1.4 Geometry Technical Drawing

Geometry design sketching was performed by the aid of AUTOCAD 2012 software prior to actual simulation trials. This is because AUTOCAD is highly convenient in designing the model to gain optimum accuracy in terms of dimensions.

Previous ONEBaja studies has focused on cylindrical microchannel with a diameter length of 100 μm . In variation, a square-shaped microchannel is preferred in this project with a given dimension of 100 μm by 100 μm , continuous throughout out the system.

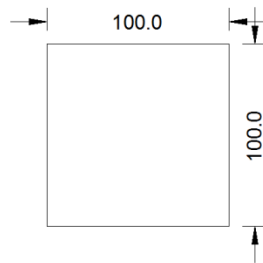


Figure 3.2: Microchannel dimension

A square microchannel is selected for this study as it may reveal certain changes in the results such as flow system or pattern as compared to a cylindrical channel. Furthermore, better data range can be obtained for the simulation trials. This is because the meshing quality is improved with a system working at perfect angles in contrast to previous studies. Several mesh properties are key factors to different results such as; a finer mesh quality would increase the number of nodes which in turn influences the element factor and simulation period.

3.4.1.1 Model A

Proposed design geometry A was generated based on the working principles of the coanda effect for cylindrical-shaped microchannel. Obviously, this has to be modified to suit a square shaped microchannel to obtain the re-direction of stream effect. The configuration is a repetition of splitting a stream into two to form a coarsely shaped semi-triangle. Two streams are then re-joined to a single stream just as a triangle would. This semi-triangle design was then flipped over to top for the same action.

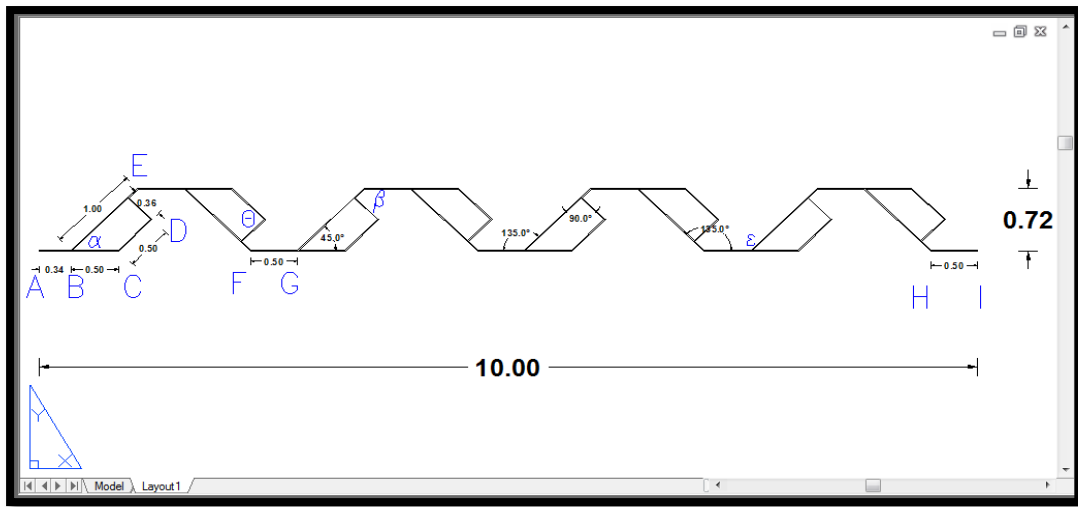


Figure 3.3: Technical drawing of the Model A system

From the figure above, sketching parameters are as stated below;

- Length of straight line inlet represented by point A to B = 0.34 cm
- Length of first split stream of line represented by points A to E = 1.00 cm
- Angle at inlet offset on line BE represented by $\alpha = 90^\circ$
- Length of second split stream of line represented by points B to C = 0.50 cm
- Distance of second split stream represented by points C to D = 0.50 cm
- Distance of second split stream represented from D to meet AE line = 0.36 cm
- Angle \ominus on all similar right-angle line D to stream AE = 90°
- Length of straight line gap prior to next cycle represented by F to G = 0.50 cm

- Angle β from line AE to FG = 135°
- Angle ε opposite α in splitting stream representation = 135°
- Length of straight line outlet stream represented by points H to I = 0.50 cm
- Total width of system = 0.72 cm
- Total length of system = 10.00 cm

3.4.1.2 Model B

The second design configuration was an adaptation of a popular geometry design which is utilized in previous studies; the zig-zag configuration. This configuration has been used in the past by other researchers for analysis of a microreactor. Although, for this study, the zig-zag configuration was taken to another level by re-arranging the pattern to the y-axis as well as applying some fundamental oscillatory principles.

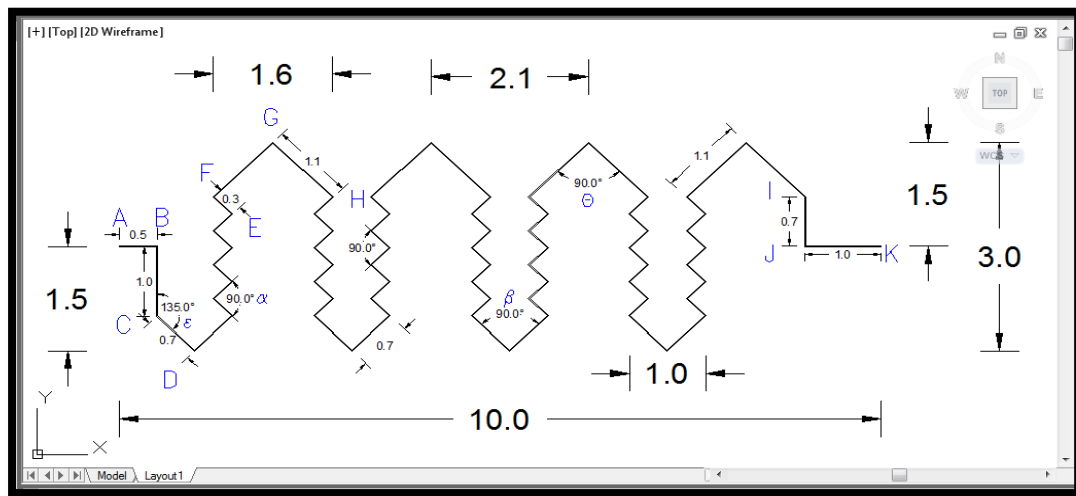


Figure 3.4: Technical drawing of the Model B system

From the figure above, sketching parameters are as stated below;

- Length of Inlet represented by points A to B = 0.5 cm
- Pitch height represented by points B to C = 1.0 cm
- Bottom angled width represented by points C to D = 0.7 cm

- Angle ε on line BD = 135°
- Small zig-zag length represented by points E to F = 0.3 cm
- Angle α on all similar parallel lines as EF line = 90°
- Distance of top angle width represented by points G to H = 1.1 cm
- Angle Θ on all similar parallel lines as FH line = 90°
- Angle β on all similar perpendicular lines = 90°
- Width of outlet pitch height represented by points I to J = 0.7 cm
- Length of Outlet represented by points J to K = 1 cm
- Total linear width of system represented by points D to G = 3 cm
- Total linear length of the system represented by points A to K = 10 cm

3.4.1.3 Model C

The third geometry design is was another modification of the previous analysis based on a serpentine model. However, this third design is similarly squared-shaped channel. Furthermore it is prevalently a grid system microreactor which is aimed at increasing residence time for mixing of gases to occur. The technical drawing using can seen below as is provided in the appendices for viewing.

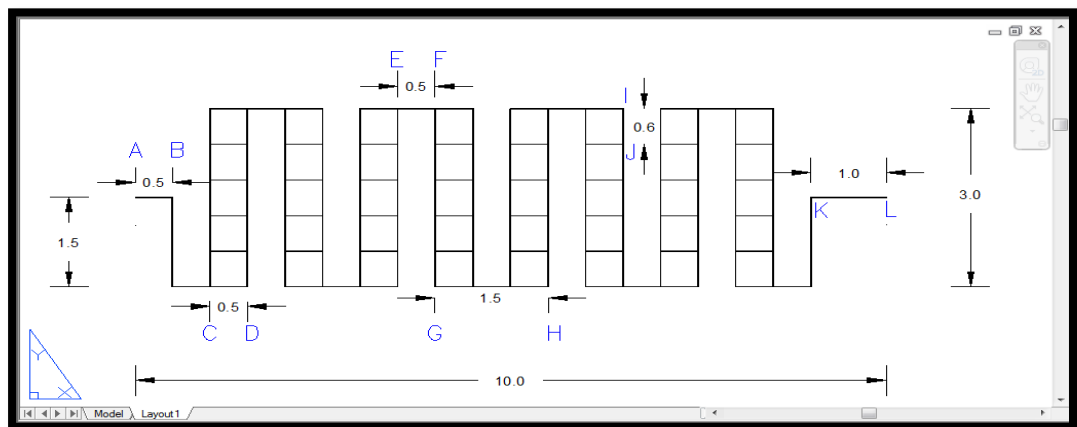


Figure 3.5: Technical drawing of the Model C system

From the figure above, sketching parameters are as stated below;

- Length of Inlet represented by points A to B = 0.5 cm
- Pitch height represented by points B to C = 1.5 cm
- Grid box length represented by points C to D = 0.5 cm
- Gap between grid system represented by points E to F = 0.5 cm
- Distance between two grid system represented by points G to H = 1.5 cm
- Width of each grid box represented by points I to J = 0.6 cm
- Length of Outlet represented by points K to L = 1 cm
- Total linear width of system represented by points F to G = 3 cm
- Total linear length of the system represented by points A to L = 10 cm

3.2 Mesh Generation

After geometry creation, a mesh is to be generated using ANSYS Meshing. Meshing properties has to be specified for most appropriate mesh quality in order to obtain best accuracy results. There are several factors that will be taken into consideration; number of nodes, elements and orthogonal quality.

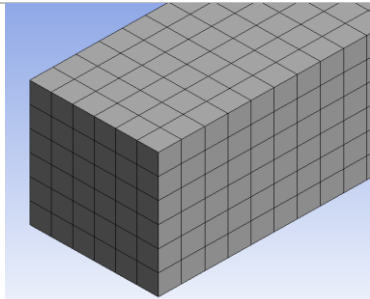
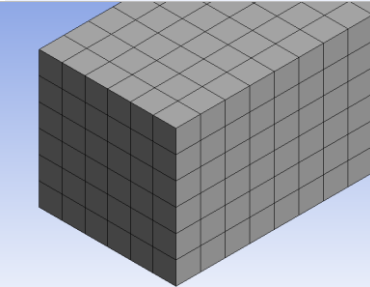
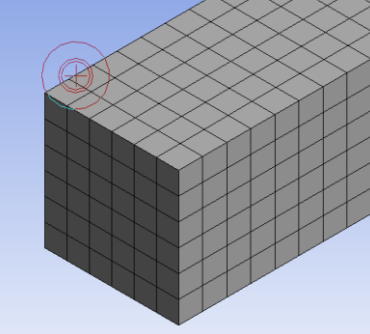
Development of mesh is to discretize the geometry by varying the number of mesh elements - coarse, medium and fine – to study the effect of mesh quality towards the simulation outcomes. Both Liaw (2013) and Amadin (2013) had performed meshing from 300000 nodes up to 4000000 thus, a similar mesh sensitivity parameters were performed in this study.

The Orthogonal quality is one of the methods to evaluate the generated mesh. Generally, the orthogonal quality range from 1 to 0. The best cells will have an orthogonal quality will converge towards 1.

3.2.1 Mesh Data

Mesh generation was performed at stage two of the process, after drawing geometry.

Table 3.1: Meshing data for three models A, B and C.

Model	No of Nodes	No of Elements	Sample	Meshing time (hr)
A	95,685	697,272		3
B	1,577,884	1,158,768		22
C	2,175,460	1,600,392		25

In a simulation program, a node is a point that is connected to another node by an element. Hence, elements and nodes are interconnected by a mesh.

The mesh quality was fixed at fine condition and the governing parameter was that the number of elements must not exceed 512,000. It had to be done by trial and error whereby author had to approximate the values of cell sizes and then run the mesh simulation before getting the number of elements as the result. It is clear that the number of elements obtained after meshing was completed did not meet the requirement as they were well above the required value of 512,000. This is because of the limitation set on the software license were maximum up to 512,000 only.

Nevertheless, the mesh shows that cell size and arrangement looked the same from figures given in Table 4.1 across all the models. This meant that the mesh

sizing input were consistent thus, the accuracy of the results will depend on the number of elements. For a refined mesh, the number of cells per unit area is approaching maximum, therefore this will affect the required time to simulate and generates better solution for data.

It was also observed that the simulation time required to complete the mesh were proportionate to the number of mixing chamber installed. For example; the control model (Model A) could complete the mesh time shorter as the design does not have any mixing chambers. Whereas, the micromixers Model B and C were at a difference from Model A and by themselves in terms of mesh time as there was increment in the array of mixing chambers.

3.3 Flow Parameter Setup and Governing Equations

Prior to the simulation, fluid properties and parameters for the flow has to be set up during Pre-CFX section. For the selection of flow rates or gases velocity, references are also utilized from previous projects.

Table 3.2 Fluid Properties

Fluids Properties	
Fluids	H2 Ideal Gas N2 Ideal Gas
Fluid Inlet Ratio	0.25/0.75
Fluids Morphology	Continuous Fluids
Buoyancy Model	Non Buoyant
Reference Pressure	1 atm
Heat Transfer Model	Isothermal (25°C)
Turbulence Model	k-epsilon
Fluids Inlet Velocity	3.33 m/s
Relative Pressure	0 Pa

The table above reflects the parameters input from Amadin (2013) and Liaw (2013) as during the Pre-CFX studies. Therefore, the same properties input will be done in this study. Reactant components are assumed to be incompressible fluids as

the mach number at inlets are expected as 0.01. A Newtonian (incompressible) fluid in a microchannel may be explained by Navier-Stokes equation as well as the Continuity equation;

Navier – Stokes Equation

$$\rho \left(\frac{\partial \mathbf{v}}{\partial t} + \mathbf{v} \cdot \nabla \mathbf{v} \right) = -\nabla p + \nabla \cdot \mathbf{T} + \mathbf{f} \quad (5)$$

Where \mathbf{v} = flow velocity, ρ = fluid density, p = pressure, \mathbf{T} = deviatoric component of the stress tensor, \mathbf{f} = body forces (per unit volume) acting on the fluid.

Under the assumption of incompressibility, the density of fluid parcel is constant and when using the substantive derivative it follows easily that the continuity equation simplifies to;

$$\nabla \cdot \mathbf{v} = 0 \quad (6)$$

Momentum Equation

$$\frac{\partial(\rho v_j v_k)}{\partial x_j} = \frac{\partial}{\partial x_j} \left(-p \delta_{ij} + \mu \left(\frac{\partial v_i}{\partial x_j} + \frac{\partial v_j}{\partial x_i} \right) \right) = \rho g_i \quad (7)$$

Where X is the Cartesian coordinate direction, subscripts i, j and k are Cartesian axis, δ_{ij} are 1 if $i=j$ and 0 if otherwise; μ = dynamic viscosity and ρ = fluid density. Furthermore, species distribution follows the diffusion convective equation under assumption of non-slip boundaries.

$$\frac{\partial c}{\partial t} + \frac{\partial v_k(c)}{\partial x_k} = D \frac{\partial^2 c}{\partial x^2} \quad (8)$$

CHAPTER 4

RESULTS AND DISCUSSION

In post-processing phase, the results obtained from the simulated computation will be examined by extraction of useful data. ANSYS 15 offers a complete set of post-processing tools for display of the results on models in the form such as contour plots and velocity plots. Furthermore, improvement and optimization can also be done at this phase by analyzing the result data, where parameters such as physical models, boundary conditions and mesh quality can be redefined and improved by observing the output of the simulated computation.

4.1 Pressure Contours

This contour is obtained from the results by way of inserting a plane across the micromixer. The plane is located midway on the Z-X axis of the microchannel. This inserted plane will then read off the gas pressure inside the microchannel in variable colour representation.

The results obtained were for the velocities at 1.67 m/s, 3.33 m/s as well as 10.99 m/s. The Figures presented in the proceeding pages reflects the pattern of fluid pressure difference across the micromixer system. Variable that is measured is the absolute total pressure of the micromixer. Absolute Pressure was measured by rule of thumb because the elements that are concerned with are in gaseous phase. In gas system, it is recommended to record pressure measurements using absolute values because it is zero-referenced against a perfect vacuum, hence giving the total pressure. This is essential as the project is dealing with small reactors/mixers at the micro scale. The findings also reflect the total pressure of the system and not per component.

4.1.1 Pressure Contours for 1.67 m/s Inlet Velocity

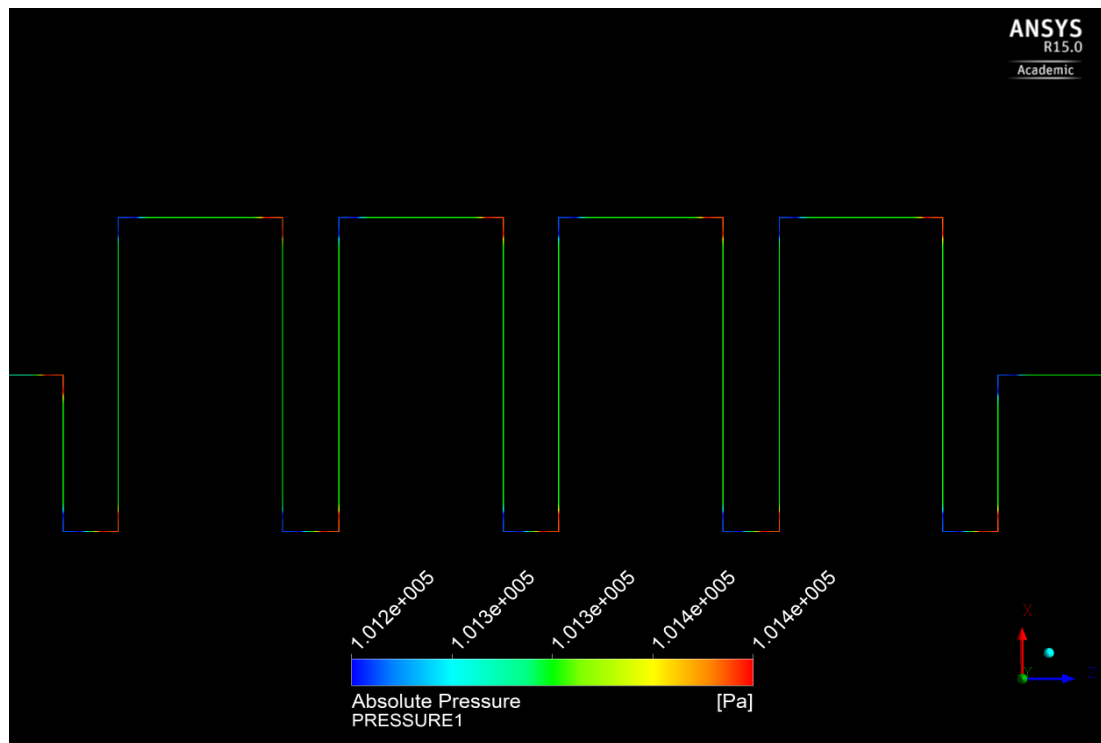


Figure 4.2: Pressure Contour of Model A

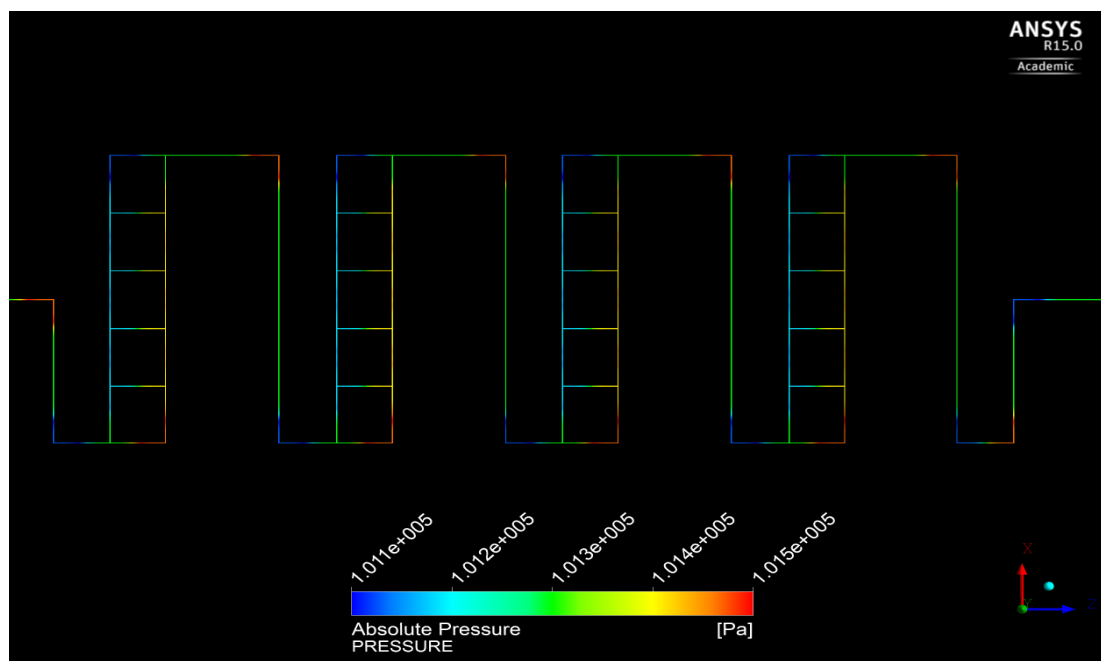


Figure 4.3: Pressure Contour of Model B

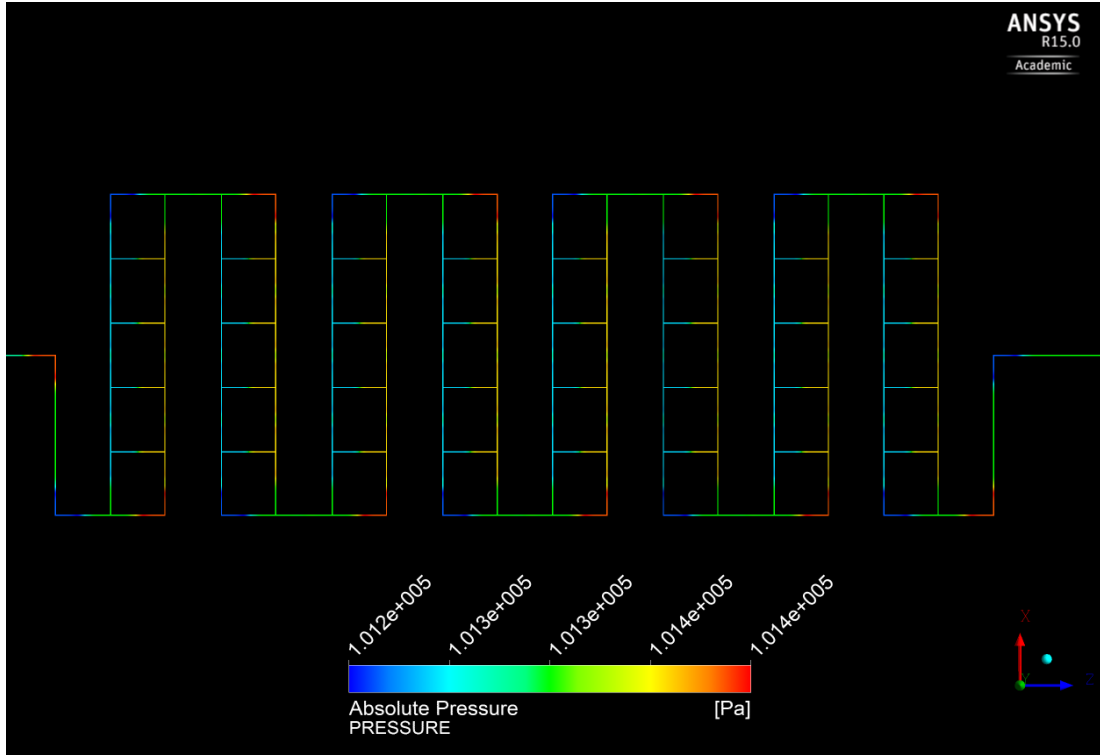


Figure 4.4: Pressure Contour of Model C

Figure 4.2 to 4.3 shows, the pressure distribution is across the system varies and does not present convergence towards pressure increment at relatively small velocity. The system in fact operates at approximately atmospheric pressures for all models ranging from 101.1 kPa to 101.5 kPa.

One of the similarities found across the models is that the gas pressures at inlet (from left) will increase at the first intersection, expressed in red color and stabilizes then, reduces at the second intersection shown in blue and vice-versa before exiting the mixer. This is much more pronounced in the Model A whereby repeating patterns of pressure increase and decreases after each intersection is observed throughout the system.

Obviously, this is expected in microchannels with sharp angular turns at 90° geometrical pattern. The increment in pressure may be produced by the reduction in velocity at said intersections of the micromixer. Bernoulli's principle states that for an inviscid fluid flow, an increase in the speed of the fluid occurs simultaneously with the decrease in pressure or potential energy and vice versa.

4.1.2 Pressure Contours for 3.33 m/s Inlet Velocity

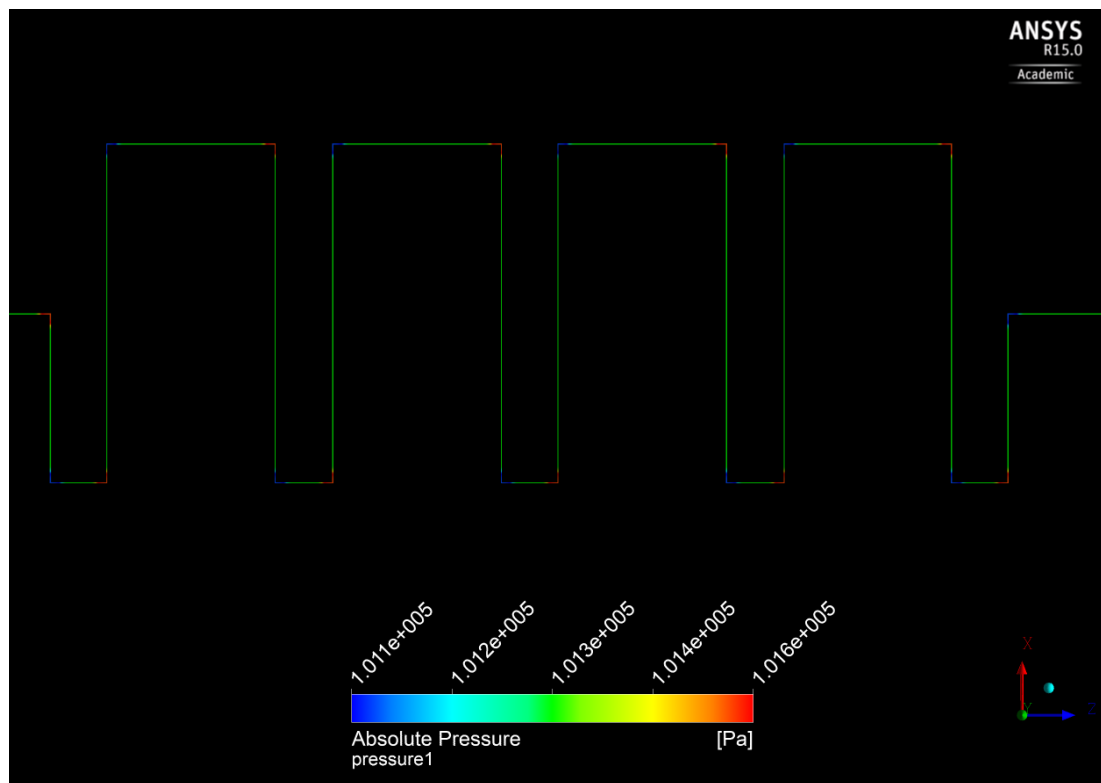


Figure 4.5: Pressure Contour of Model A

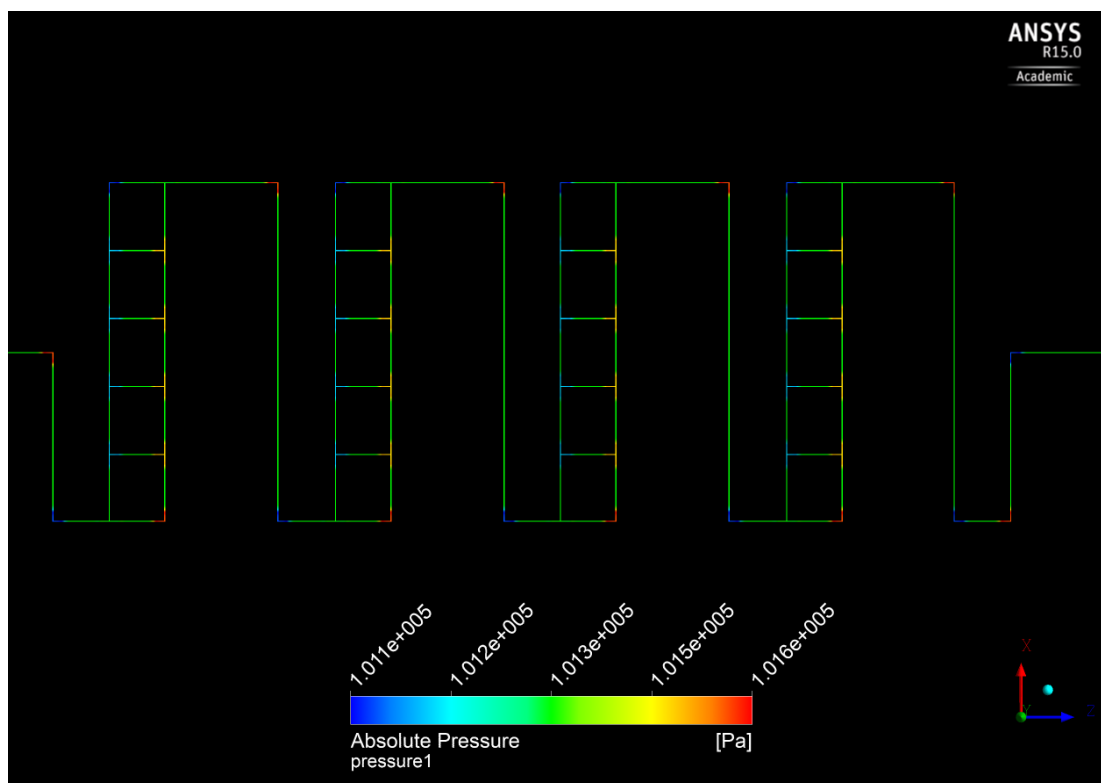


Figure 4.6: Pressure Contour of Model B

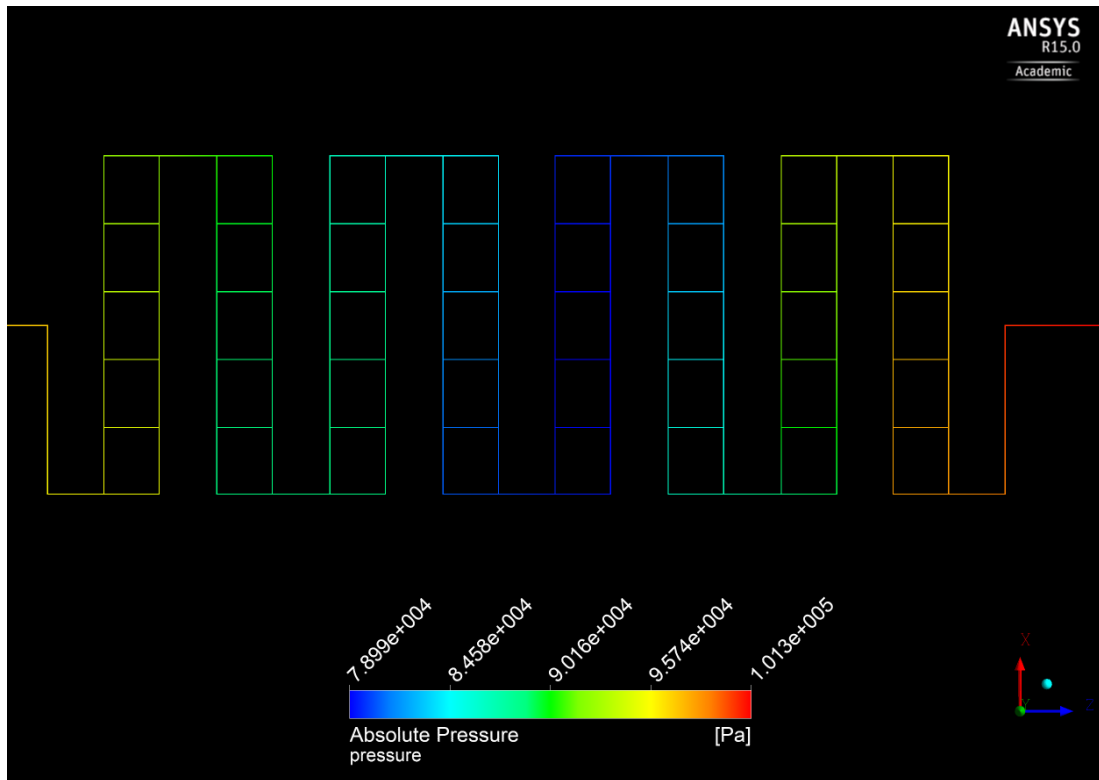


Figure 4.7: Pressure Contour of Model C

At medium velocity, the length of pressure reduction and increment before each intersection are shorter as compared to the 1.67 m/s inlet velocity. This meant since the fluid is moving at faster speed, pressure increase on intersection still occurs but at a faster rate thus not effecting the path length as much. For model A similar pattern is observed but for model B the pressure system is much more stable as gas flow velocity is increased.

Interestingly, pressure contour presented in Figure 4.6 reveals a new pressure pattern in Model C configuration. At higher inlet velocity, the pressure of the system conforms to a steady variation from high to low pressure around the middle region of the mixer and increases again towards exiting the micromixer.

Furthermore, by approximation, differential pressure in this geometry is higher because the range of values has widened. There pressure drop towards the middle region amplified so much to the extent that it has fallen below atmospheric pressure approaching approximately 79 kPa. However, good mixing characteristics can be observed because low pressure in the middle accounts for rise in fluid speed which is best for mixing.

4.1.3 Pressure Contours for 10.99 m/s Inlet Velocity

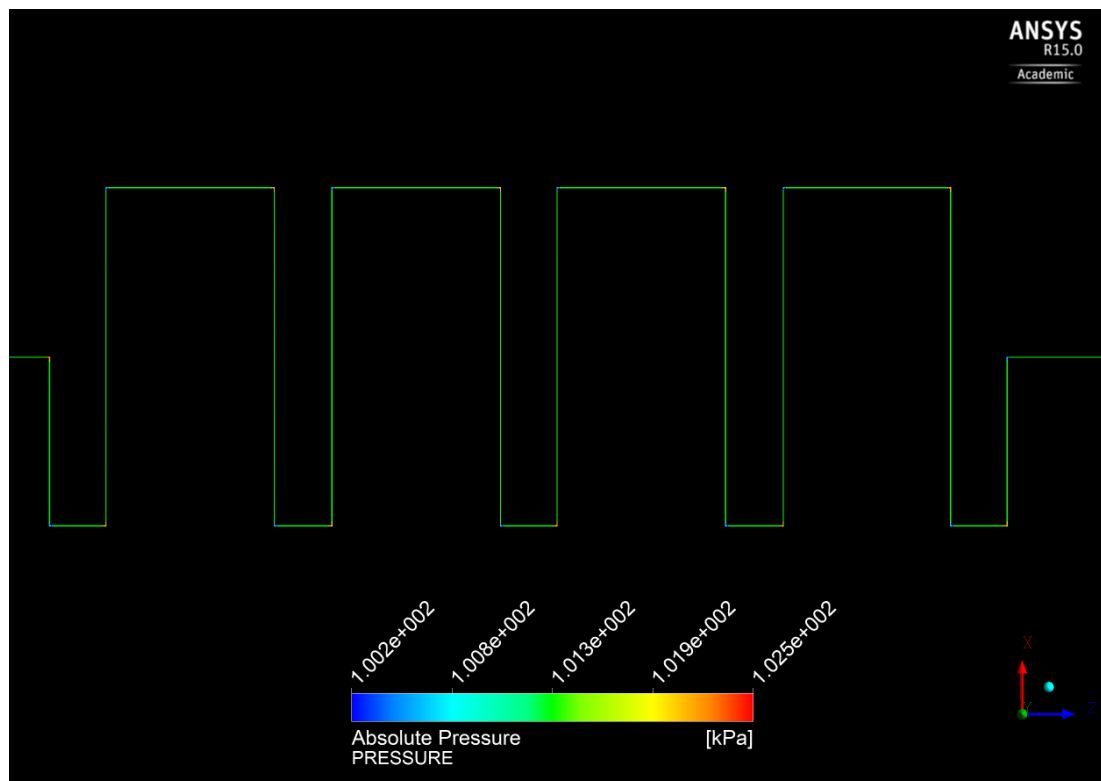


Figure 4.8: Pressure Contour of Model A

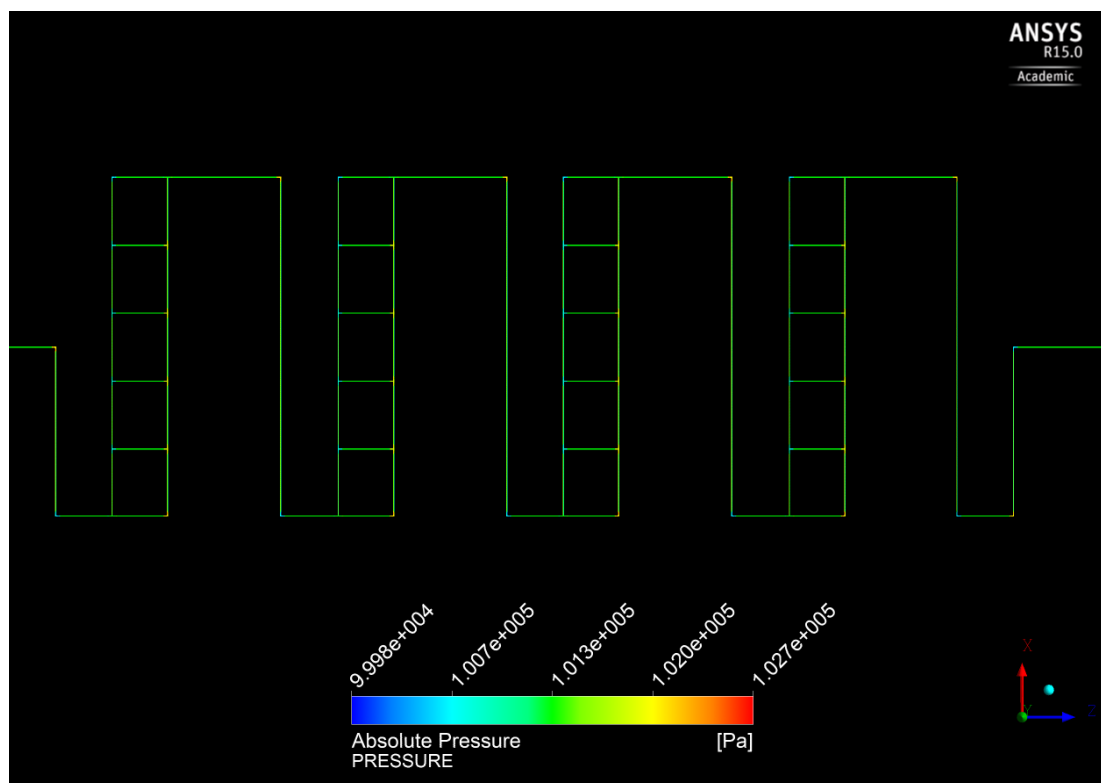


Figure 4.9: Pressure Contour of Model B

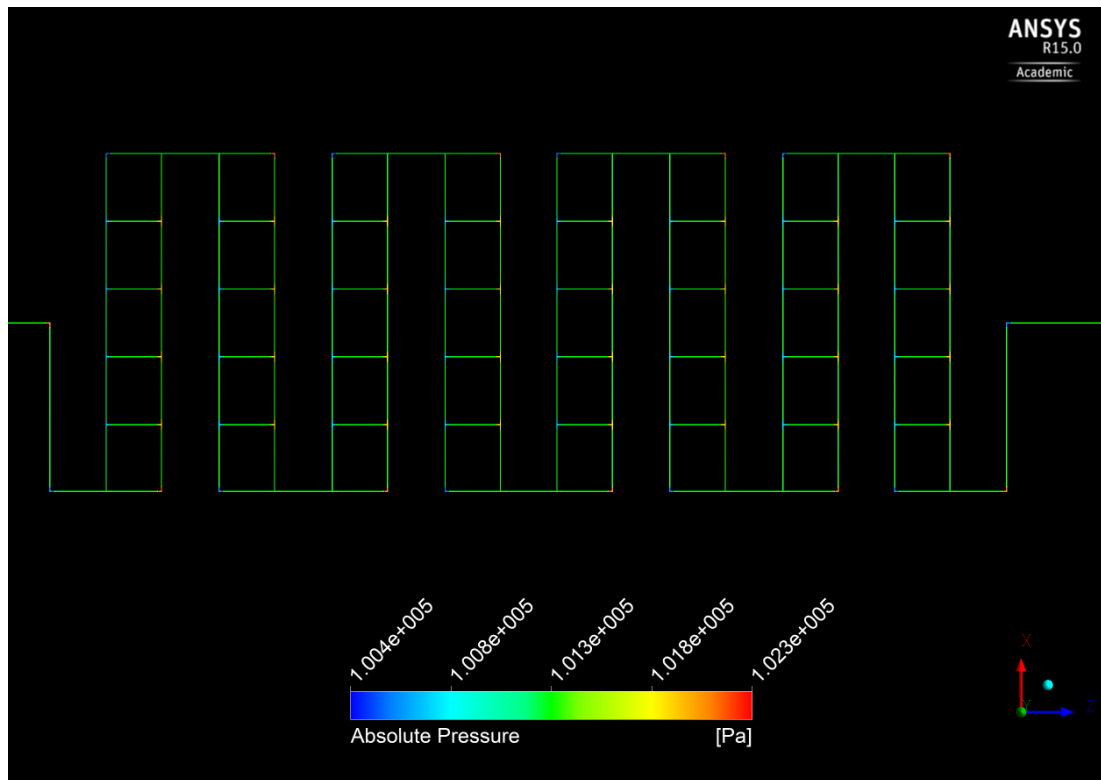


Figure 4.10: Pressure Contour of Model C

In Figures 4.7 to 4.9, there variations in pressure are not as intense. Due to the high inlet speed, atmospheric pressure was much more prevalent until mixer outlet. This is quite different than models simulated with lower velocities. There are minor pressure surges at intersections which are the norm but largely, stable conditions and uniform across the mixer.

In reference to the Bernoulli's principle, uniform atmospheric pressures entails uniform speed across the system however, due to the increase in speed of fluid, mixing is better because of high velocity is maintained throughout. At intersections where there are pressure losses, good mixing behaviour can take place.

On indication of pressure alone, all of the mixers exhibits mediocre mixing characteristics because there are no large pressure drop between inlet and outlet of mixer.

4.2 Nitrogen Velocity Contours

This contour is obtained from the results by way of inserting a plane across the micromixer. The plane is located midway on the Z-X axis of the microchannel. This inserted plane will then read off the gas velocity inside the microchannel in variable color representation.

The diagrams presented are configured into two views or representation; Axial and Radial. In axial view, as previously shown, the diagram will show contour details for overall mixer. Whilst radial view will show the flow's velocity distribution by the plane located on the X-Y axis. In this study, the contour plots are situated at specified locations on the mixer. They are arranged in the order shown the figure below; and placed within midsections of the proposed mixing chambers.

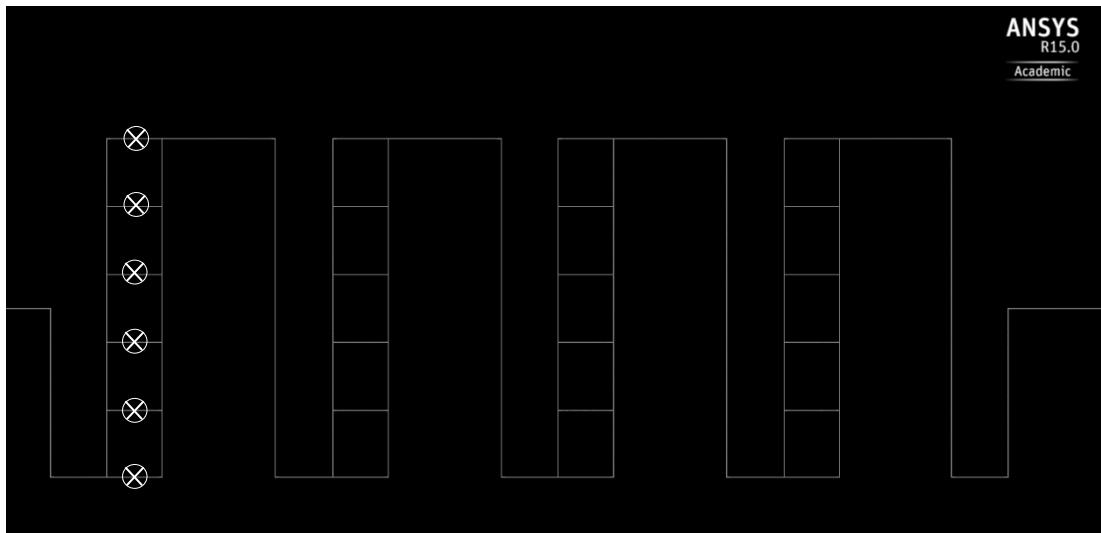


Figure 4.11: Location of Radial Contour Plots sample

4.2.1 Axial Contours for 1.67 m/s inlet velocity

The velocity contour of nitrogen gas component at the outlet in the direction of its microchannel height is referenced in Figures 4.12 to Figure 4.14. Velocity profile is often used to measure the flow condition of fluids within a pipe. In this study, nitrogen gas component enters the microchannel tube at a speed of 1.67 m/s and it is also expected to exit the channel at similar speed for all models.

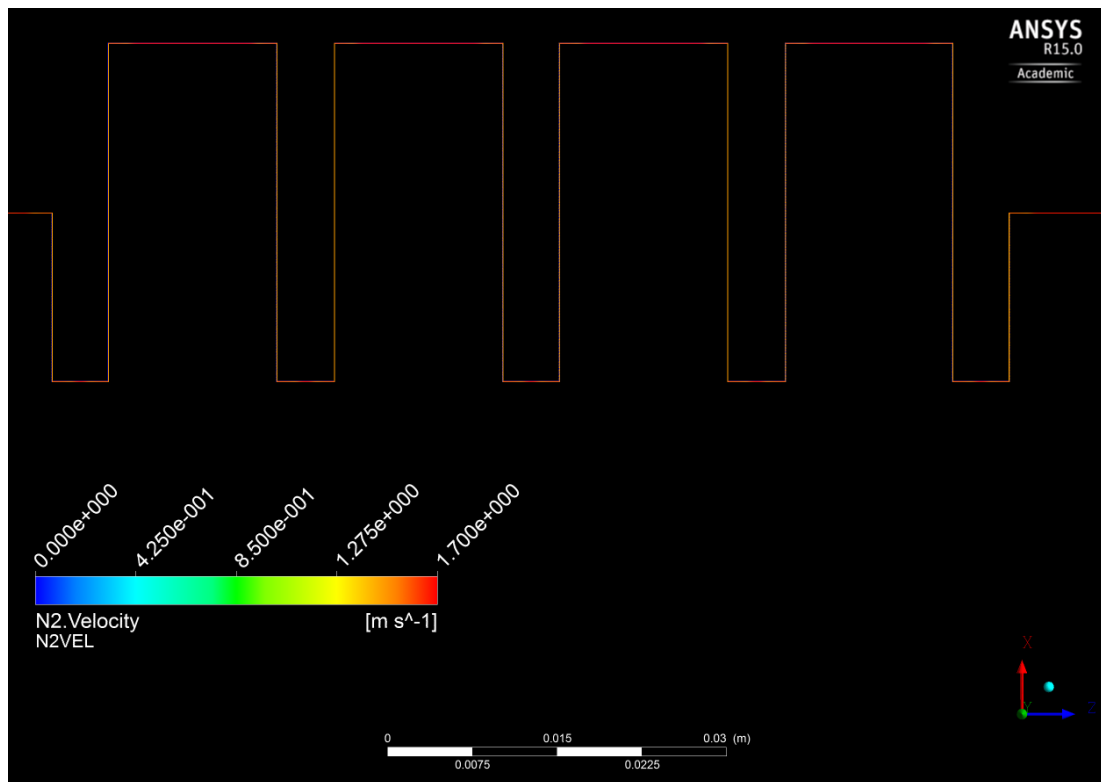


Figure 4.12: Axial Velocity Contour of Model A

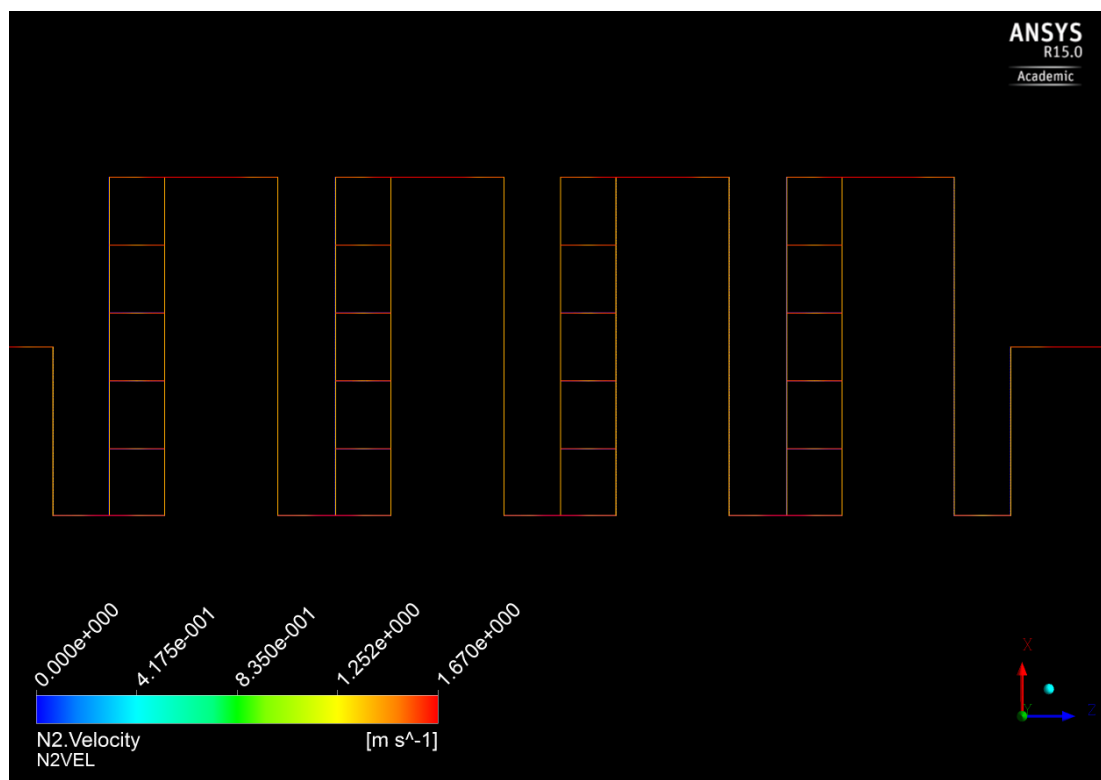


Figure 4.13: Axial Velocity Contour for Model B

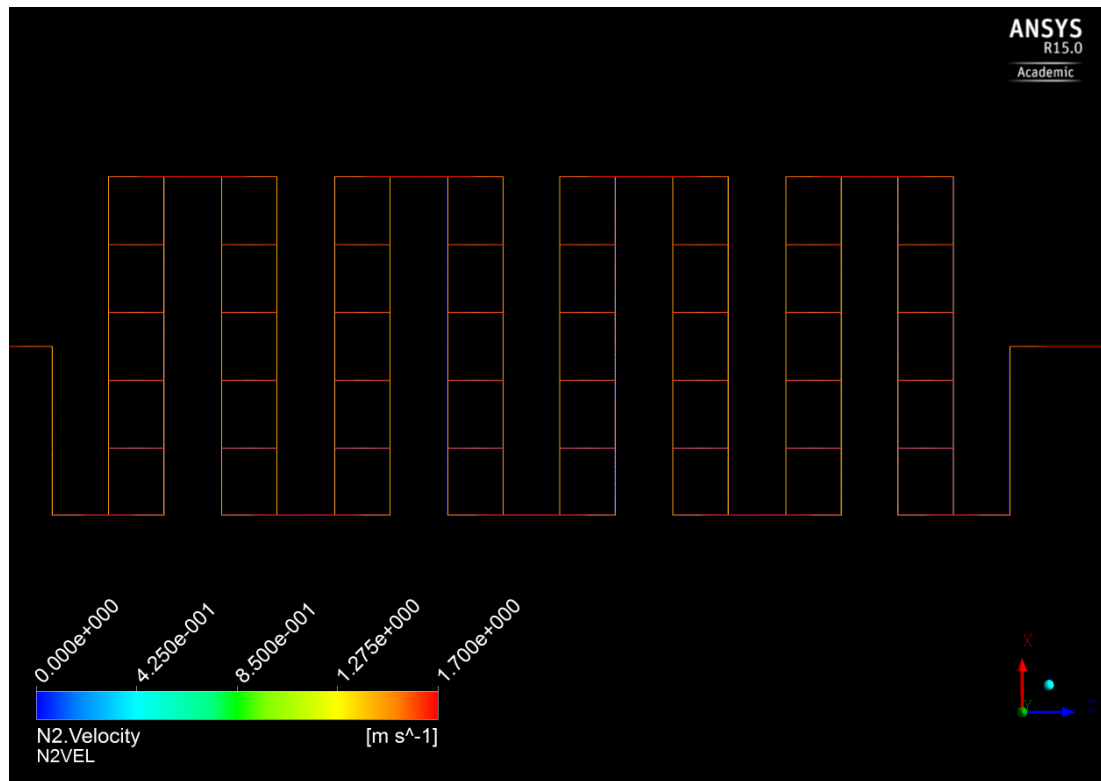


Figure 4.14: Axial Velocity Contour of Model C

In terms of velocity, Nitrogen is able to maintain speed close to inlet speed of 1.67 m/s. This is evident in the figure given shown in red. This is can be due to difference in volume fraction of the component gas. Nitrogen accounts for 25% of total flow volume.

Represented by the red color, Model A can sustain maximum velocity for nitrogen at 11 sections of the micromixer. While, Model B can sustain maximum velocity for Nitrogen gas for 26 sections of the micromixer. Model C can sustain maximum velocity for Nitrogen gas at 50 sections of the micromixer.

4.2.2 Radial Contours for 1.67 m/s inlet velocity

Radial contours were completed for Models B and C only because these models contain the mixing chamber configurations. Furthermore, these contours are placed on the first array of mixing chamber of each model and not on the all subsequent. This is because when examined, the mixing chamber has flow patterns which are repetitive throughout the system. As such, it is assumed the contours will account for all subsequent mixing chambers in the system.

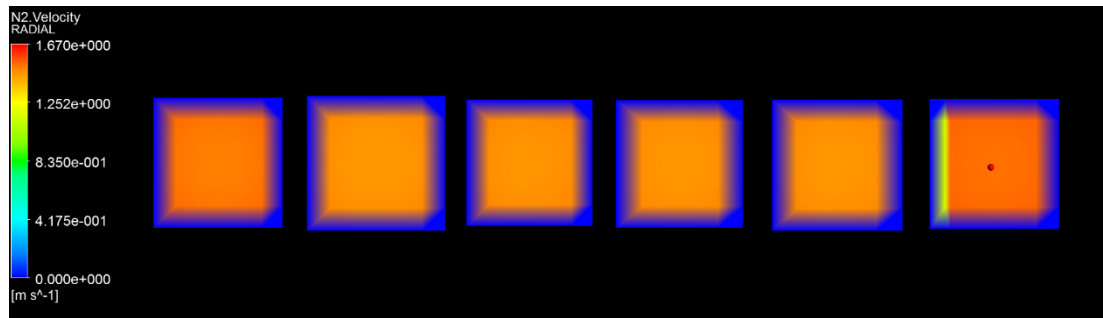


Figure 4.15: Series of Radial Contours for Model B

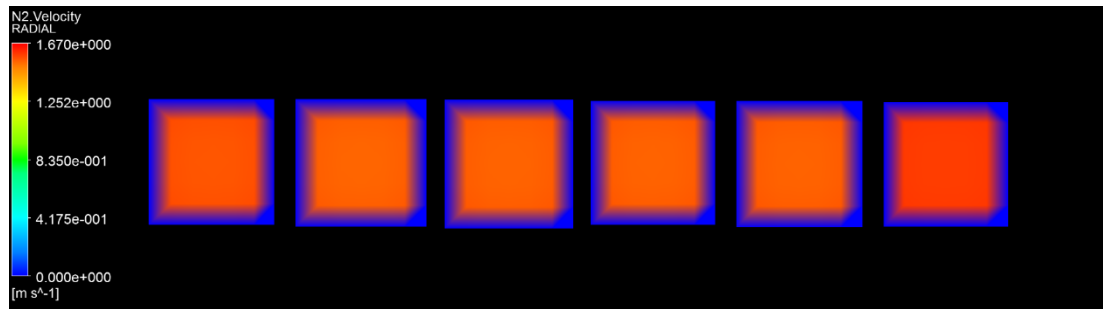


Figure 4.16: Series of Radial Contours for Model C

From the contours given in the figures above, there is a clear distinction in the color from model B to C. This means that the velocity distribution for the two models are different. Nevertheless, the radial contours can display the blue line around the rectangular channel. This represents that the flow is at no-slip condition on the channel wall.

In Model B, Nitrogen flow is generally slower compared to Model C even at the same inlet velocity. The flow is nearer to approximately 1.25 m/s. Similarly, Model C shows uniform flow can be seen radially although this configuration can maintain Nitrogen flow at faster speed. The speed is approximately above 1.4 m/s.

4.2.3 Axial Contours for 3.33 m/s velocity

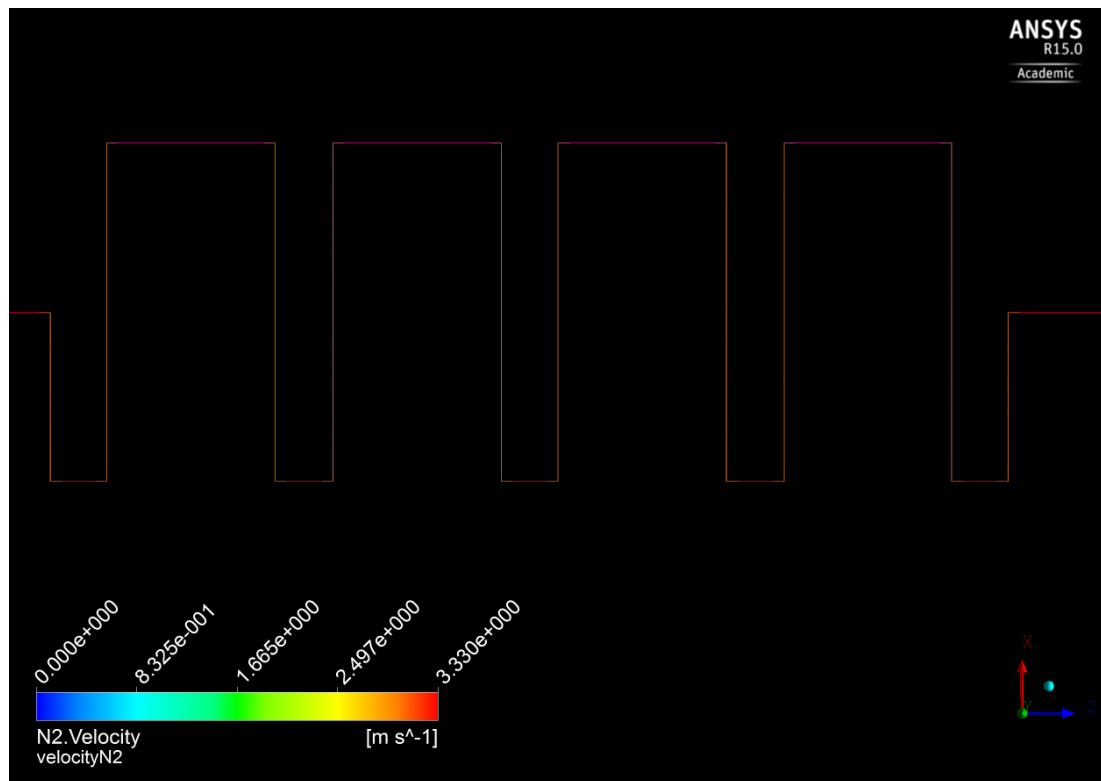


Figure 4.17: Axial Velocity Contour for Model A

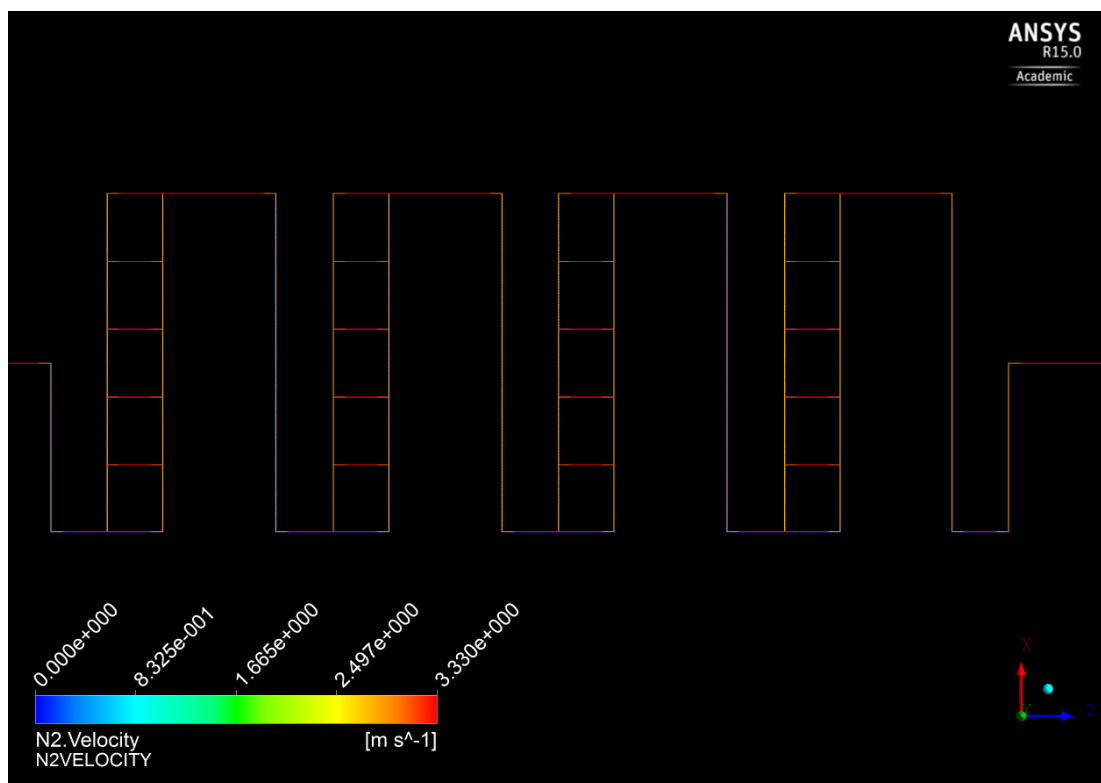


Figure 4.18: Axial Velocity Contour for Model B

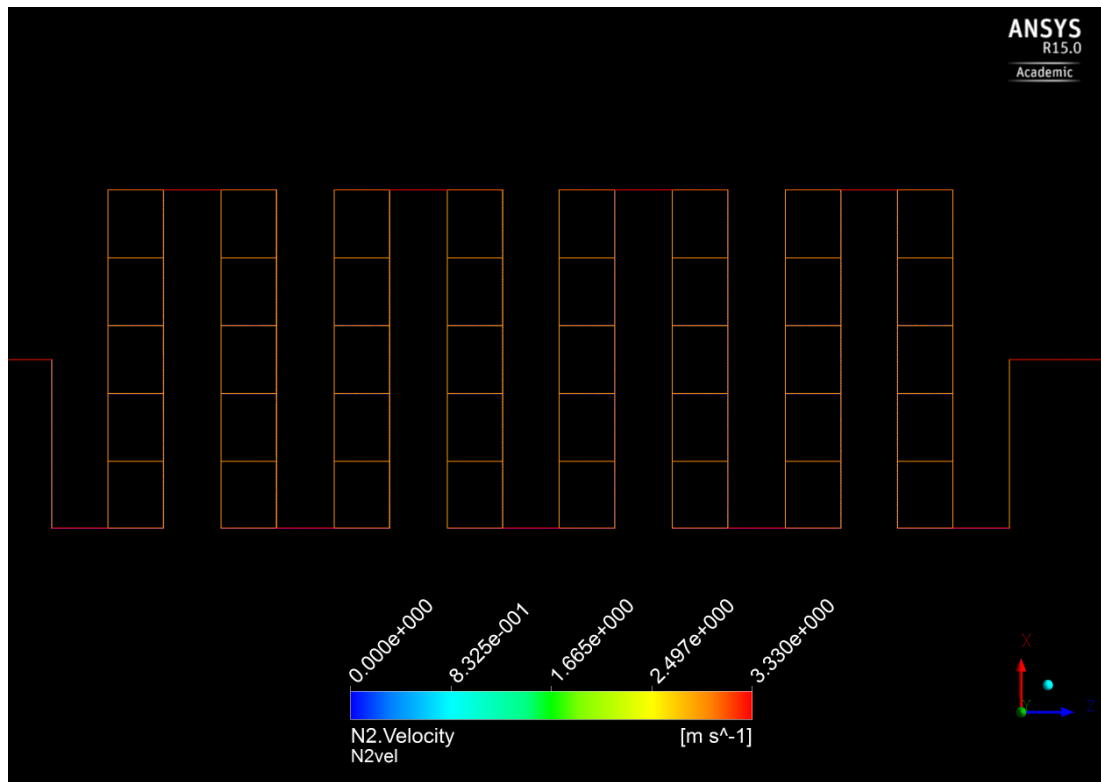


Figure 4.19: Axial Velocity Contour for Model C

In terms of velocity, Nitrogen is able to maintain speed close to inlet speed of 3.3 m/s. This is evident in the figure given shown in red. This can be due to difference in volume fraction of the component gas. Nitrogen accounts for 25% of total flow volume.

Represented by the red color, Model A can sustain maximum velocity for nitrogen at 11 sections of the micromixer. While, Model B can sustain maximum velocity for Nitrogen gas for 26 sections of the micromixer. Although, Model B shows maximum velocity are achieved in the center of mixing chamber sections. This is different from the 1.67 m/s speed because the contour showed that highest velocity achieved at more length of the intersection. This time. Model C can only sustain maximum velocity for Nitrogen gas at 11 sections of the micromixer and this does not relatively reflect good mixing behaviour even though surface area for molecule interaction was increased.

4.2.4 Radial Contours for 3.33 m/s inlet velocity

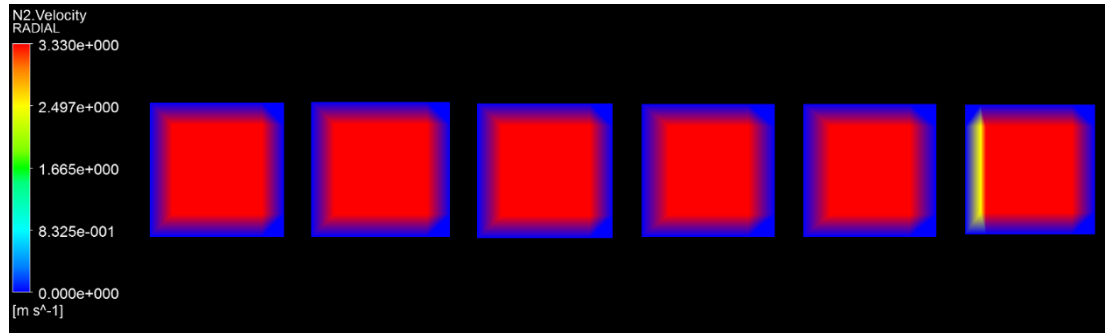


Figure 4.20: Radial Velocity Contour for Model B

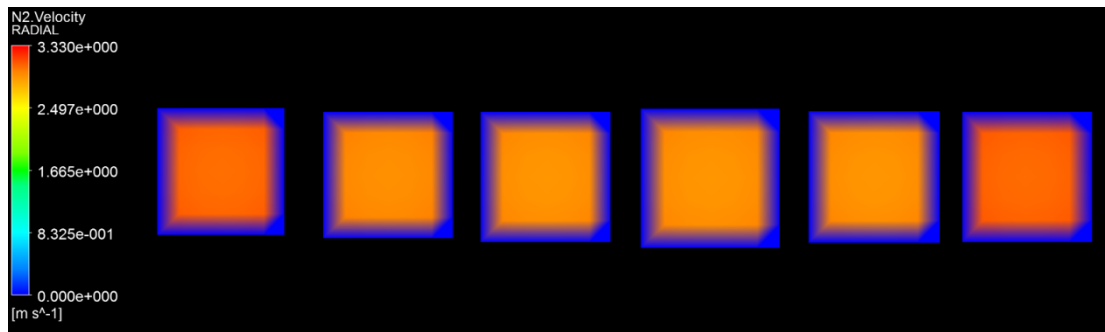


Figure 4.21: Radial Velocity Contour for Model C

In this case, Nitrogen velocity was able to achieve speed of 3.33 m/s in the center of the mixing chamber. There is a clear distinction in the color from model B to C. This meant that the velocity distribution for the two models are different. Nevertheless, the radial contours displays the blue line around the rectangular channel. This represents that the flow at no-slip condition on the channel wall.

In Model B, Nitrogen flow is generally faster compared to Model C even at the same inlet velocity. The flow is nearer to approximately 3.33 m/s and similar pattern is shown across the 6 intersections. By observation there is a minor yellow section of the contour on the left wall after the non-slip boundaries. The channel shows flow is slow after the turn on that particular wall and is dominant towards right. Similarly, Model C shows uniform flow can be seen radially although this configuration can maintain Nitrogen flow at slower speed. Yet, the speed is approximately above 2.9 m/s region. Furthermore, faster fluid flow is observed at the first and last channel which represents mixing chamber inlet and outlet.

4.2.5 Axial Contours for 10.99 m/s velocity

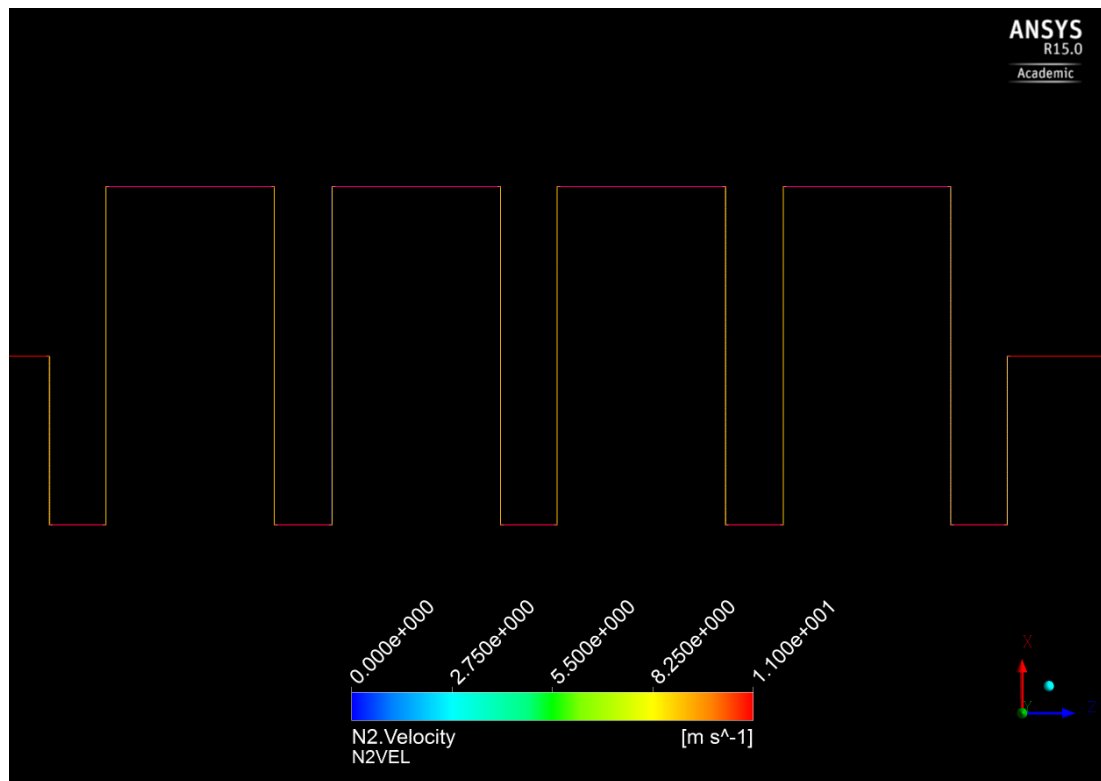


Figure 4.22: Axial Velocity Contour for Model A

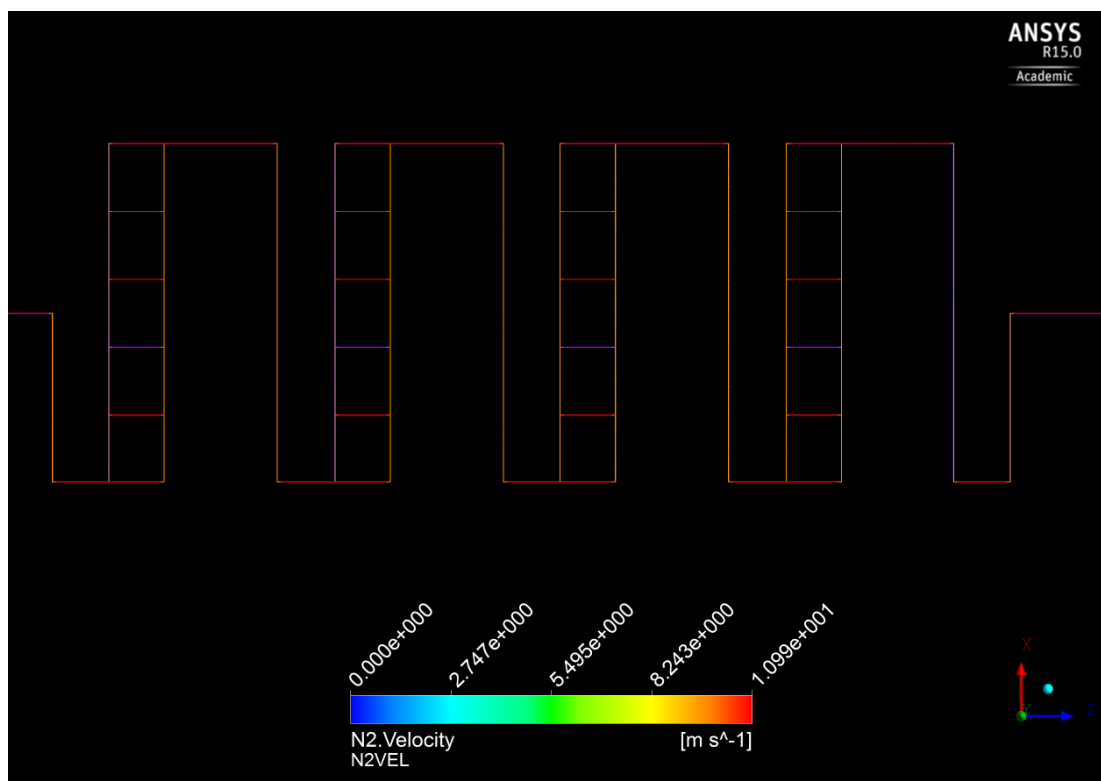


Figure 4.23: Axial Velocity Contour for Model B

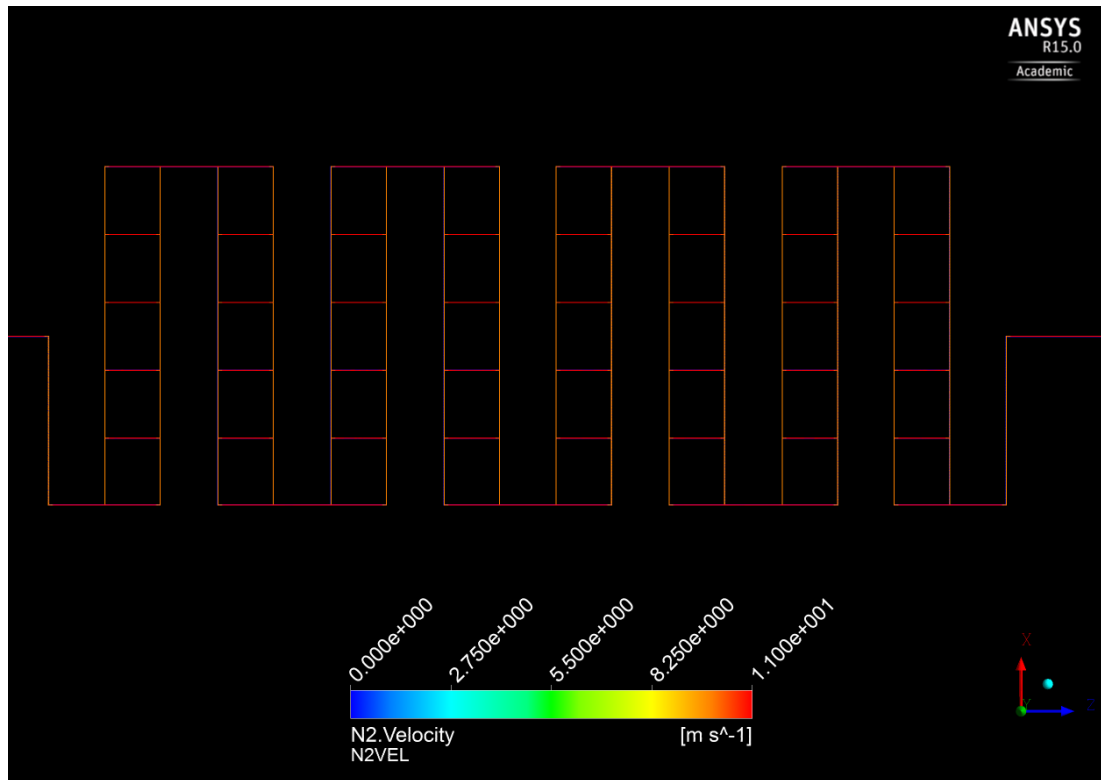


Figure 4.24: Axial Velocity Contour for Model C

In terms of velocity, Nitrogen is able to maintain speed close to inlet speed of 10.99 m/s. This is evident in the figure given shown in red. This can be due to difference in volume fraction of the component gas. Nitrogen accounts for 25% of total flow volume.

Represented by the red color, Model A can sustain maximum velocity for nitrogen at 11 sections of the micromixer. While, Model B can sustain maximum velocity for Nitrogen gas for 26 sections of the micromixer. Model C can sustain maximum velocity for Nitrogen gas at 60 sections of the micromixer. Similar trend was found on all of the models whereby fluid velocity was highest and maintained at longer length in the mixers. Therefore, maximum velocity was achieved with more surface area. Therefore, at 10.99 m/s, mixing for Nitrogen component is best with Model C configuration.

4.2.6 Radial Contours for 10.99 m/s inlet velocity

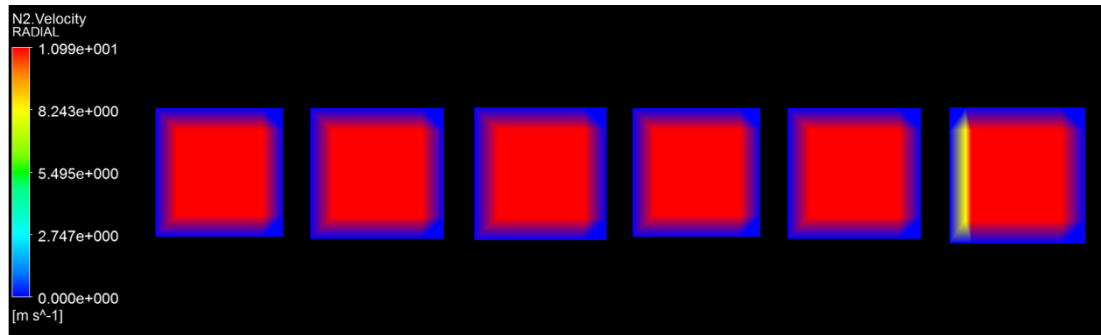


Figure 4.25: Radial Velocity Contour for Model B

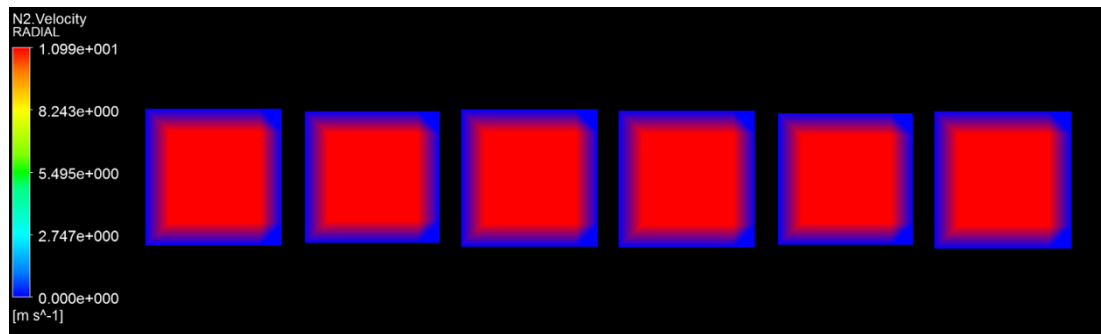


Figure 4.26: Radial Velocity Contour for Model C

In reference to the figures above, the radial contours suggests that mixing, at relatively high velocity, is good for both Models B and C. Nitrogen flow is generally uniform and similar and similar pattern is shown across the 6 intersections. In contrast, Model B shows a minor yellow section of the contour on the left wall after the non-slip boundaries. The channel shows flow is slow after the turn on that particular wall and is dominant towards right. Although, the same phenomena is not found in Model C. Maximum flow speed was achieved across the whole width of the mixing chamber outlet section. This may be attributed to the increment in mixing chambers which meant more pressure reduction thus flow is more uniform across the mixer.

4.3 Hydrogen Velocity Contours

This contour is obtained from the results by way of inserting a plane across the micromixer. The plane is located midway on the Z-X axis of the microchannel. This inserted plane will then read off the gas velocity inside the microchannel in variable color representation.

The diagrams presented are configured into two views or representation; Axial and Radial. In axial view, as previously shown, the diagram will show contour details for overall mixer. Whilst radial view will show the flow's velocity distribution by the plane located on the X-Y axis. In this study, the contour plots are situated at specified locations on the mixer. They are arranged in the order shown the figure below; and placed within midsections of the proposed mixing chambers.

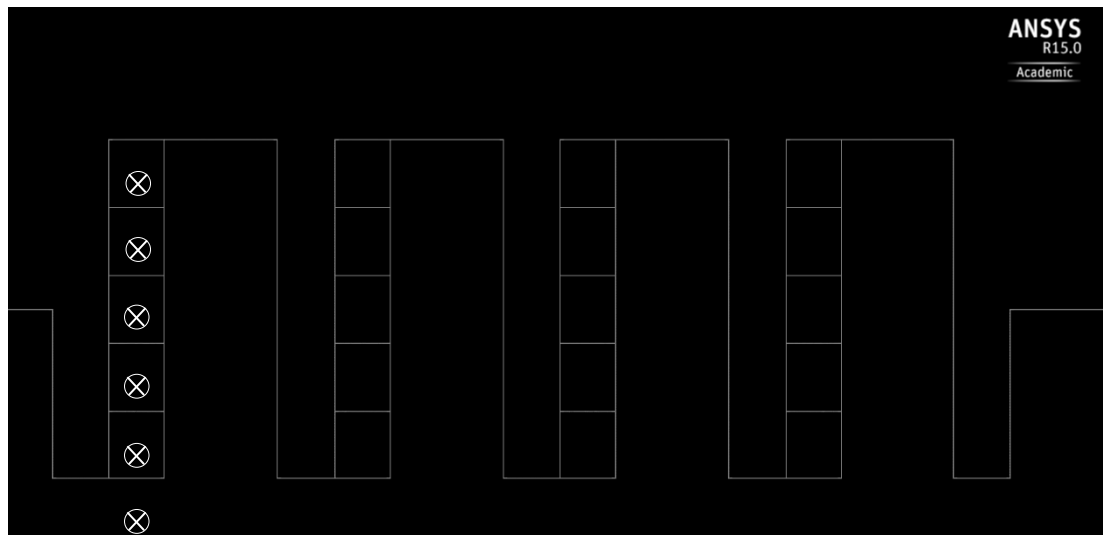


Figure 4.27: Location of Radial Contour Plots sample

4.3.1 Axial Contours for 1.67 m/s inlet velocity

The velocity profiles of Hydrogen gas component at the outlet in the direction of its microchannel height are referenced in Figure above. Velocity profile is often used to measure the flow condition of fluids within a pipe. In this study, Hydrogen gas component enters the microchannel tube at a speed of 1.67 m/s, and it is also expected to exit the channel at similar speed for all models.

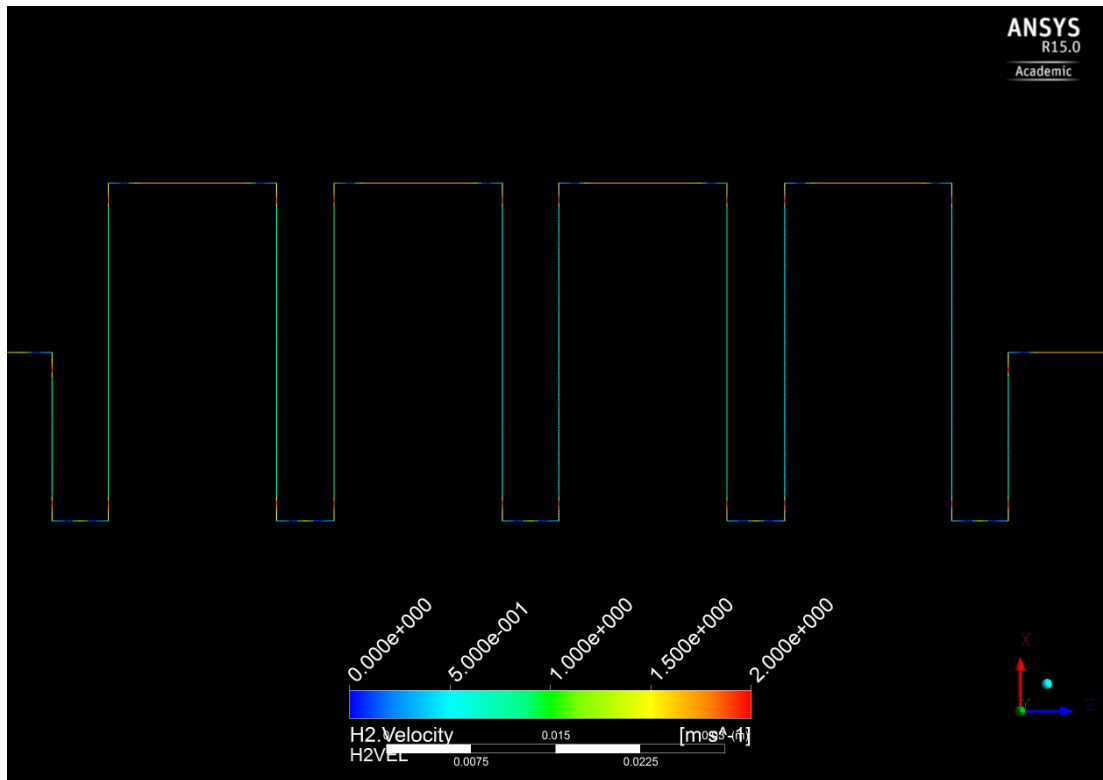


Figure 4.28: Axial Velocity Contour of Model A

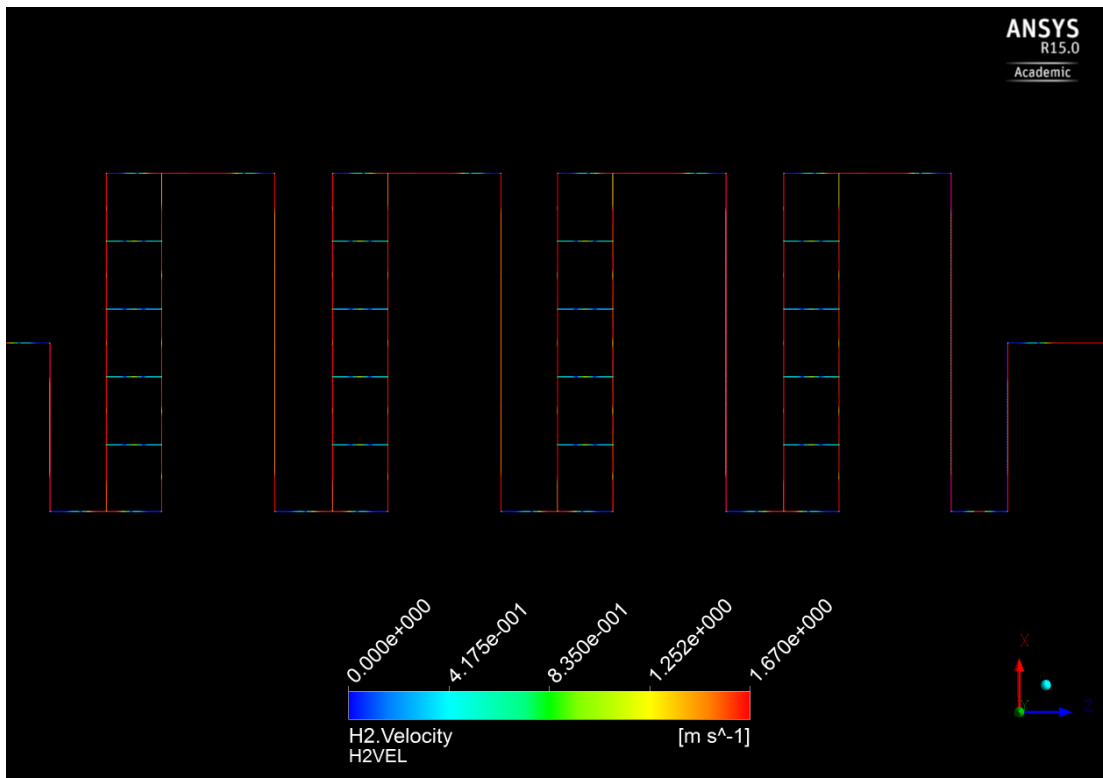


Figure 4.29: Axial Velocity Contour of Model B

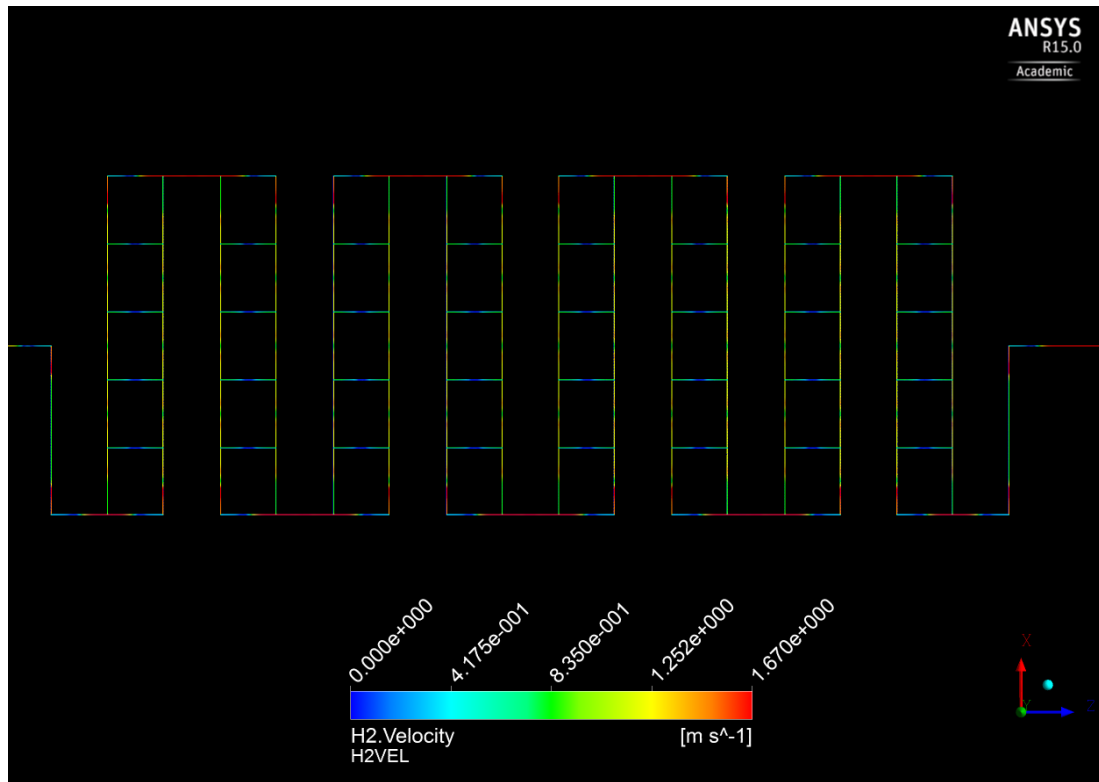


Figure 4.30: Axial Velocity Contour of Model C

In terms of Hydrogen velocity, the Contour Diagrams shows that color variations in the system is much more prominent than Nitrogen at the same velocity, signifying more variation in fluid velocity throughout the system. This is can be due to difference in volume fraction of the component gas as Hydrogen accounts for 75% of total flow volume.

In Model A, flow is steady with minor speed increment before and after junctional turns. This does not reflect well mixing behaviour because maximum velocity can't be sustained a larger distance in length. Whilst Model B, can sustain maximum velocity for Hydrogen gas at more than 26 sections of the micromixer. At straight line sections between mixing chamber inlet and outlet, the red color markers are obtained along the channel. This indicates good mixing are to occur along the vertical channel going from mixing chamber inlet to outlet. Whilst in Model C, velocity for Nitrogen gas flow are generally steady below 1.25 m/s region. Vibrant colors across the spectrum indicating flow is gradual and is not uniform as Nitrogen gas is. However, red streams are more visible on the interconnecting horizontal channels but at smaller length before it slows down again.

4.3.2 Radial Contours for 1.67 m/s inlet velocity

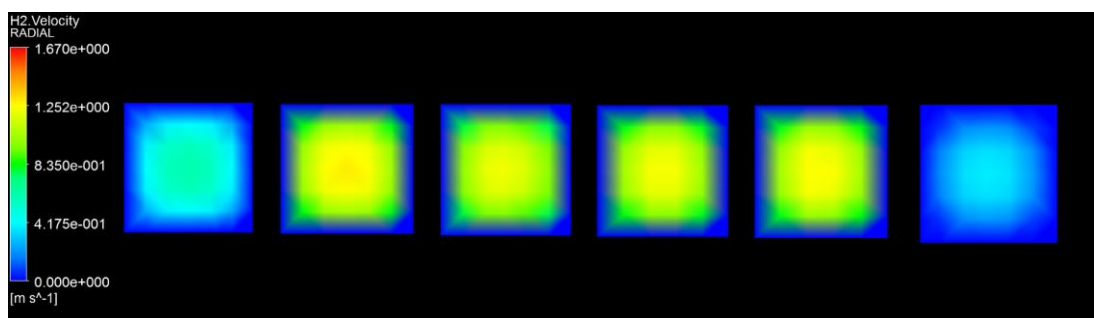


Figure 4.31: Radial Velocity Contours for Model B

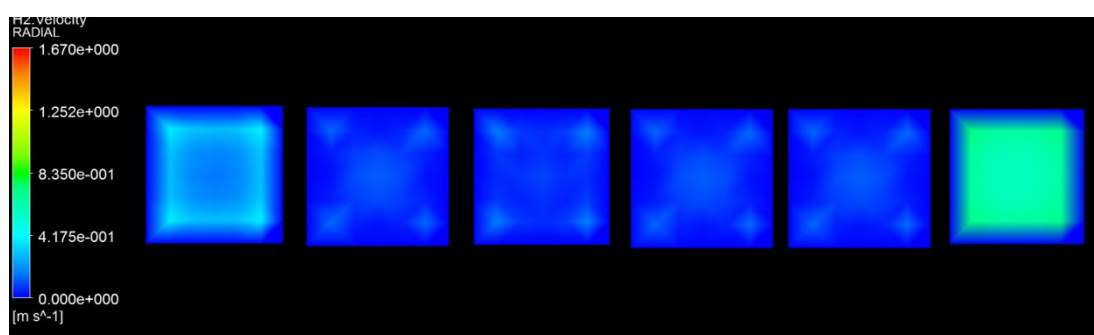


Figure 4.32: Radial Velocity Contours for Model C

Interestingly, Model B shows that Hydrogen flow is greater at mixing chambers and not at inlet and outlet channels which differs from Nitrogen flow. The flow is nearer to approximately 1.00 m/s in the 4 mixing-chambers and is slower up to approximately 0.4175 m/s on the inlet/outlet channels. Secondly, the flow is no longer uniform across the radial plane. As reflected in the contour, the flow gradually increases from the wall towards the center which is represented in yellow. This suggests that Hydrogen gas flows in laminar pattern.

In contrast, Model C flow at the center of mixing chambers are approaching zero. Although there are fragments of Hydrogen gas manage to flow near wall but not at enough speed. Furthermore, faster fluid flow is observed at the first and last channel which represents mixing chamber inlet and outlet. The radial contours obtained for Model C indicates that the addition of mixing-chamber numbers is increasing the pressure of the fluid towards the center. Thus, uniform flow distribution is disrupted and almost no mixing can occur in the center of mixing chamber.

4.3.3 Axial Contours for 3.33 m/s velocity

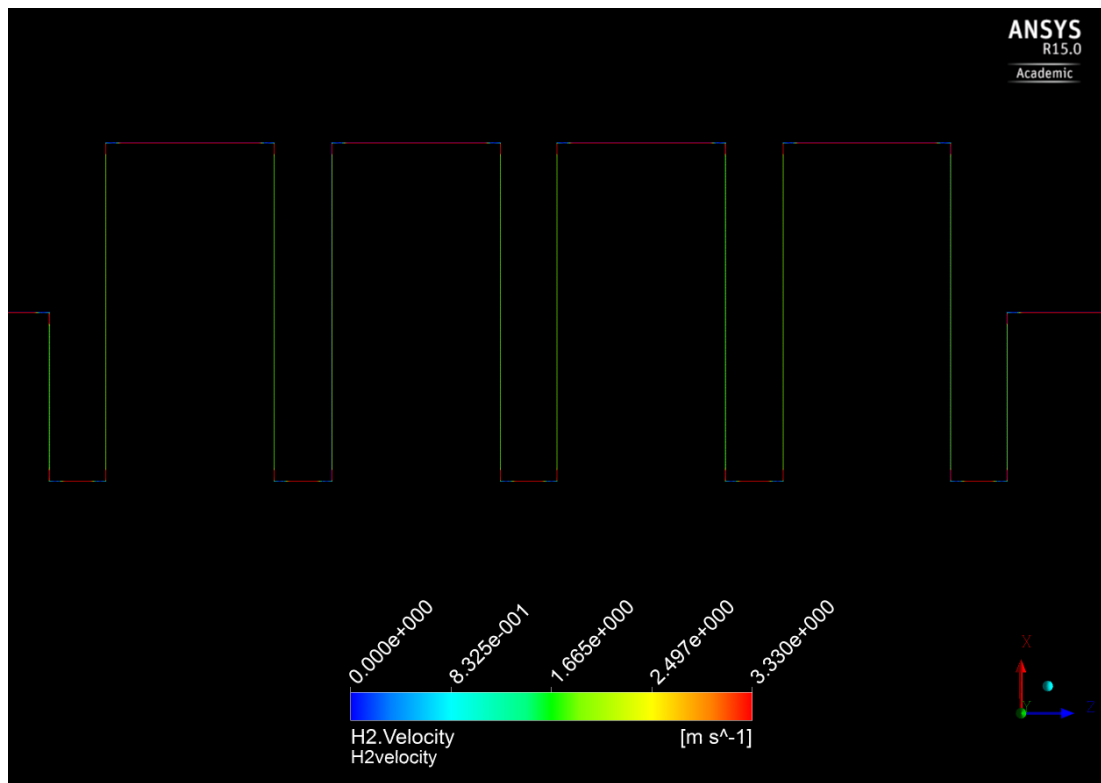


Figure 4.33: Axial Velocity Contour of Model A

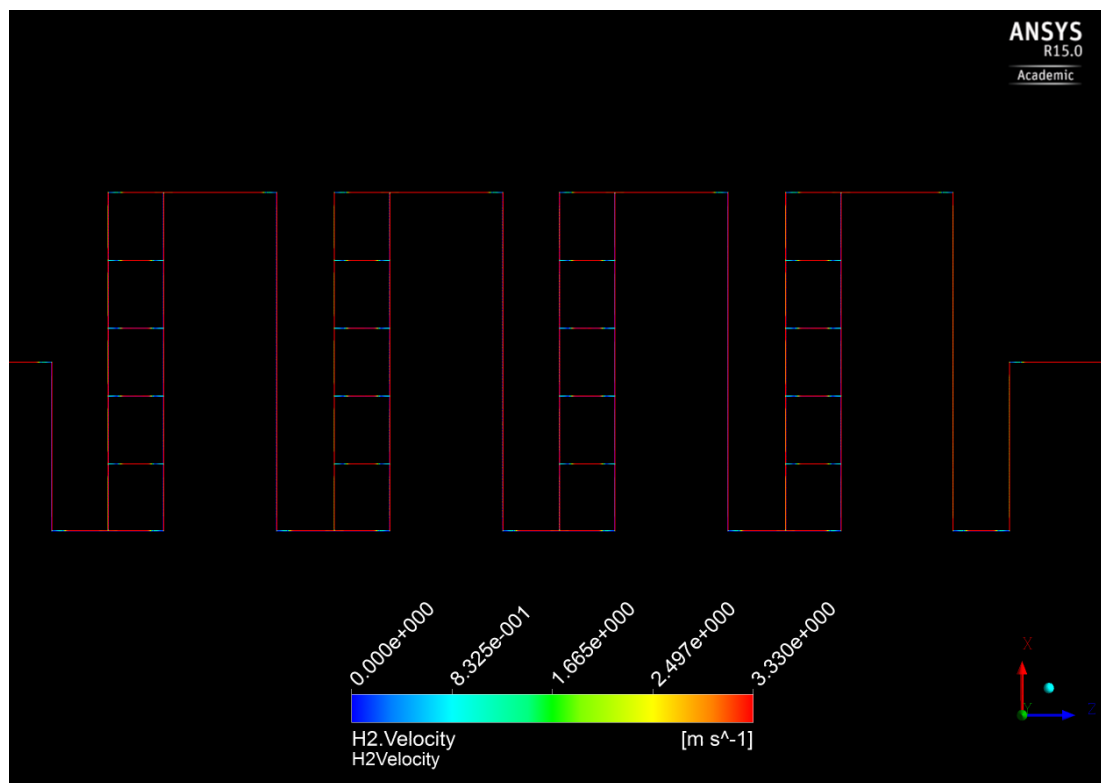


Figure 4.34: Axial Velocity Contour of Model B

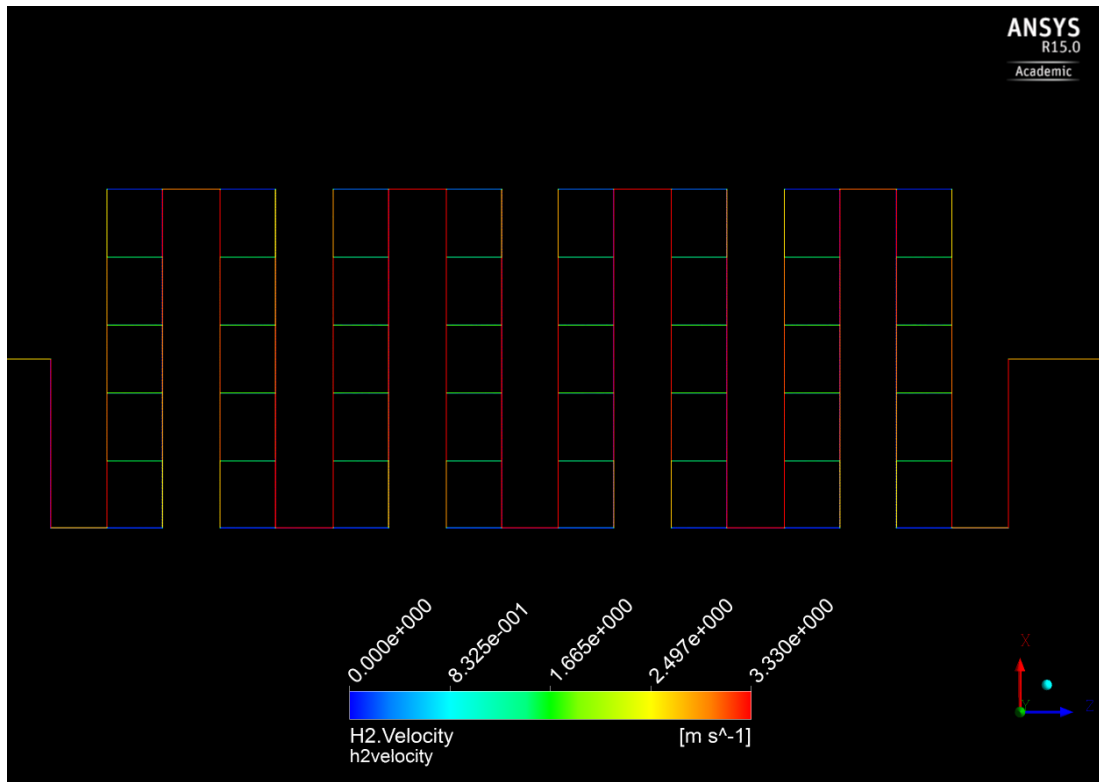


Figure 4.35: Axial Velocity Contour of Model C

At 3.33 m/s, all of the model was obtain maximum velocities at considerable length. Model A was able to obtain the speed on all horizontal microchannels and is considered good for mixing. On all vertical streams, the speed is approximately 1.67 m/s which meant it has reduced almost half of its original speed.

Although Model B was able show red color at more sections in the contours. This points to significant mixing along the micromixer as compared to model A. Apart from velocity drop at intersections, Hydrogen flow is quite fast throughout the microchannel mostly above ≈ 3.0 m/s. Furthermore, mixing is indicated at center of the mixing chambers as it is presented in red.

Model C presents a contour with more variation in color, hence greater velocity distribution. Some red streams can be seen on mixing chamber vertical channels and at interconnecting streams. Although least flow velocity are found on the connecting streams also whereas horizontal mixing chamber streams are green thus contain some mixing. In general, increasing number of mixing chambers has increased the pressure towards the middle of the mixer and slowed the fluid velocity.

4.3.4 Radial Contours for 3.33 m/s inlet velocity

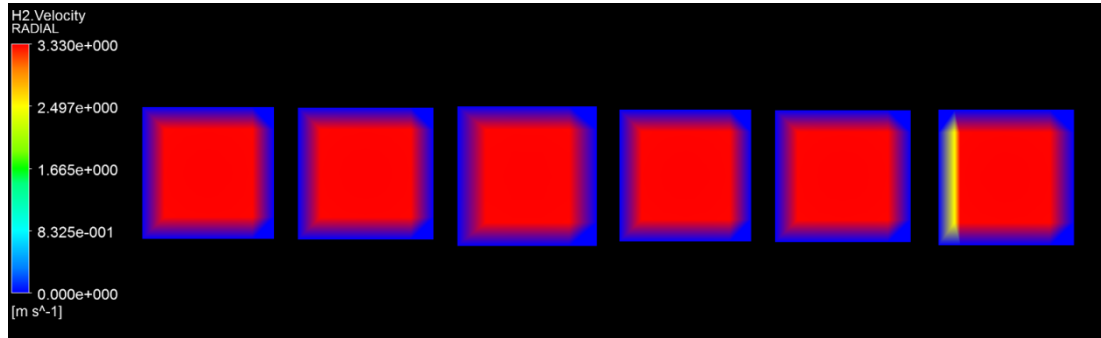


Figure 4.36: Axial Velocity Contour for Model B

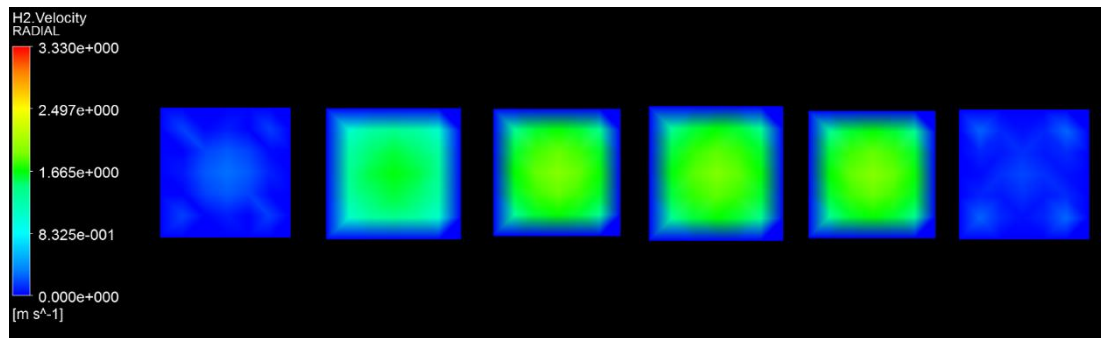


Figure 4.37: Axial Velocity Contours for Model C

In this case, Hydrogen velocity was able to achieve speed of 3.33 m/s in the center of the mixing chamber. There is a clear distinction in the color from model B to C. This meant that the velocity distribution for the two models are different. Nevertheless, both radial contours displays the blue line around the rectangular channel. This represents that the flow at no-slip condition on the channel wall.

In Model B, Hydrogen flow is generally faster compared to Model C even at the same inlet velocity. The flow is nearer to approximately 3.33 m/s and similar pattern is shown across the 6 intersections. By observation there is a minor yellow section of the contour on the left wall after the non-slip boundaries. The channel shows flow is slow after the turn on that particular wall and is dominant towards right.

Model C shows uneven flow can be seen radially yet, the speed is approximately below 2.2 m/s region. Velocity is lower in the second contour.

Furthermore, almost no fluid flow is observed at the first and last channel which represents mixing chamber inlet and outlet. Slightly, laminar flow is indicated.

4.3.5 Axial Contours for 10.99 m/s velocity

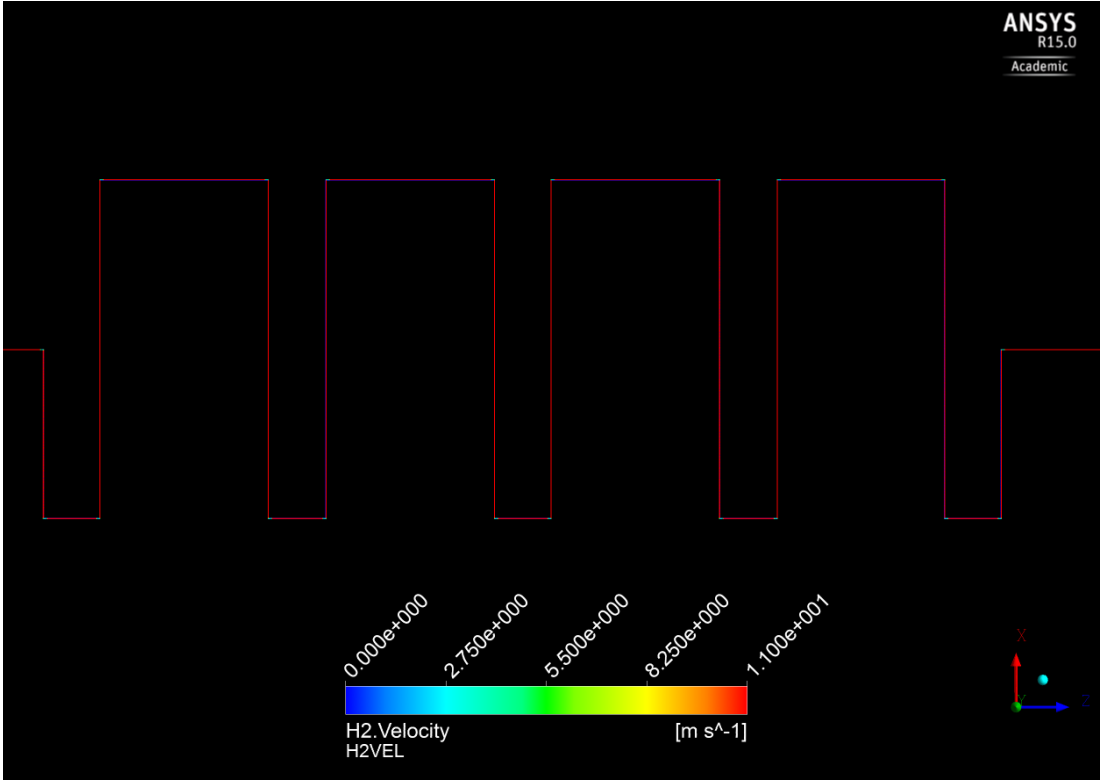


Figure 4.38: Axial Velocity Contour of Model A

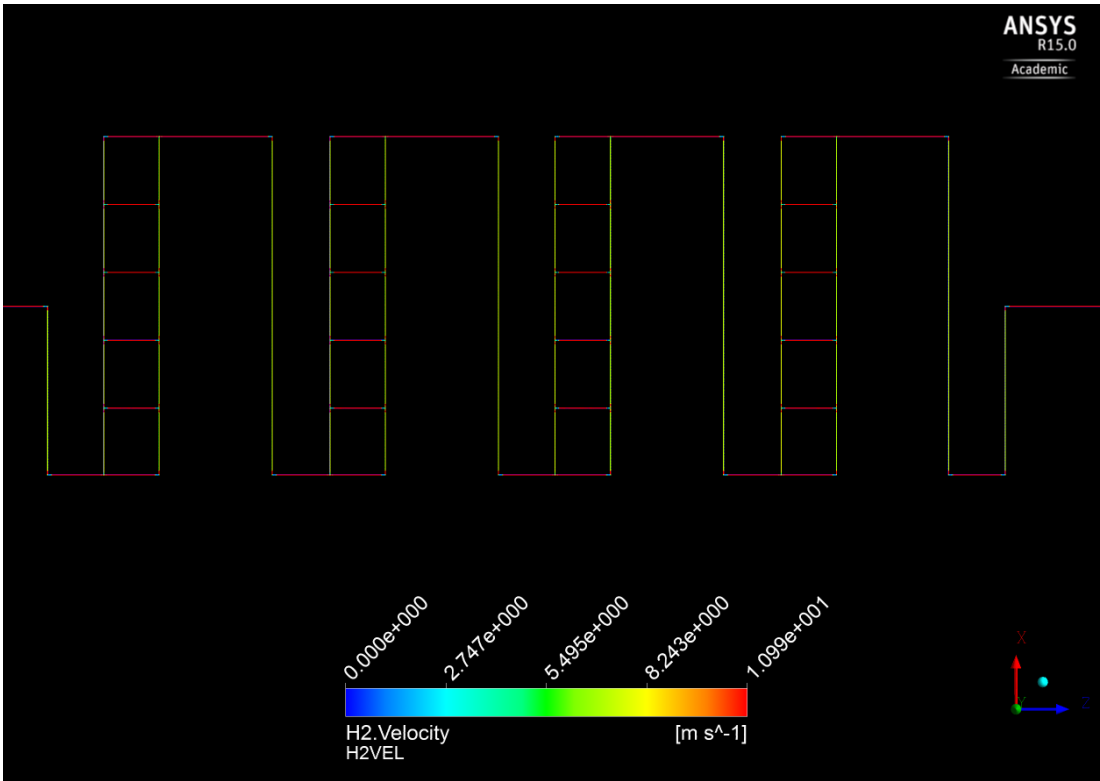


Figure 4.39: Axial Velocity Contour of Model B

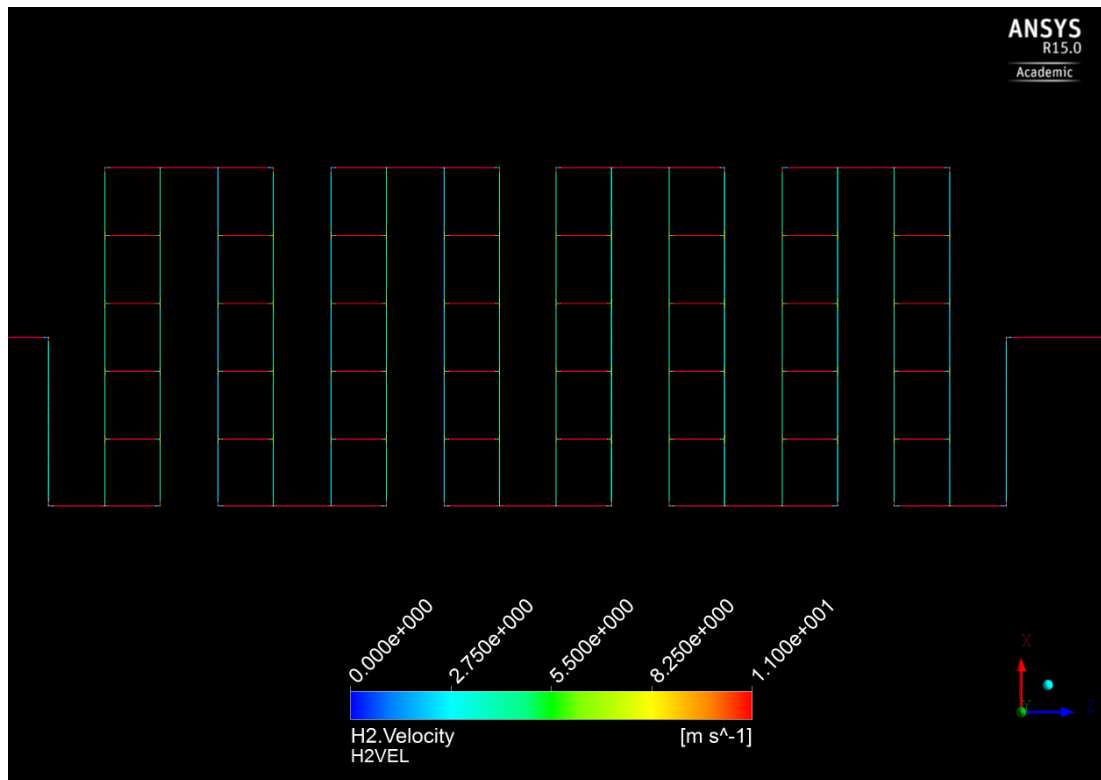


Figure 4.40: Axial Velocity Contour of Model C

In terms of velocity, Hydrogen is able to maintain speed close to inlet speed of 10.99 m/s. This is evident in the figure given shown in red. This can be due to difference in volume fraction of the component gas as Hydrogen accounts for 75% of total flow volume.

Represented by the uniform redish color, Model A can sustain maximum velocity for Hydrogen across the micromixer suggesting good mixing characteristics because mixing occurs throughout the system in terms of length.

While, Model B can sustain maximum velocity for Nitrogen gas for 35 sections of the micromixer (on all horizontal streams) meaning the model sustains maximum velocity when path length is shorter. Good mixing behaviour can be seen in the center of each mixing chambers. This is a better model for mixing compared to Model A

Increasing the contact (surface) area of the mixer in Model C shows similar trend to that of Model B. Hence, adding more mixing chambers suggest that this

Model has better mixing capabilities than Model B at 10.99 m/s because highest velocity is obtained at greater surface area.

4.3.6 Radial Contours for 10.99 m/s inlet velocity

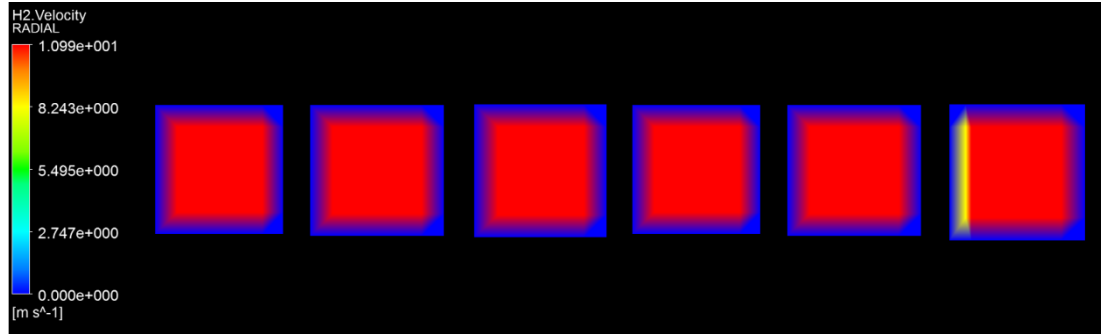


Figure 4.41: Radial Velocity Contours for Model B

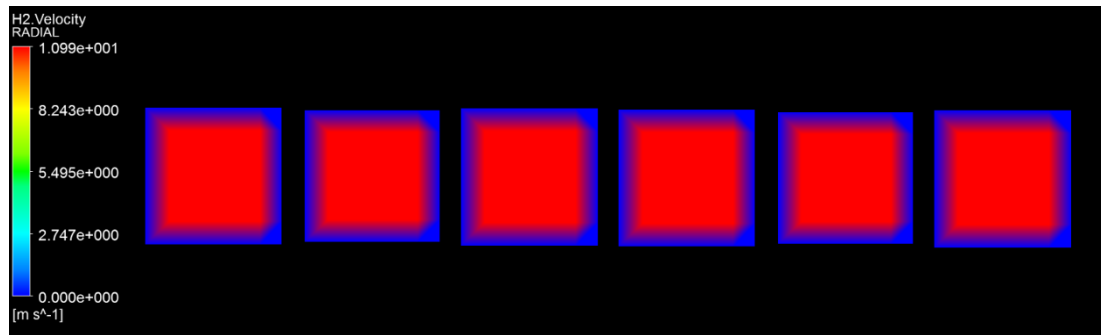


Figure 4.42: Radial Velocity Contours for Model C

In reference to the figures above, the radial contours suggests that mixing, at relatively high velocity, is good for both Models B and C. Hydrogen flow is generally uniform and similar and similar pattern is shown across the 6 intersections. In contrast, Model B shows a minor yellow section of the contour on the left wall after the non-slip boundaries. The channel shows flow is slow after the turn on that particular wall and is dominant towards right. Although, the same phenomena is not found in Model C. Maximum flow speed was achieved across the whole width of the mixing chamber outlet section. This may be attributed to the increment in mixing chambers which meant more pressure increase thus flow is able to be more uniform across the mixer.

At 10.99 m/s the flow is relatively fast enough for mixing to occur in center sections of the mixing chamber in both models. Model C having more mixing

chambers is the better option for the molecular interaction of Hydrogen and Nitrogen gases.

CHAPTER 5

CONCLUSIONS AND RECOMMENDATIONS

5.1 Conclusions

The objective of this project study is to investigate the hydrodynamics of nitrogen and hydrogen gas components during the synthesis of ammonia in a micromixer at ambient operating condition. The significant of this study is to assist in optimizing the localization of the catalyst for the ammonia synthesis reaction to take place.

Next, the micromixer with fine mesh quality is then simulated. Through CFD simulation, the velocity contour plots for both the gas components are obtained. It is observed that generally, hydrogen component have a lower velocity as the fluid flows inward towards the middle of the rectangular microchannel; whereas nitrogen component will decrease its fluid flow only each of the junctions and bend but at the parallel straight section it will flow steadily and in uniform.

Whilst in terms of pressure, the study has found that all models, the pressure in the micromixer ranged from approximately minimum 100 kPa absolute to 102.5 kPa maximum and mostly working pressure is established at 101.3 kPa. However, one exception was discovered whereby in model C with 3.33 m/s inlet speed, the fluid pressure reduced to approximately 0.79 to 0.8 kPa. This meant there is a large pressure drop in the system. In general, the pressure contours reflected that the pressures inside the simulated models were in fact, in an acceptable range. This is because one of the main objectives in this new method of Ammonia synthesis is to design a micromixer which could operate at low temperature and pressure relative to conventional method. In

this study the temperature parameter was not considered as the system undergoes process at room temperature (25 °C).

Table 5.1: Best micromixer selection based on speed

Velocity/ Model	1.67 m/s	3.33 m/s	10.99 m/s
A			
B	✓	✓	
C			✓

Table 5.1 reflects the best micro mixers for the each Models at different inlet speeds. Consideration were taken for both Nitrogen and Hydrogen components to select the micromixer model.

At 1.67 m/s Model B presents the best option because of good Nitrogen mixing capabilities and higher velocities were achieved in the center of mixing chambers as compared to Model C.

Model B was again the best option in 3.33 m/s operation because radial contours shows that mixing is better in the mixing chambers as well having more red streams representing higher velocity for both Hydrogen and Nitrogen gases.

Finally, Model C is most viable option when operated at speed of 10.99 m/s. In both Nitrogen and Hydrogen gases, the maximum speed were able to be maintained in the mixing chambers and on all horizontal streams. Therefore, the key difference from Model B and C was that by increasing surface area greater mixing capabilities can be observed. In terms of flow behaviour, Hydrogen flow pattern is more uniform across the width of channel and not towards laminar flow as observed in section 4.4.6.

5.2 Recommendations

Based on the study, catalyst loading can be performed in many sections of the mixer and even throughout the whole micromixer. The function of inserting the catalyst inside the micromixer is to enhance mixing. Considering the three selected models from section 5.1, the models has larger surface area which can be exploited for catalyst loading. Although, the effect of catalyst loading will then adjust the pressure and velocity of the whole system and thus simulation will be required.

In Model B designs, catalyst can be localized on the vertical streams of the micromixer where maximum velocity were achieved for larger surface area covered.

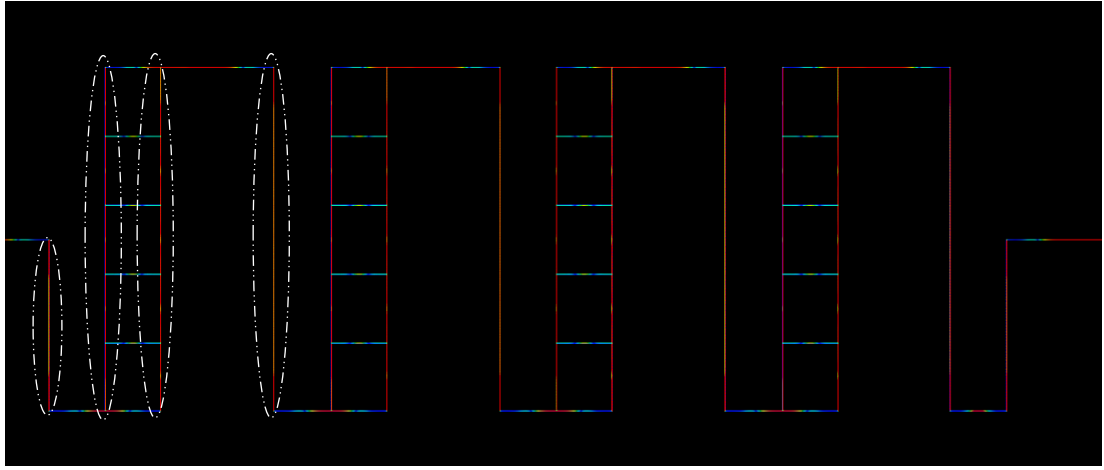


Figure 5.1: Proposed Catalyst location at 1.67 m/s operation

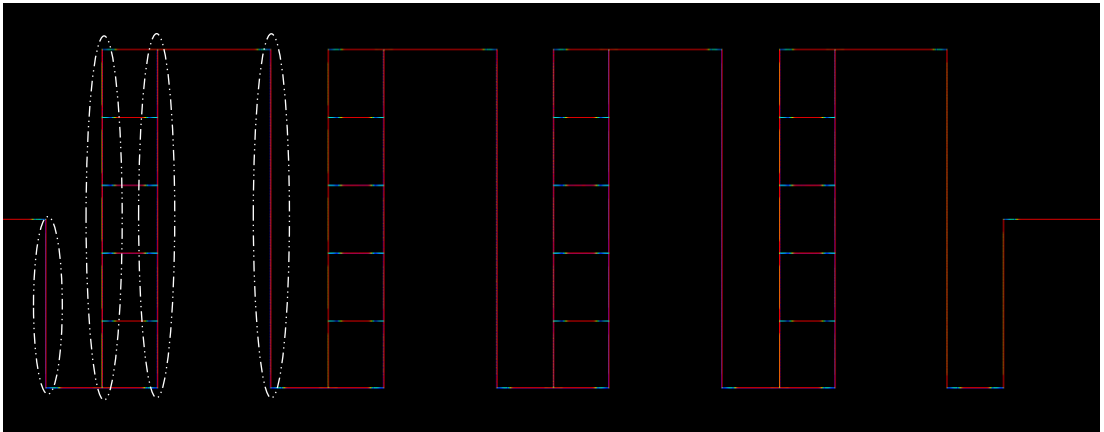


Figure 5.2: Proposed Catalyst location at 3.33 m/s operation

The dashed line on the figures above represents the location of the catalyst. This location is typical for each mixing chambers across the micromixer.

In addition, Model C requires investigation on catalyst loading on all horizontal streams of the micromixer. Simulation can be performed on a micromixer with localized catalyst in the middle and perform hydrodynamic analysis. At 10.99 m/s speed, the velocities for Nitrogen and Hydrogen were fastest at horizontal streams of the micromixer as shown in Figure 5.3. Similarly, the locations highlighted is to be repeated throughout the micromixer.

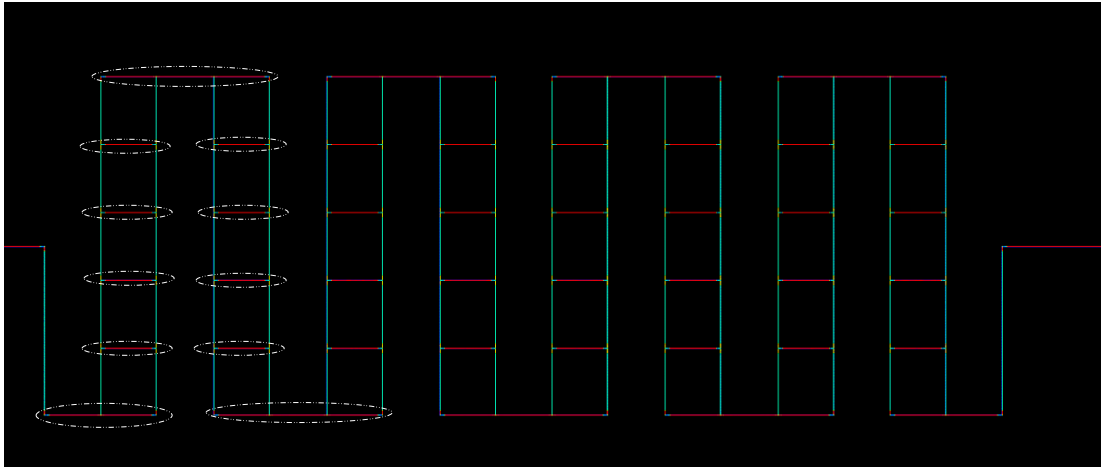


Figure 5.43: Proposed Catalyst location for Model C design

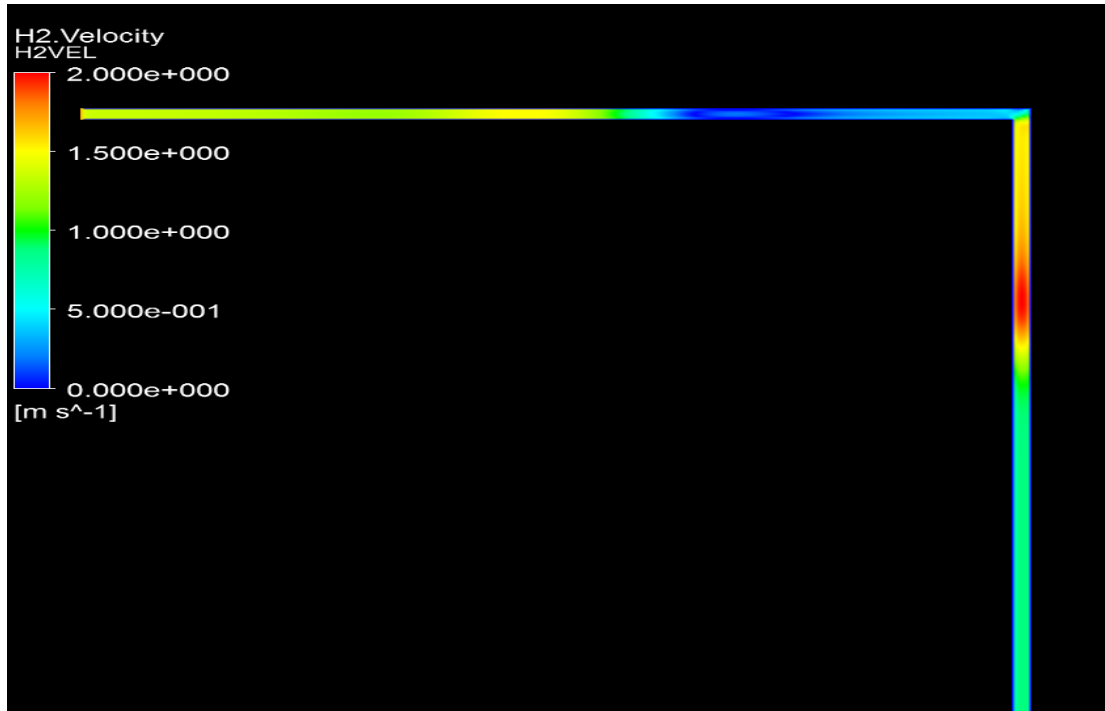
REFERENCES

- Azeman, M. K. (2012). Unpublished, CFD Modelling of The Microreactor for the Ammonia Synthesis.
- Amadin, S. I. (2013). Unpublished, Study on Various Geometry Configurations of a Microchannel For Ammonia Synthesis.
- Baldyga, J. a., & Bourne. (1990). The Effect of Micromixing on Parallel Reactions. *Chemical Engineering Science*, 907-916.
- Bhagat, A., Peterson, E., & Papautsky, I. (2007). A passive planar micromixer with obstructions for mixing at low Reynolds numbers. *J.Micromech.Microeng.* 17, 1017-1024.
- Brody, J. P., & Yager, P. (1997). Diffusion-based extraction in a microfabricated device. *Sensors Actuators A* 58, 13-8.
- Burke, B. J., & Regnier, F. E. (2003). Stopped-flow enzymes assays on a chip using a microfabricated mixer. *Anal. Chem.* 75, 1786-91.
- Cussler, E. L. (1997). *Diffusion: Mass Transfer in Fluid Systems* (2nd Edition ed.). Cambridge University Press.
- Elmabruk A. Mansur, W. Y. (2008). Computational Fluid Dynamic Simulation of Liquid-Liquid Mixing in a Static Double-T-shaped Micromixer. *The Chinese Journal of Process Engineering*, 1-3.
- Hinsmann, P., Frank, J., Svasek, P., Harasek, M., & Lendl, B. (2001). Design, simulation and application of a new micromixing device for time resolved infrared spectroscopy of chemical reactions in solutions. *Lab on a Chip* 1, 16-21.
- Ismagilov, R. F., Stroock, A. D., kenis, P. J., Whitesides, G., & Stone, H. A. (2000). Experimental and theoretical scaling laws for transverse diffusive broadening in two-phase laminar flows in microchannels. *Appl. Phys. Lett.* 76, 2376-2378.

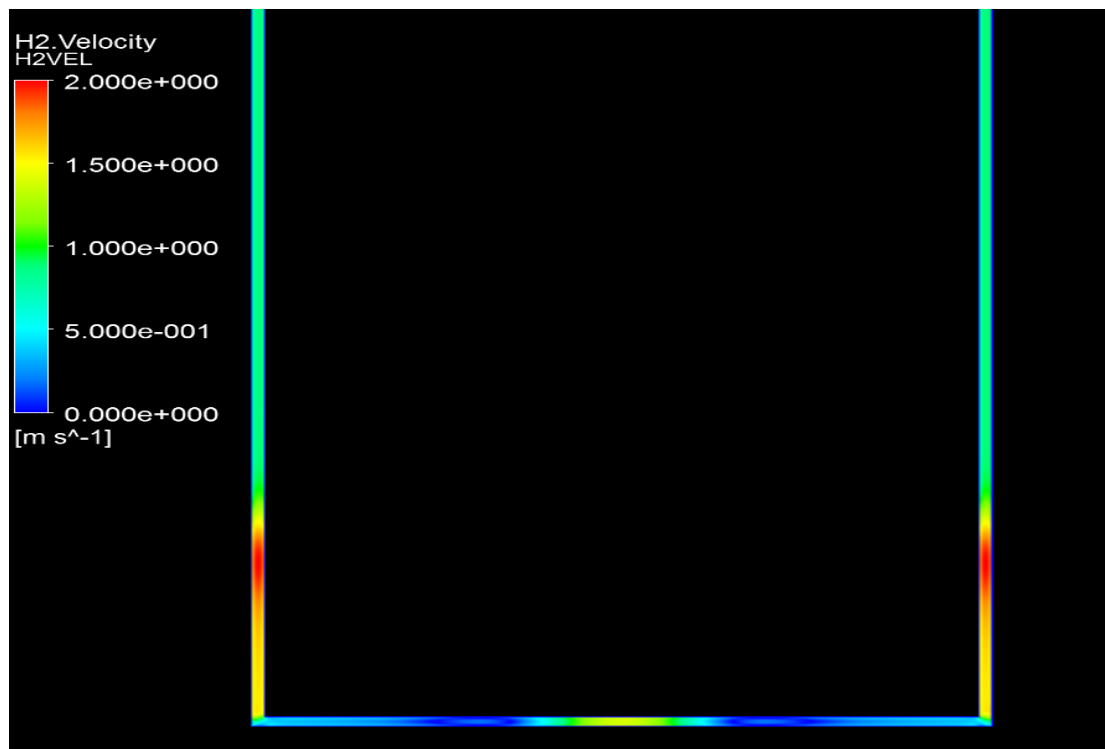
- Koch, M., Evans, A. and Brunnschweiler, A. (2000). Microfluidic technology and applications. Philadelphia, PA: Research Studies Press.
- Liaw, S. Y. (2013). Unpublished, Investigation of the Flow Behavioral dynamics of Ammonia Component Gases in a Microreactor via CFD Approach. Undergraduate. Universiti Teknologi PETRONAS.
- Mengeaud, V., Josser & Girault, H. (2002). Mixing processes in a zigzag microchannel: finite element simulations and optical study. *Analytical Chemistry*, 74 (16), 4279--4286.
- Nguyen, N., & Wu, Z. (2005). Micromixers-a review. *Microengineering* 15, R1-R16.
- Rosli, M. (2012). Unpublished, CFD Modelling of the Micro-Mixing Process for the One-Step Magnetically Induced Urea Synthesis I.
- Wang, M., & Li, W. (2005). Gases Mixing in Microchannels using the direct simulation Monte Carlo Method. *ASME International Conference of Micro and Mini Channel* (pp. 13-15). Toronto: CA.
- Wong, S., Bryant, P., Ward, M., & Wharton, C. (2003). Investigation of mixing in a cross-shaped micromixer with static mixing elements for reaction kinetics studies. *Sens. Act. B* 95, 414-424.
- Wong, S., Ward, M., & Wharton, C. (2004). Micro T-mixer as a rapid mixing micromixer. *Sensors and Actuators B: Physical*, 359-379.
- Wu, Z., Nguyen, N.-T., & Huang, X. (2004). Non-linear diffusive mixing in microchannels: theory and experiments. *J. Micromech. Microeng.* 14, 604-11.
- Yamaguchi, Y., Takagi, F., Yamashita, K., Nakamura, H., Maeda, H., Sotowa, K., et al. (2004). 3D simulations and visualization of laminar flow in a microchannels with hair-pin curves. *AIChE J.* 50, 1530-1535.
- Yi, M., & Bau, H. (2003). The kinematics of bend-induced mixing in micro-conduits. *Int. J. heat. Fluid Flow* 24, 645-656.

APPENDIX I: Velocity Contours For Hydrogen Component

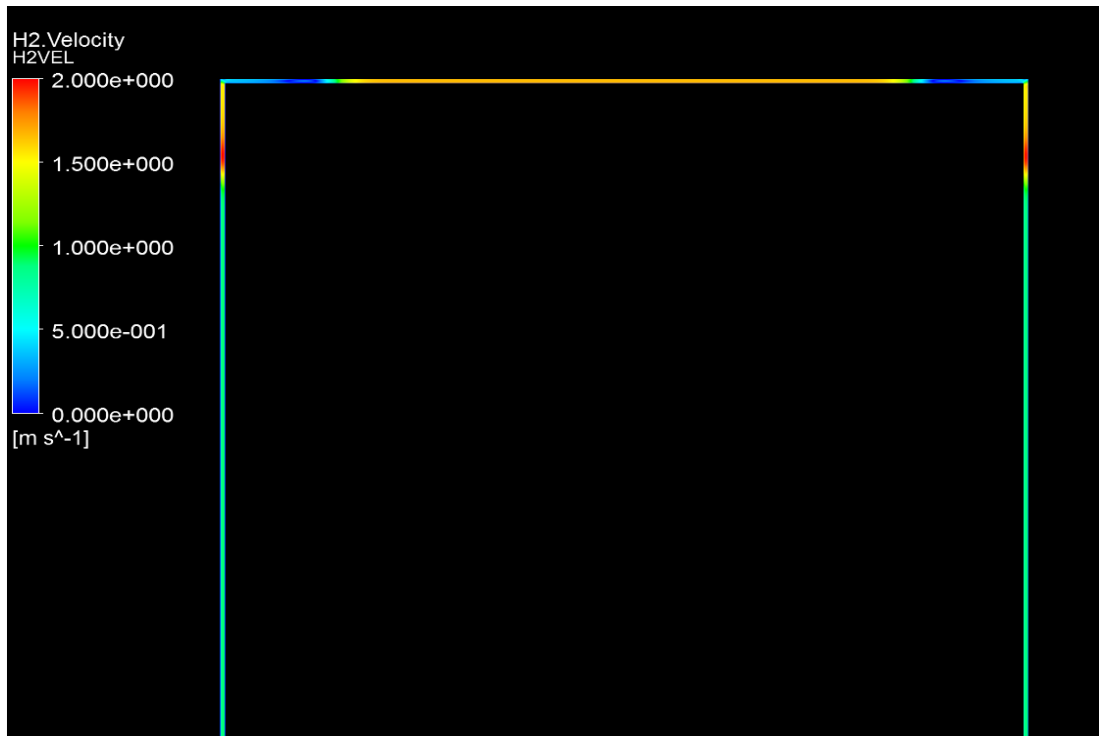
Model A at 1.67 m/s Inlet Velocity



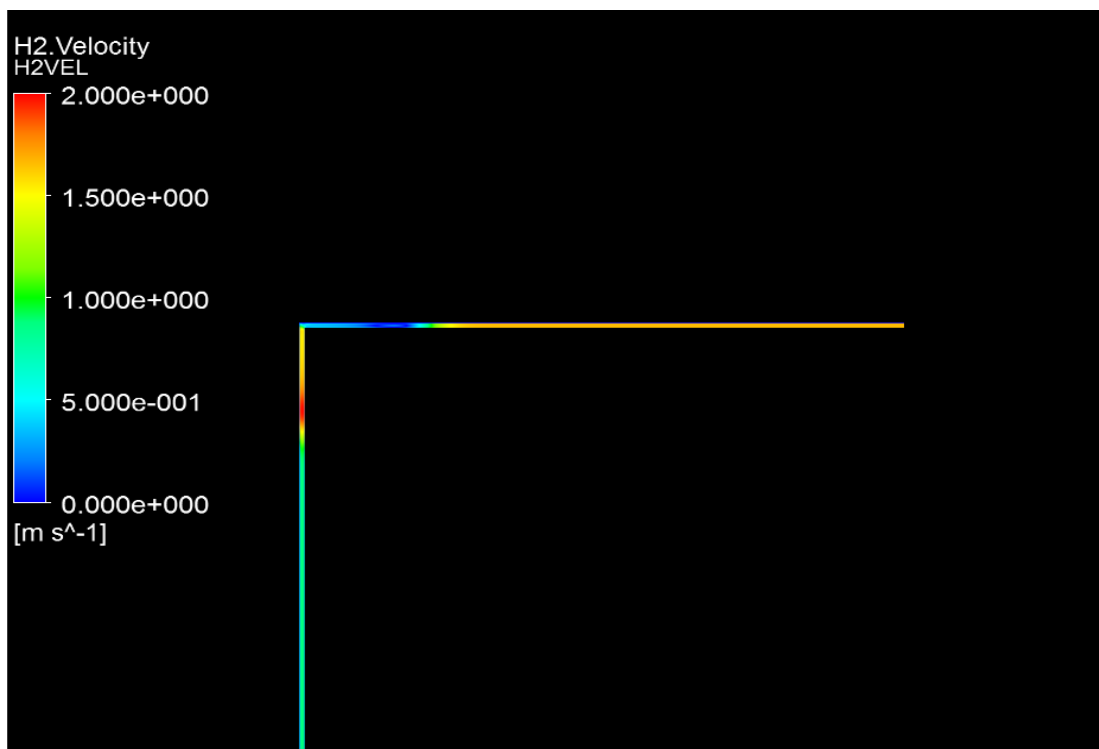
Appendice 1: Hydrogen velocity at Inlet



Appendice 2: Hydrogen Velocity at 1st Pitch

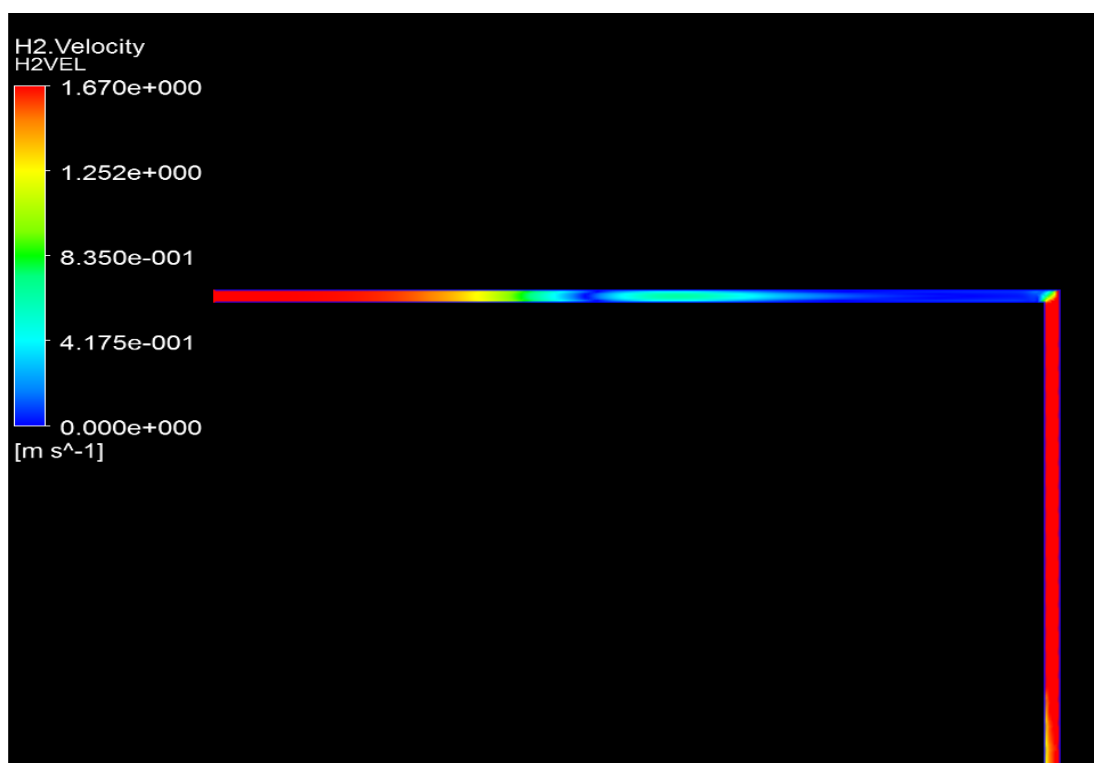


Appendice 3: Hydrogen Velocity at 2nd Pitch

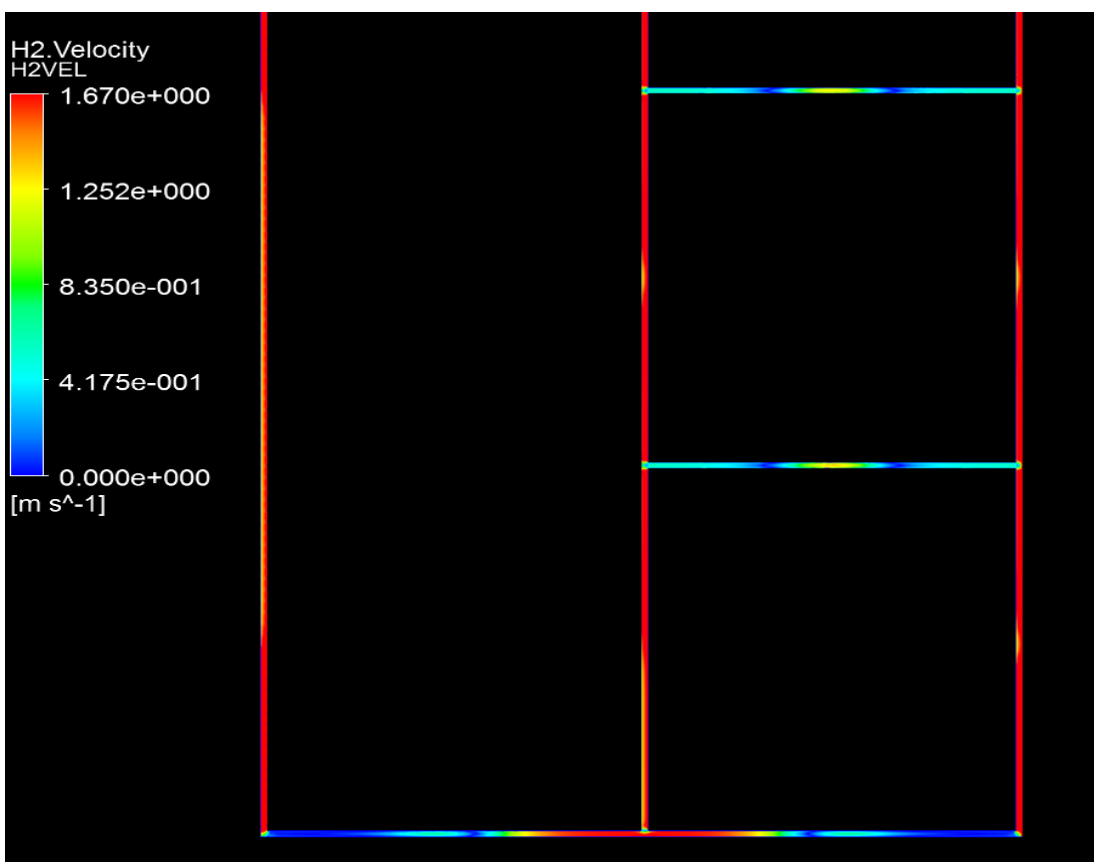


Appendice 4: Hydrogen Velocity at Outlet

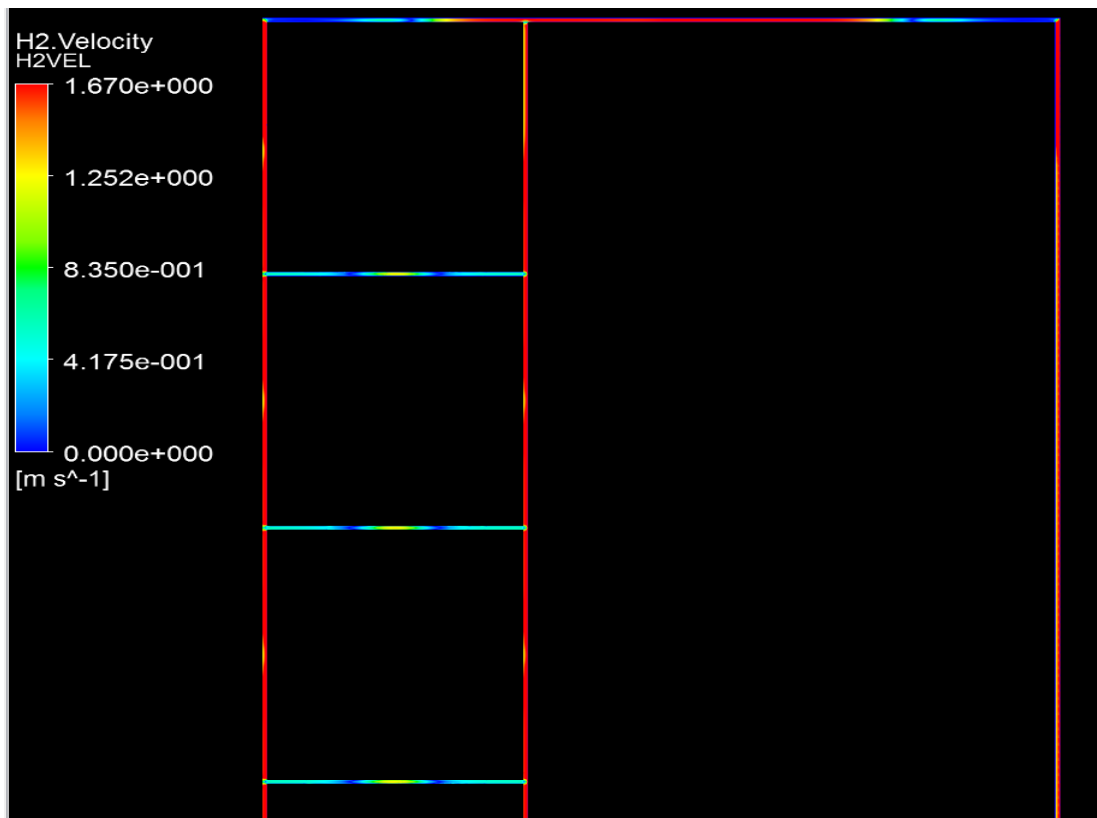
Model B at 1.67 m/s Inlet Velocity



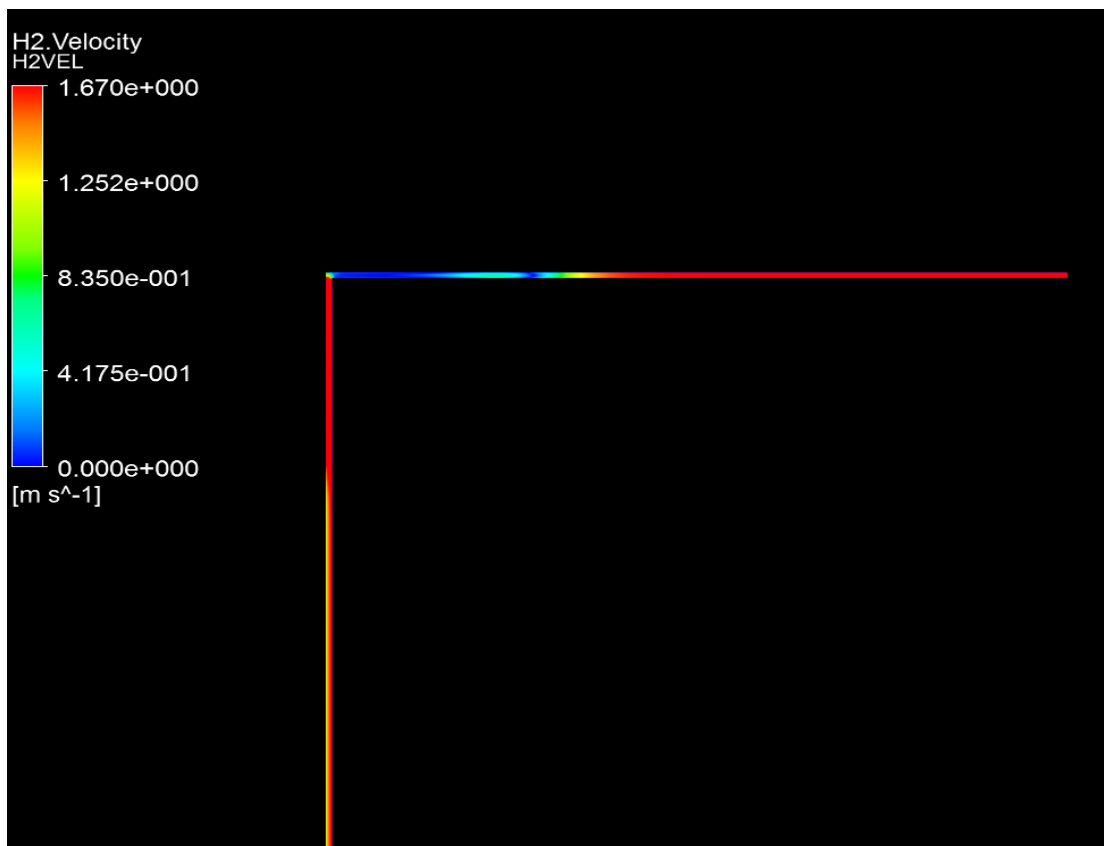
Appendice 5: Hydrogen Velocity at inlet



Appendice 6: Hydrogen velocity at 1st pitch

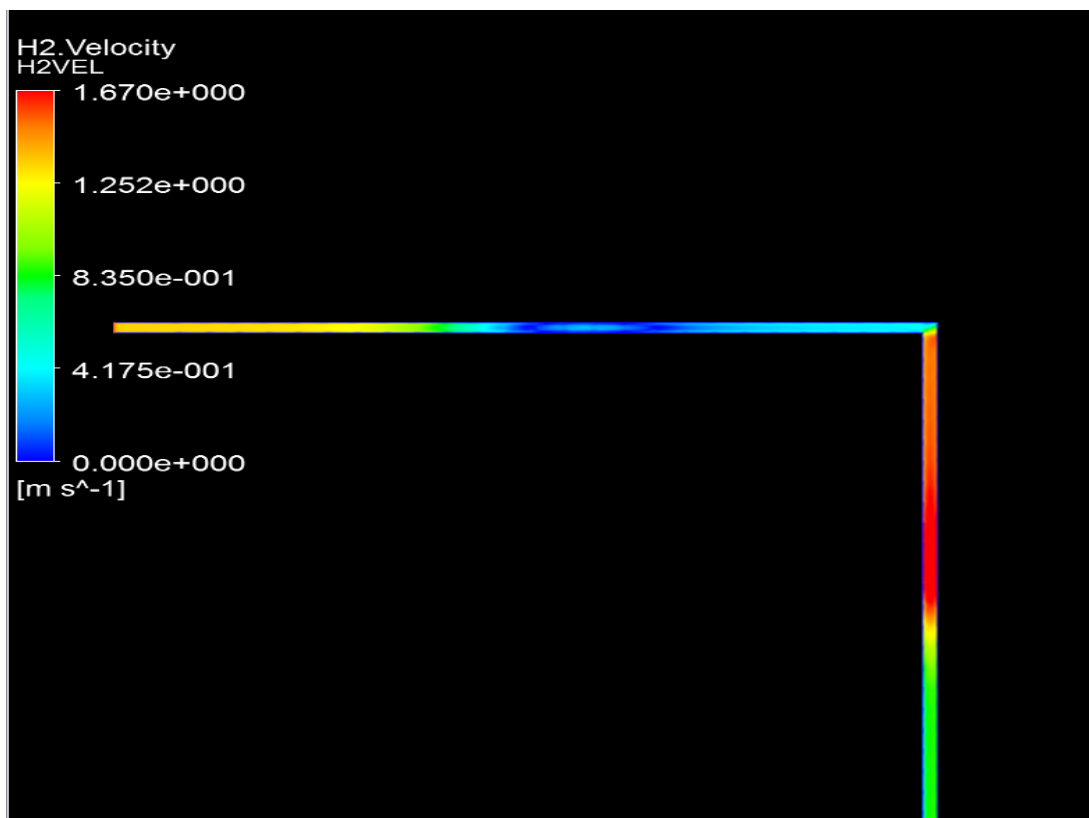


Appendice 7: Hydrogen velocity at 2nd pitch

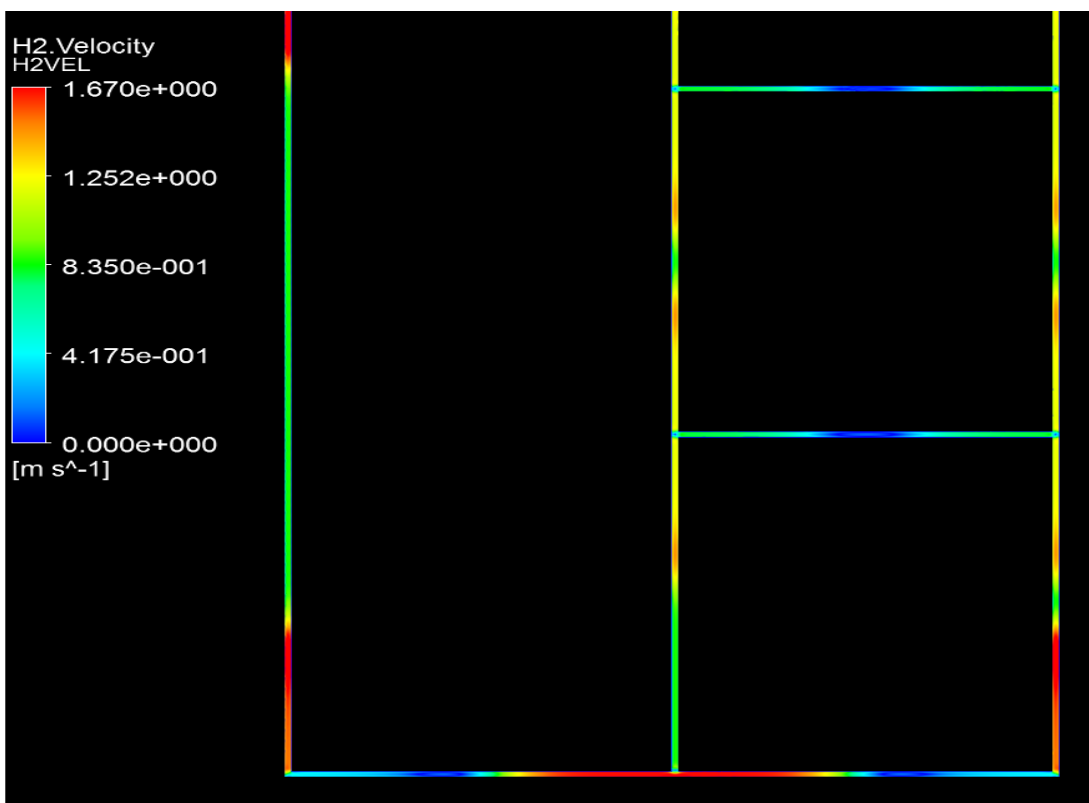


Appendice 8 : Hydrogen velocity at Outlet

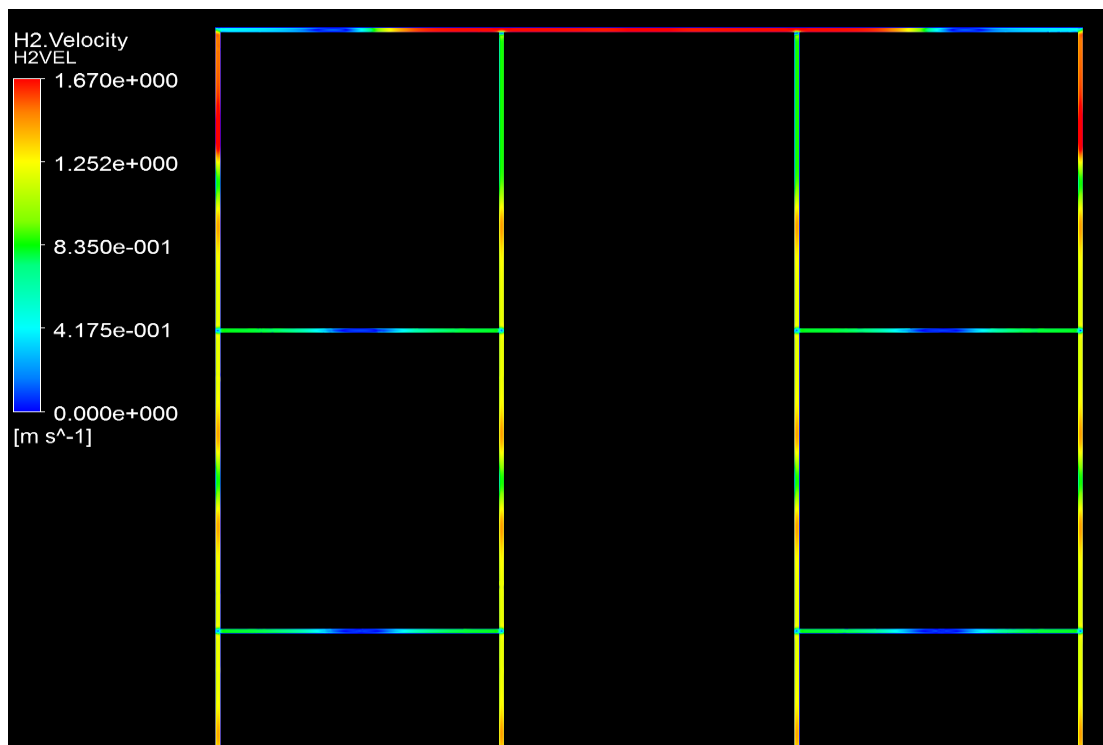
Model C at 1.67 m/s Inlet Velocity



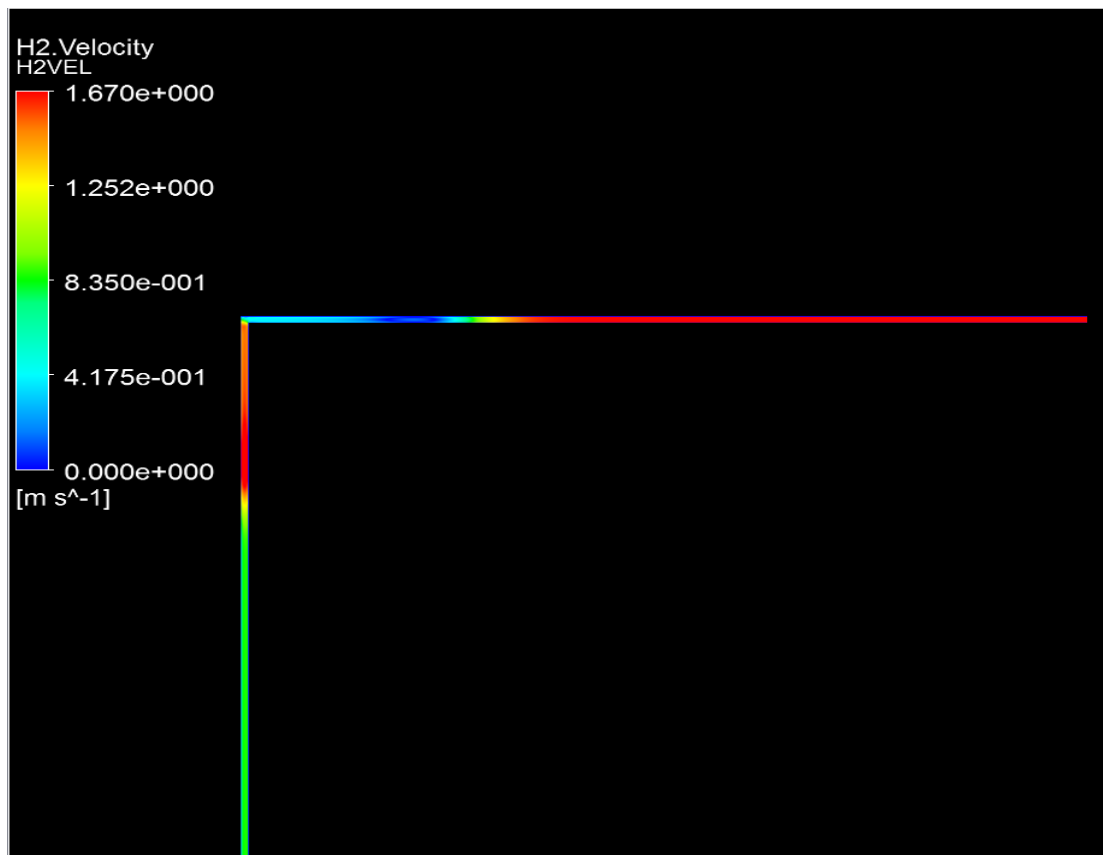
Appendice 9": Hydrogen velocity at Inlet



Appendice 10: Hydrogen velocity at 1st pitch

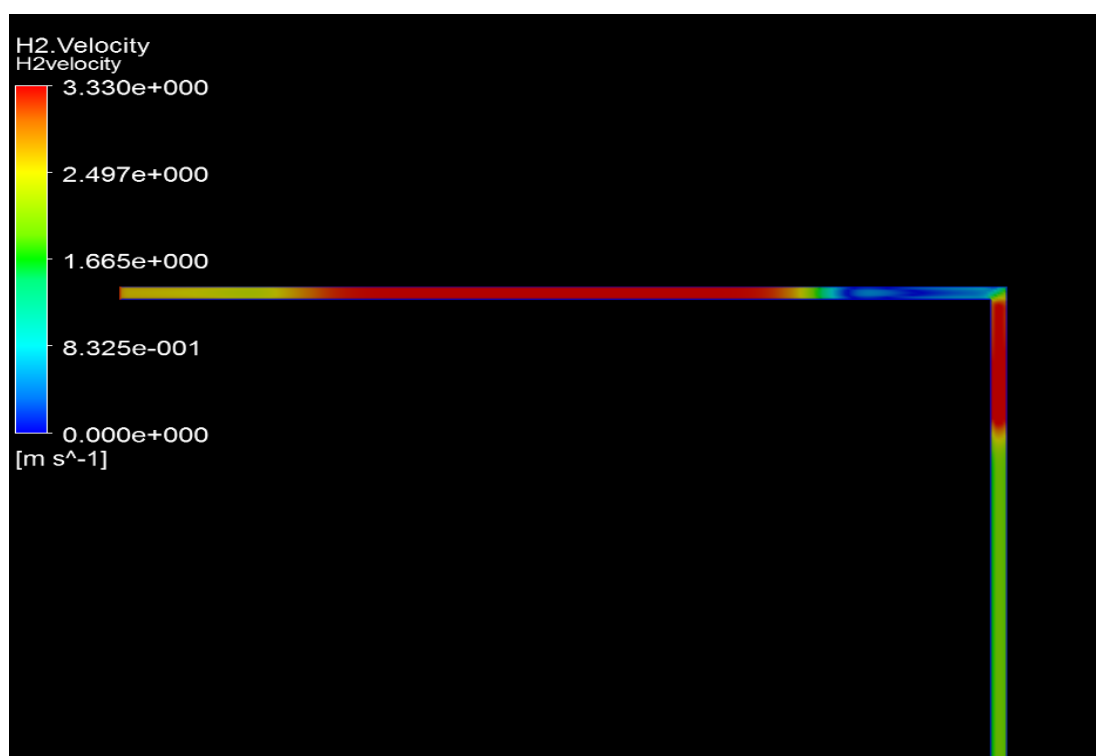


Appendice 11: Hydrogen velocity at 2nd pitch

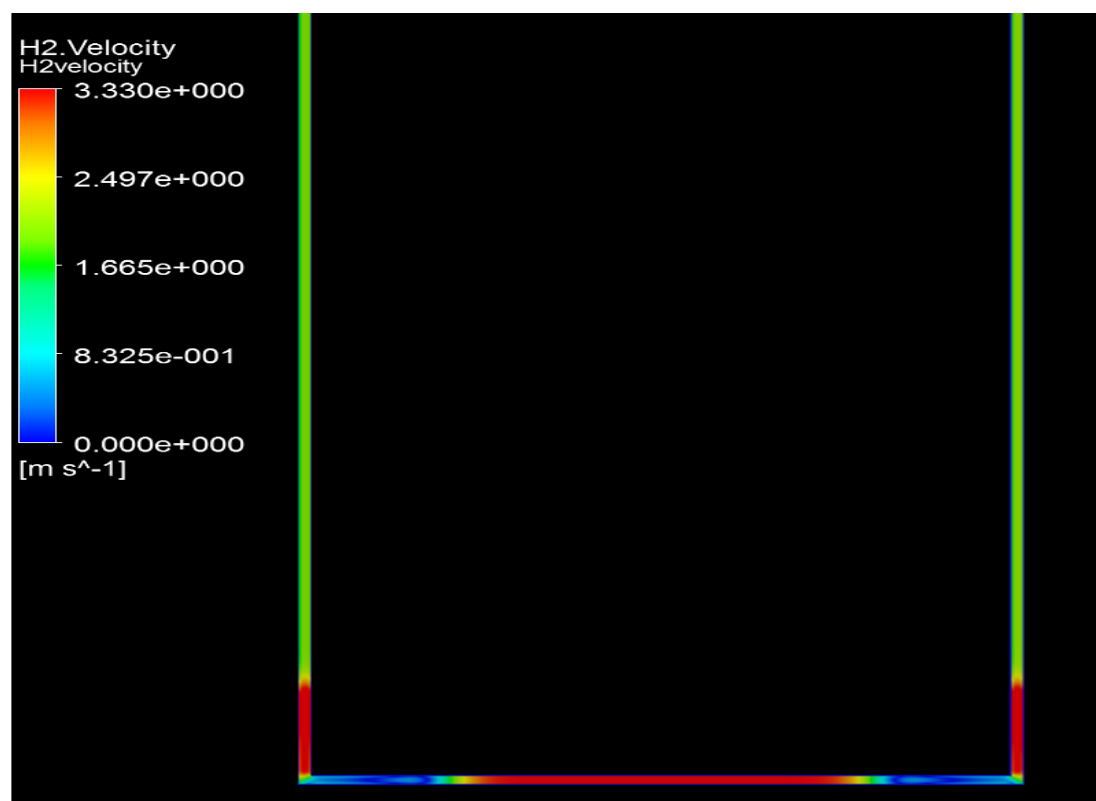


Appendice 12: Hydrogen velocity at Outlet

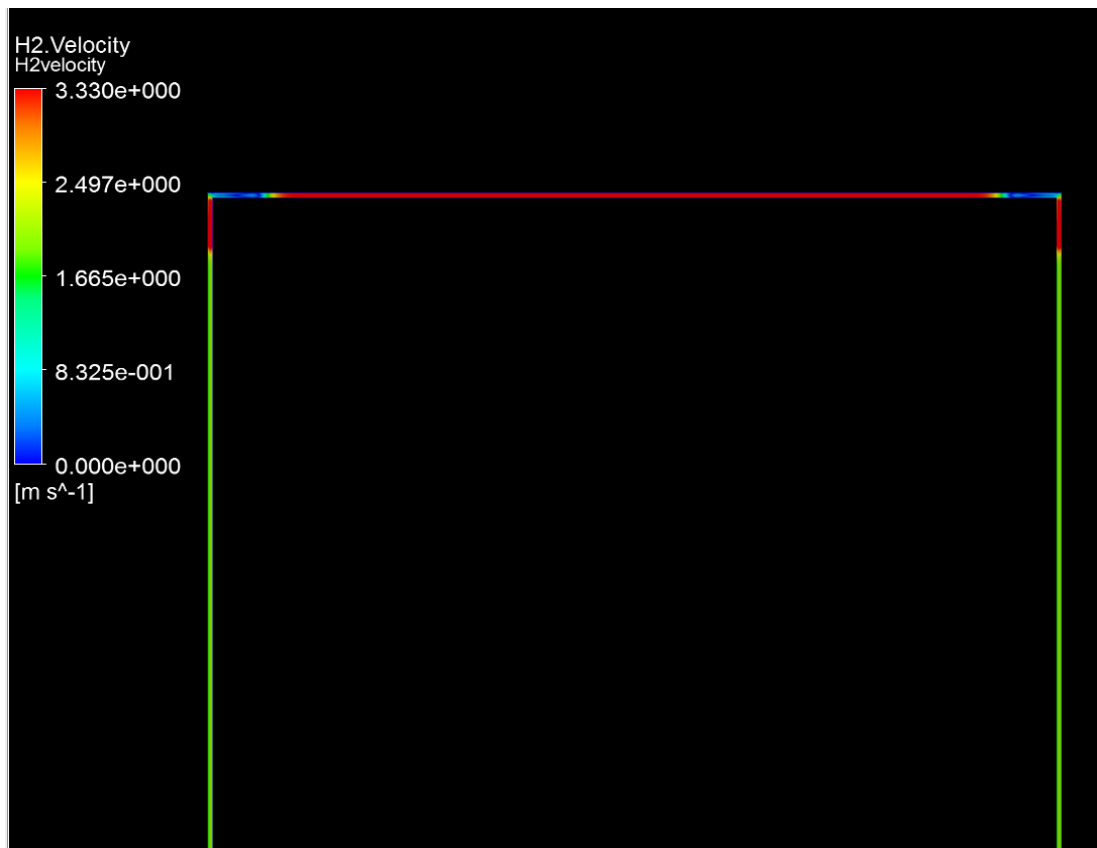
Model A at 3.33 m/s Inlet Velocity



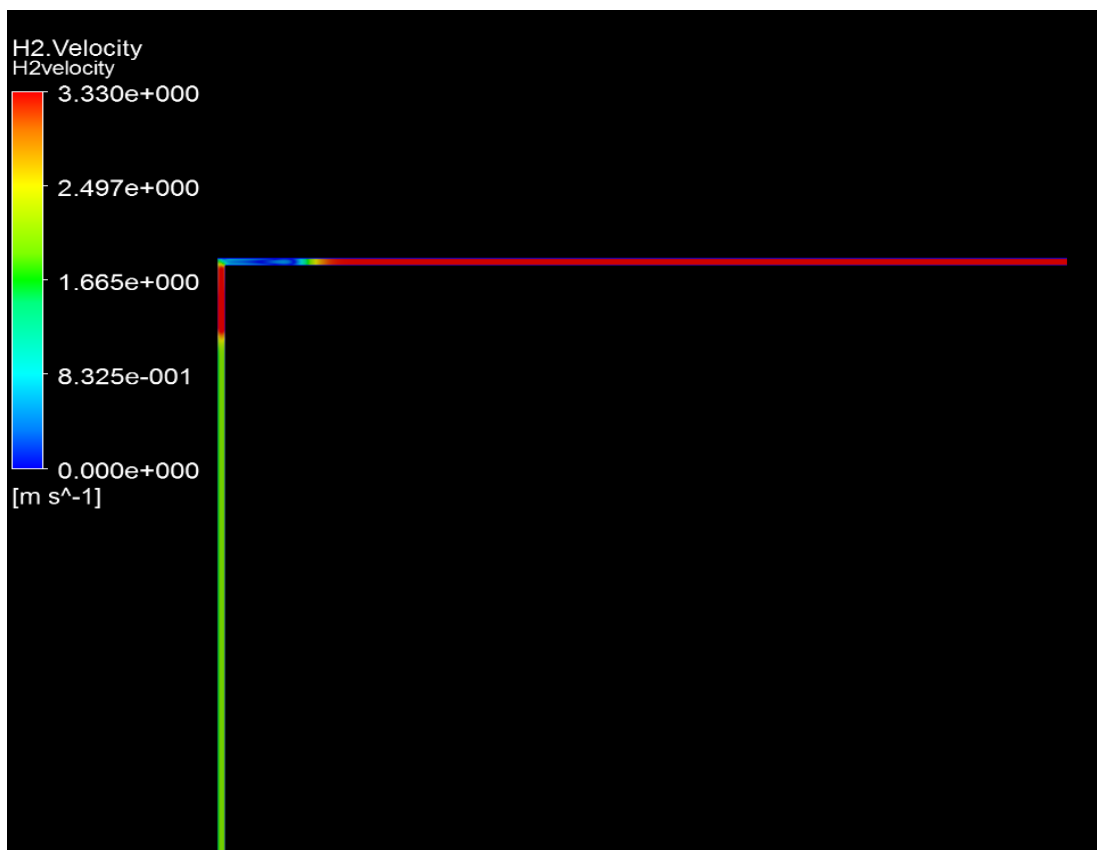
Appendice 13: Hydrogen velocity at inlet



Appendice 14: Hydrogen velocity at 1st pitch

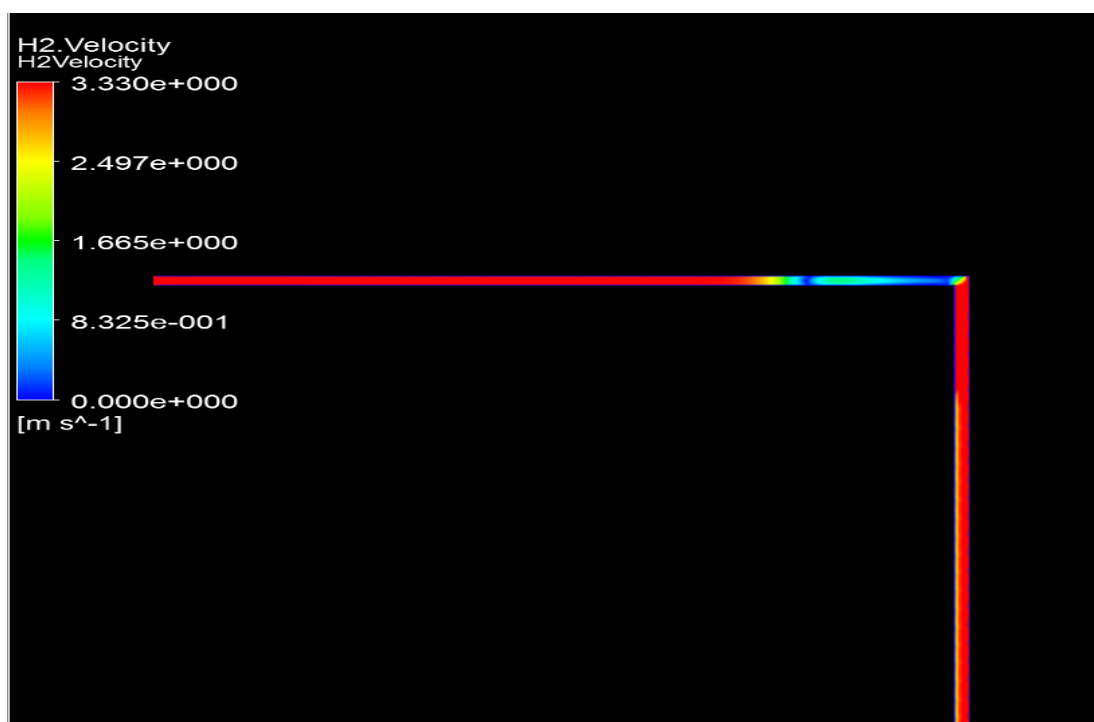


Appendice 15: Hydrogen velocity at 2nd pitch

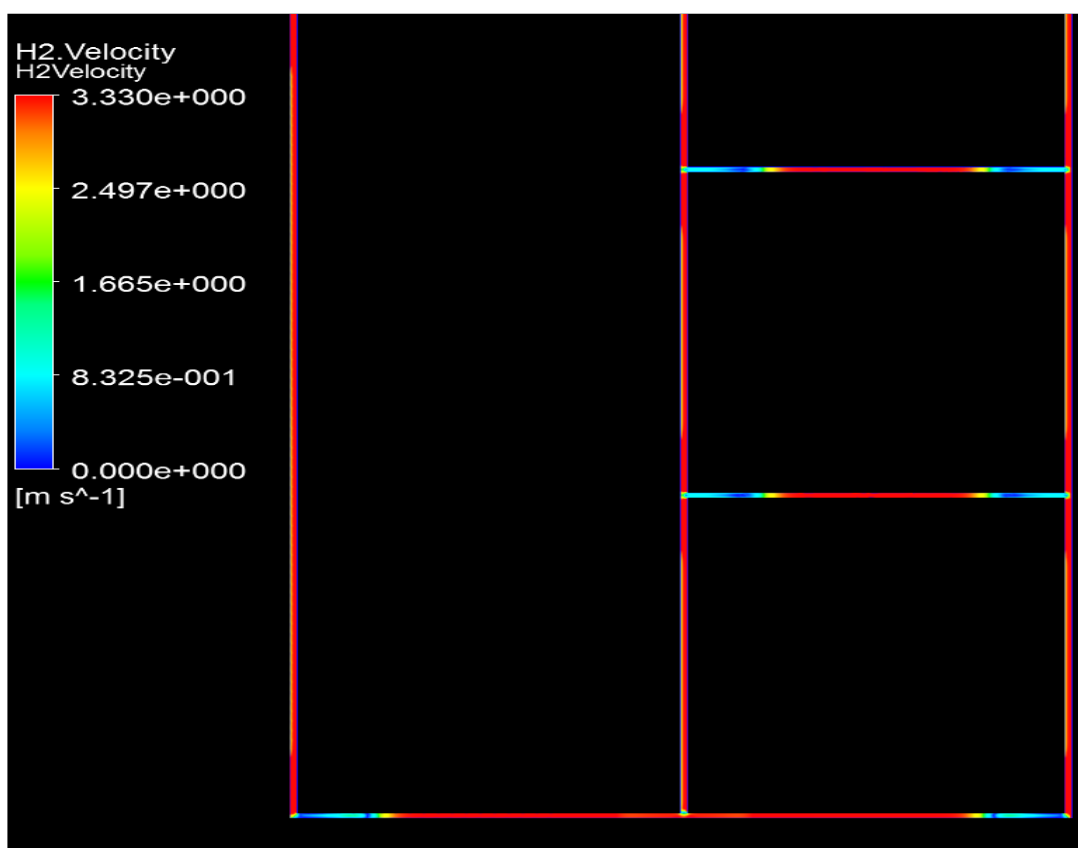


Appendice 16: Hydrogen velocity at Outlet

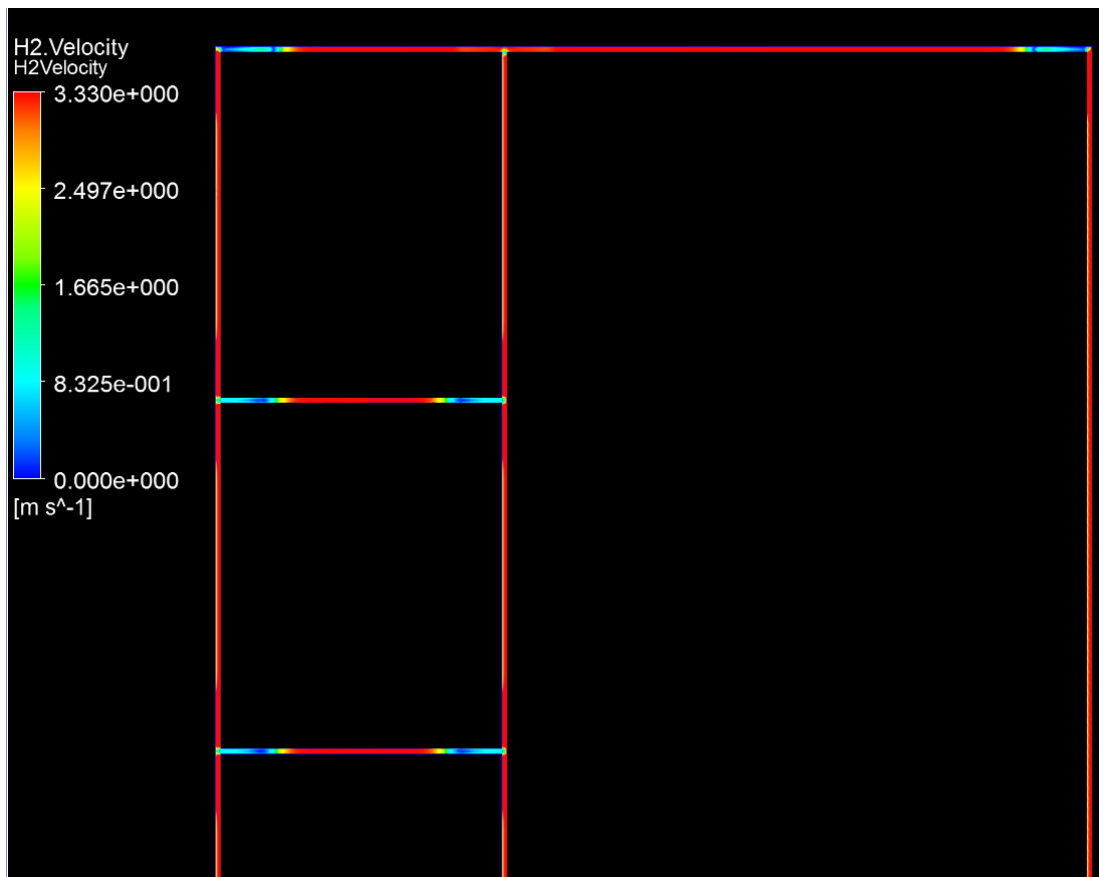
Model B at 3.33 m/s Inlet Velocity



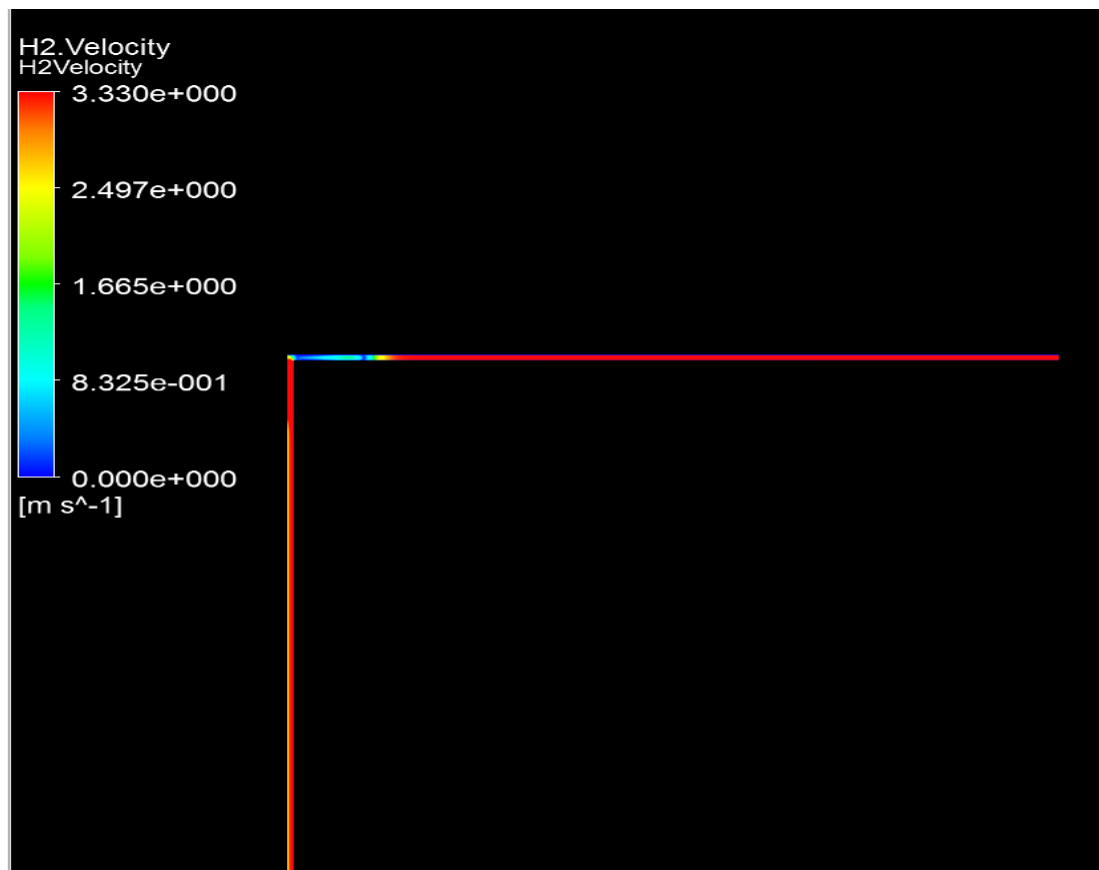
Appendice 17: Hydrogen velocity at Inlet



Appendice 18: Hydrogen velocity at 1st pitch

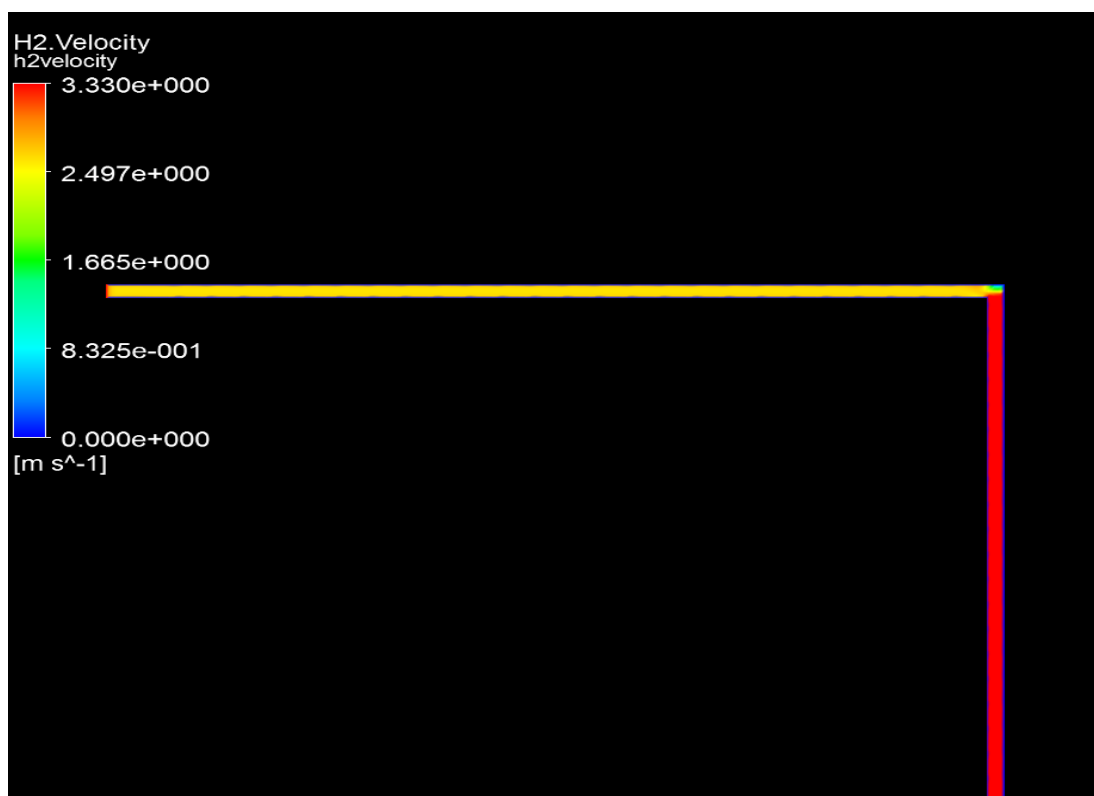


Appendice 19: Hydrogen velocity at 2nd Pitch

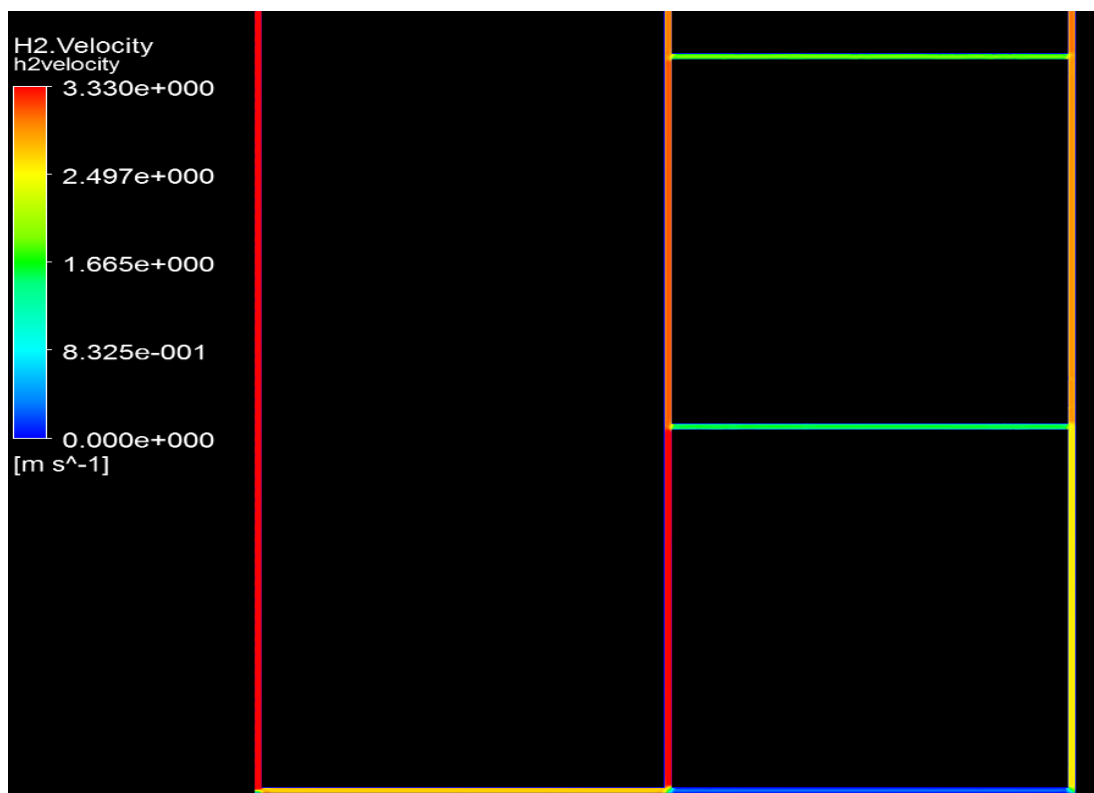


Appendice 20: Hydrogen velocity at Outlet

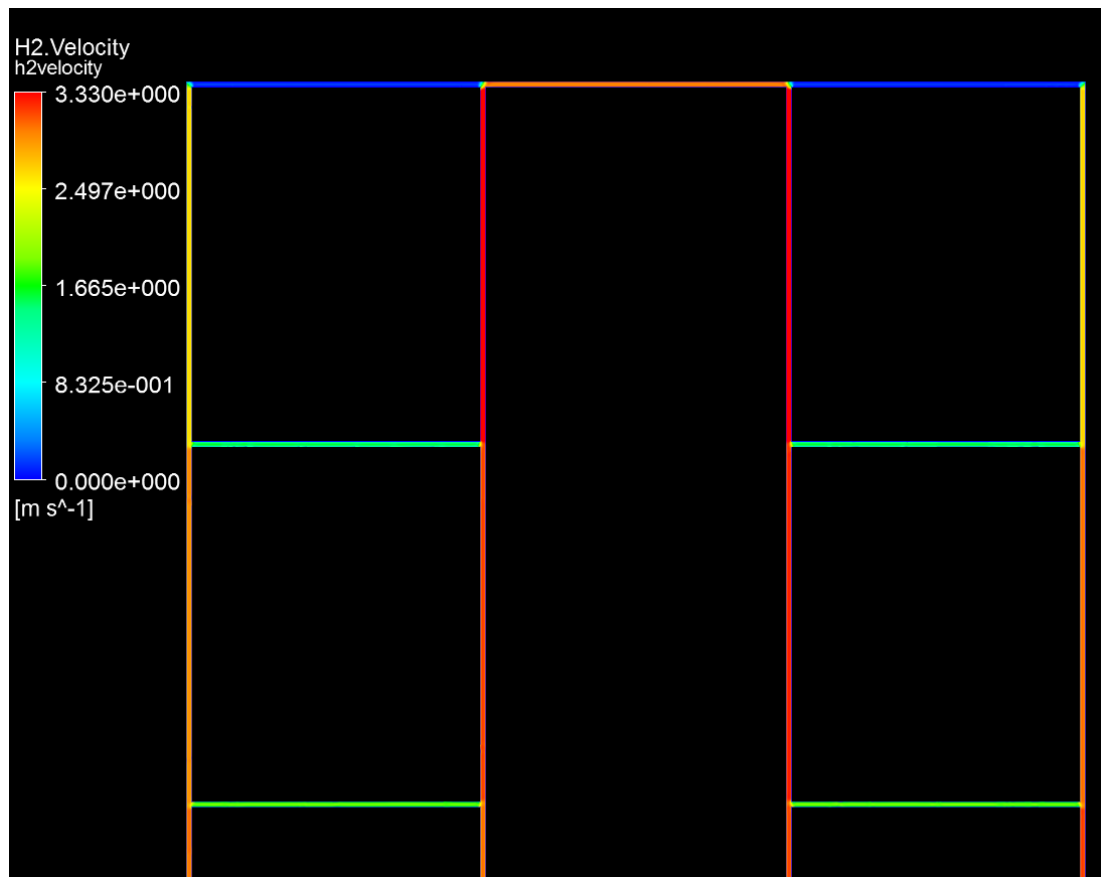
Model C at 3.33 m/s Inlet Velocity



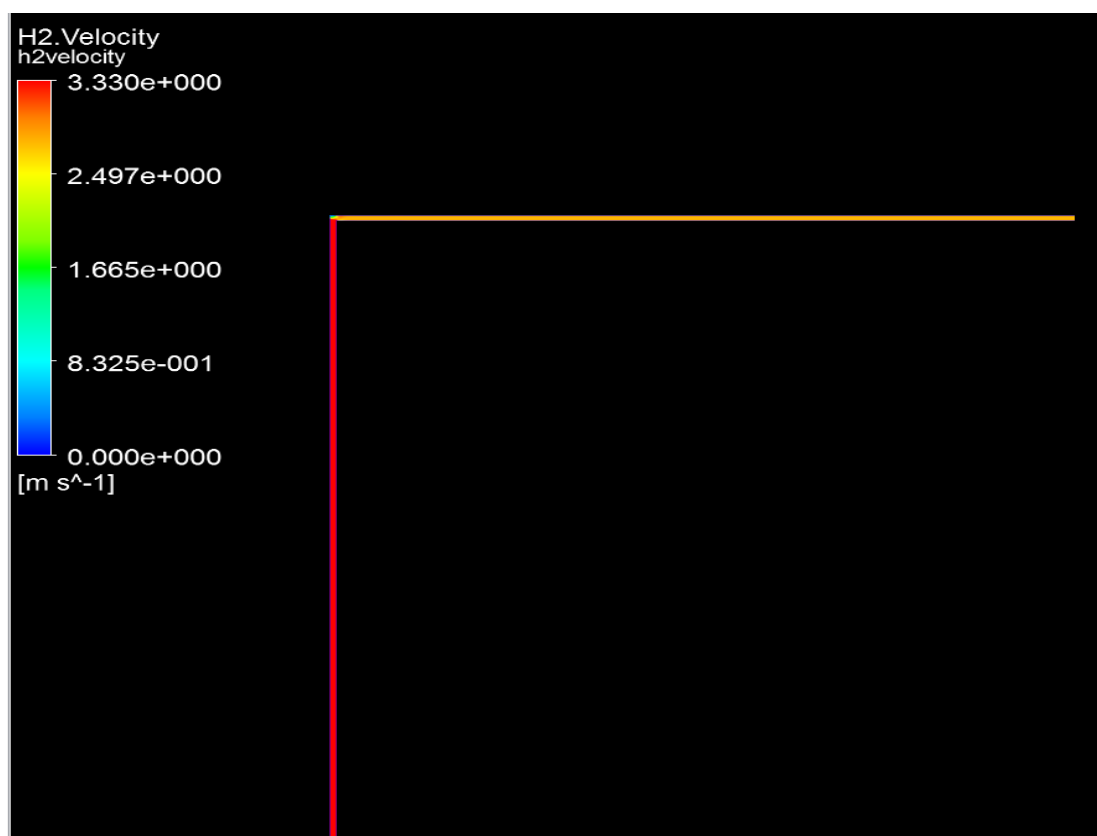
Appendice 21: Hydrogen velocity at Inlet



Appendice 22: Hydrogen velocity at 1st pitch

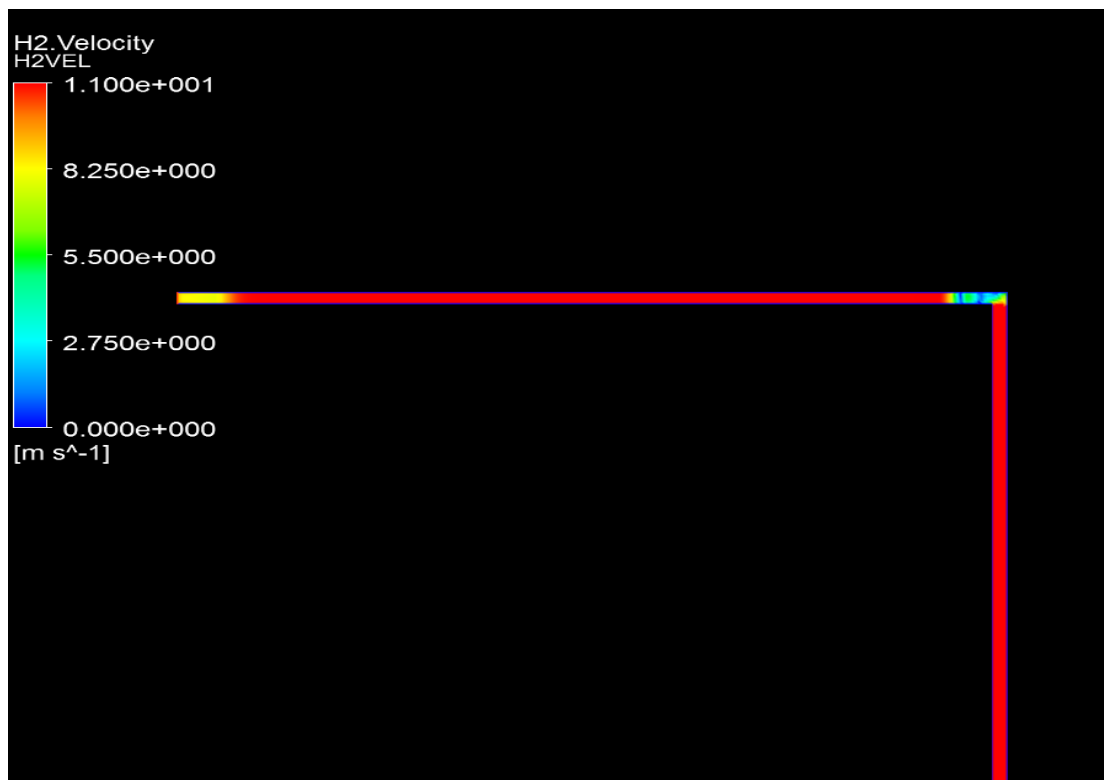


Appendice 23: Hydrogen velocity at 2nd pitch

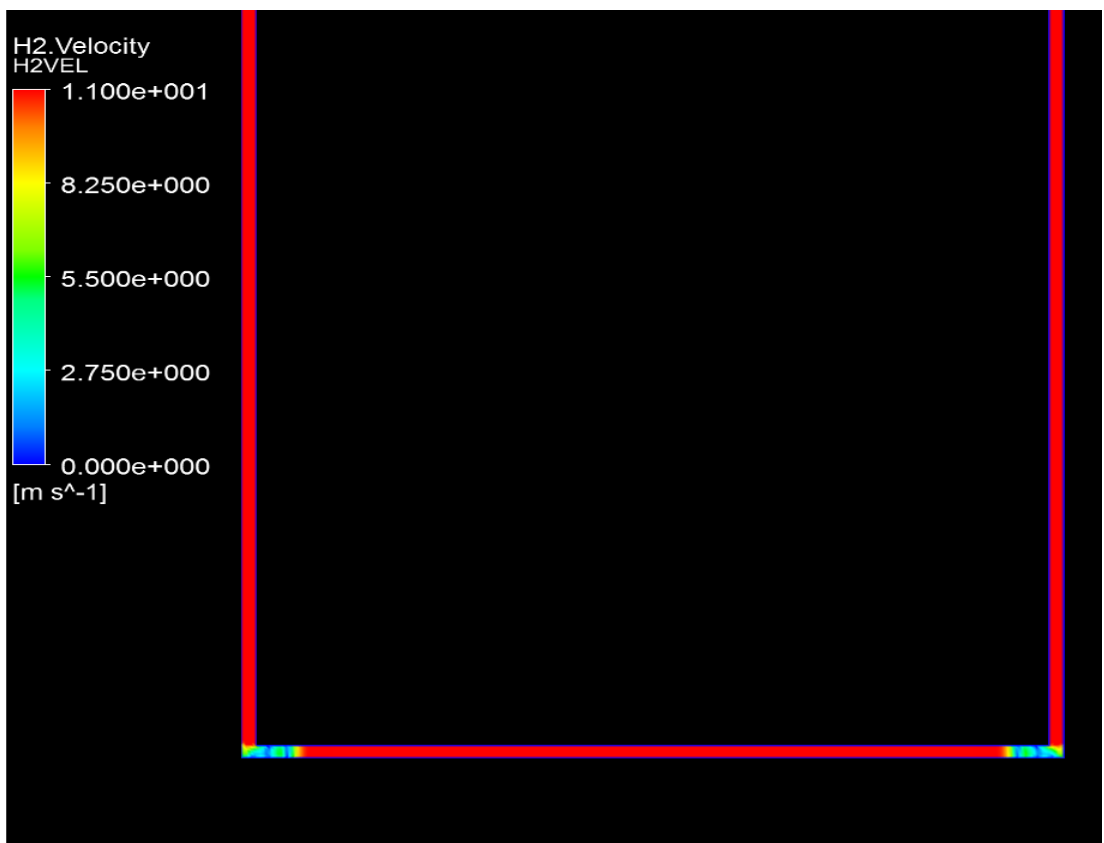


Appendice 24: Hydrogen velocity at 2nd pitch

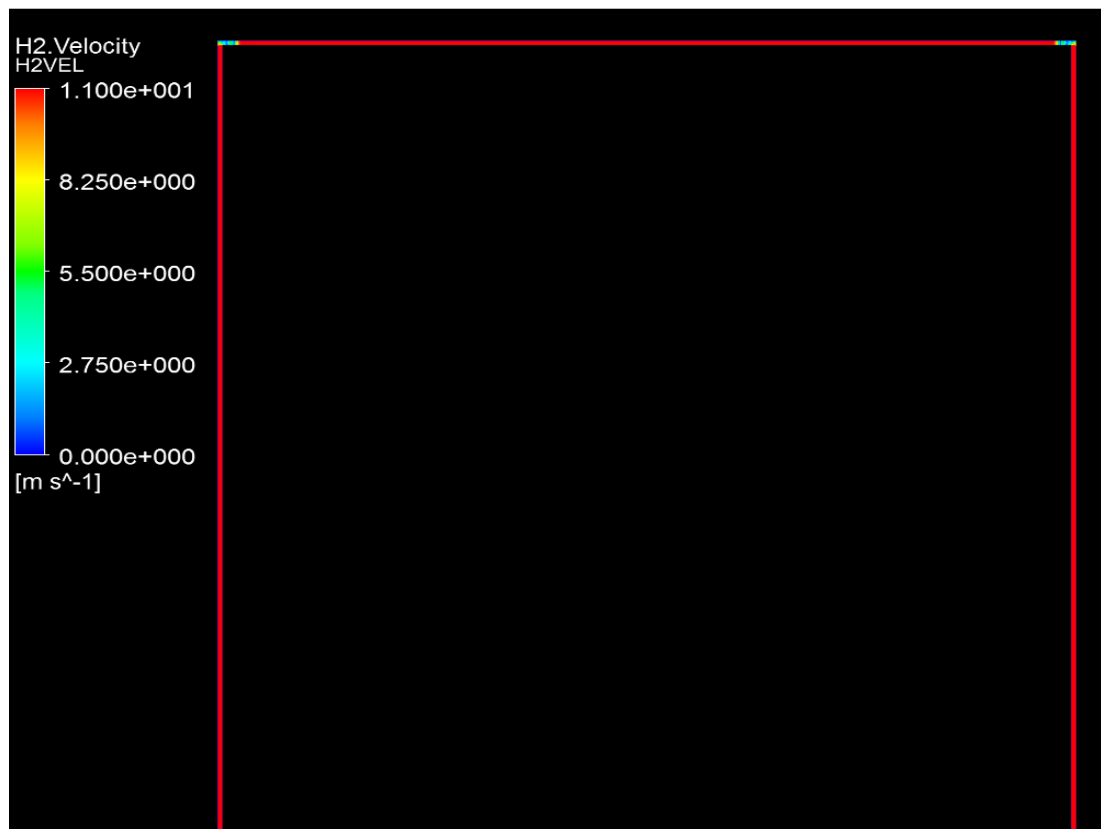
Model A at 10.99 m/s Inlet Velocity



Appendice 25: Hydrogen velocity at Inlet



Appendice 26: Hydrogen velocity at 1st pitch

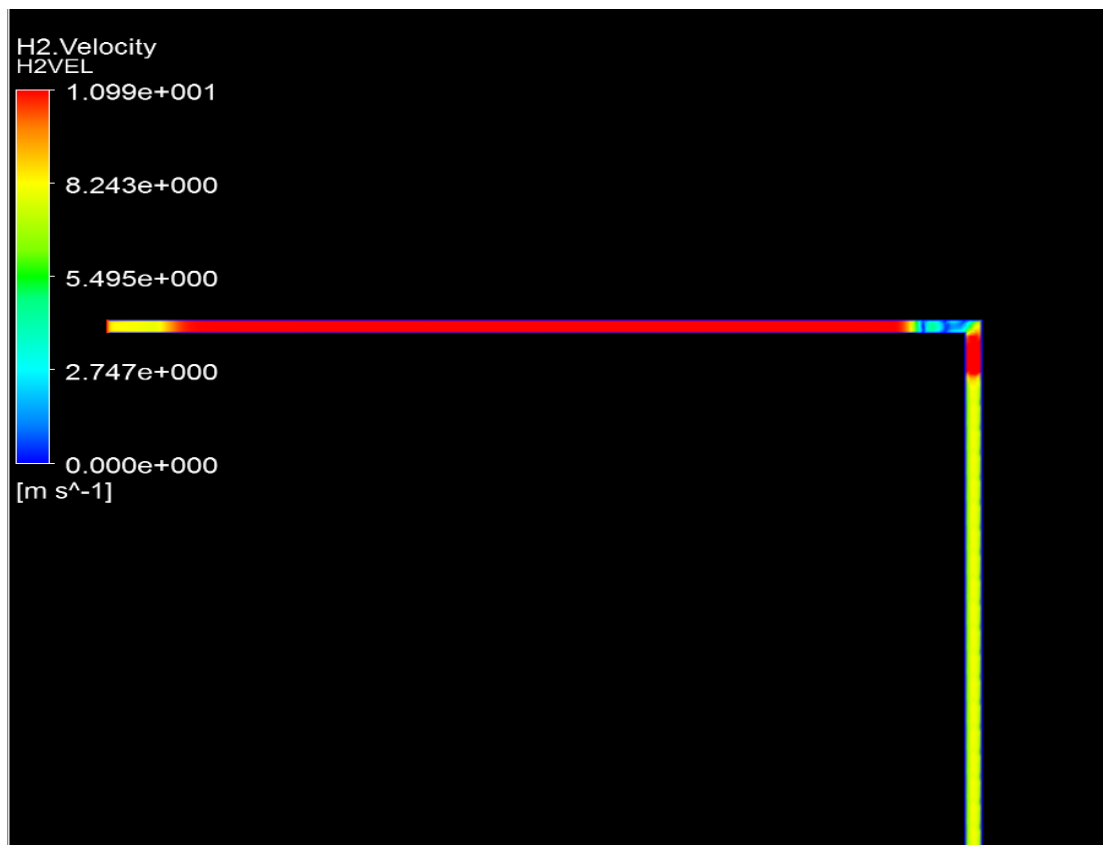


Appendice 27: Hydrogen velocity at 2nd pitch

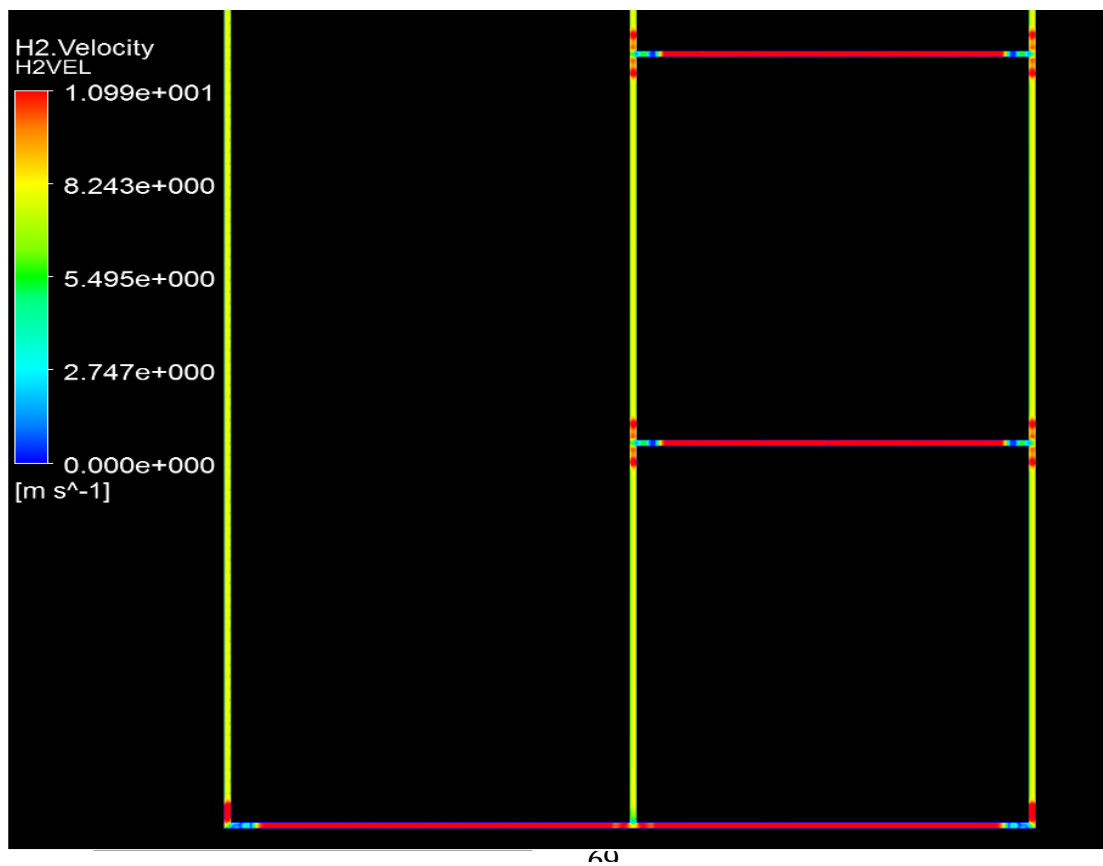


Appendice 28: Hydrogen velocity at Outlet

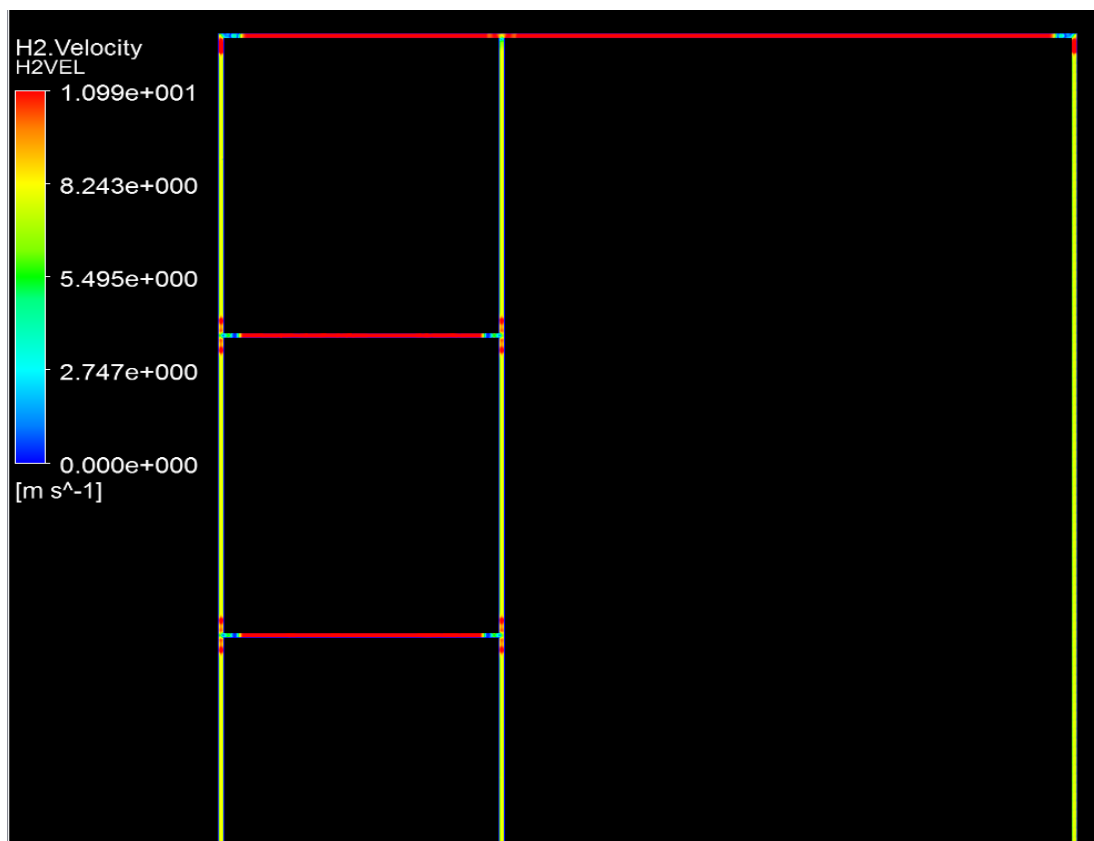
Model B at 10.99 m/s Inlet Velocity



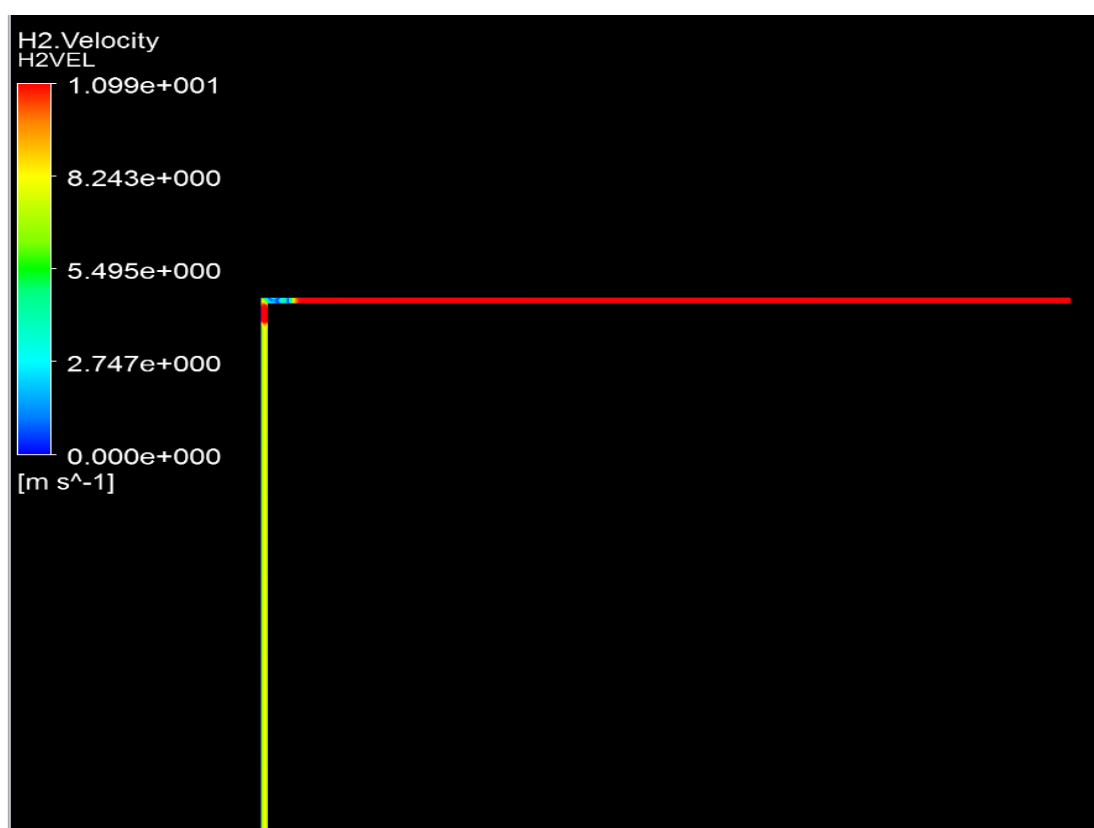
Appendice 29: Hydrogen velocity at inlet



Appendice 30: Hydrogen velocity at 1st pitch

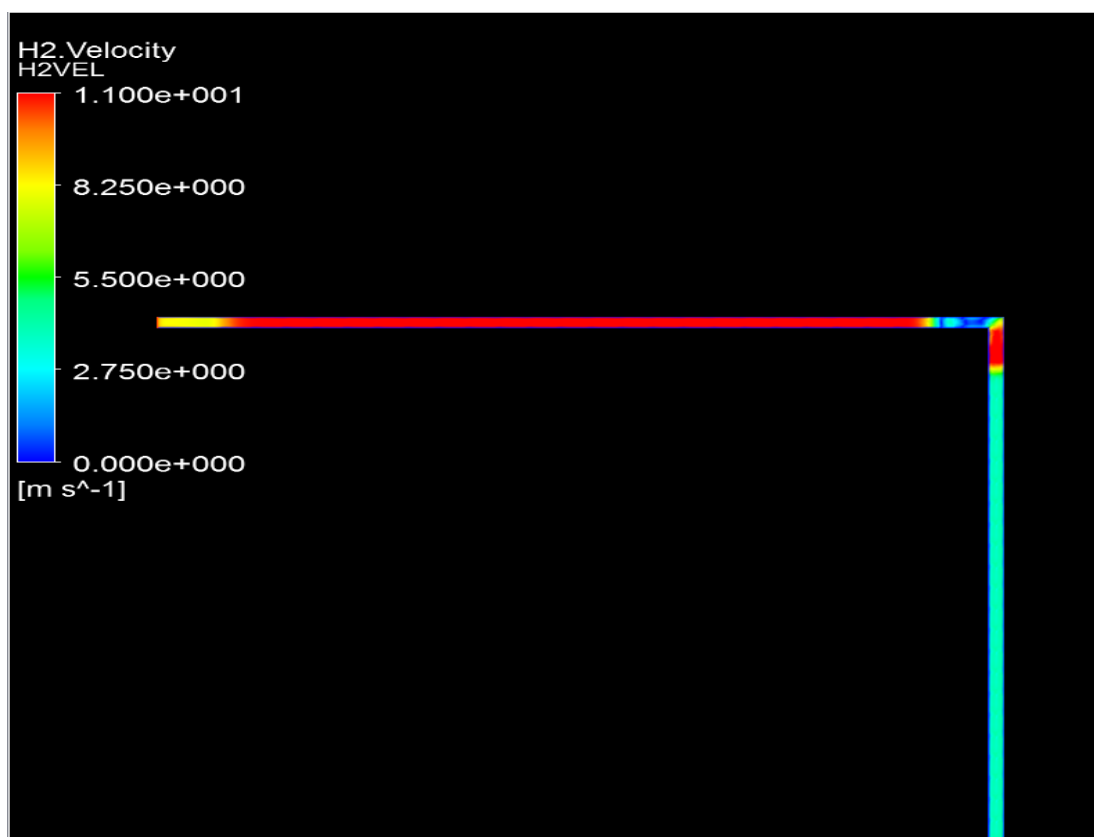


Appendice 31: Hydrogen velocity at 2nd pitch

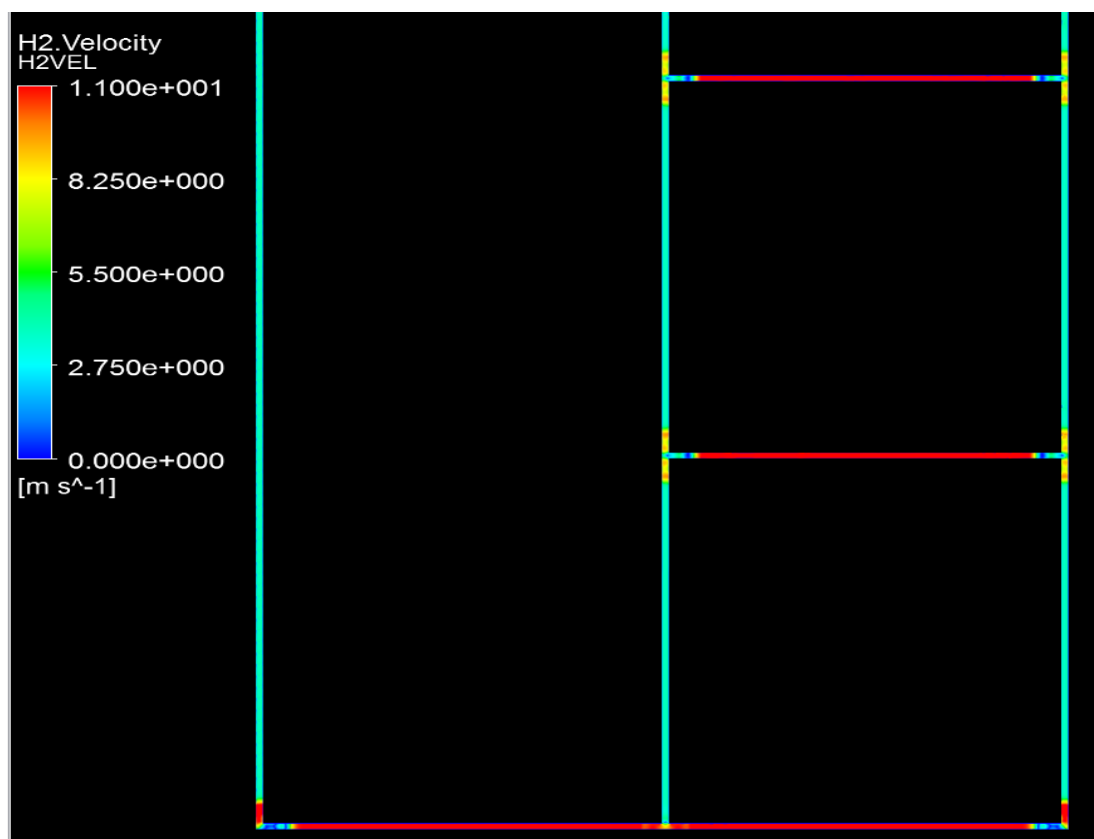


Appendice 32: Hydrogen velocity at Outlet

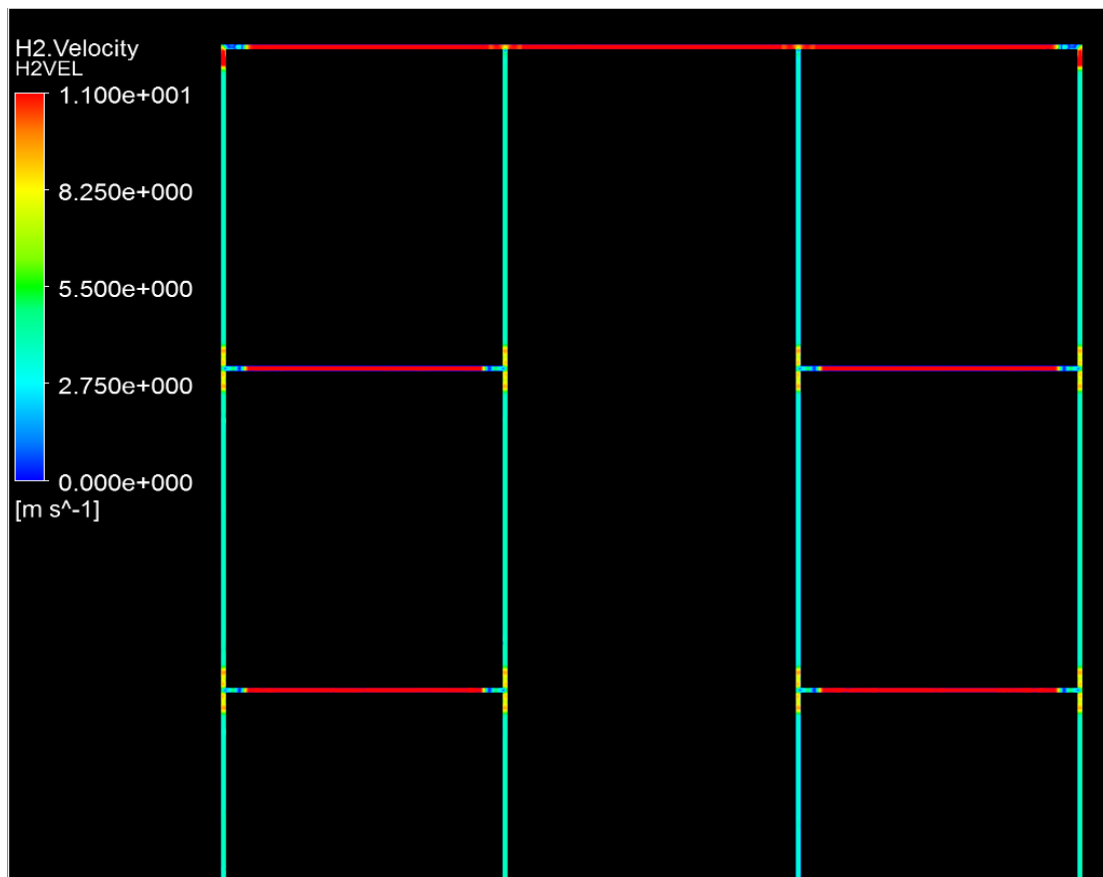
Model C at 10.99 m/s Inlet Velocity



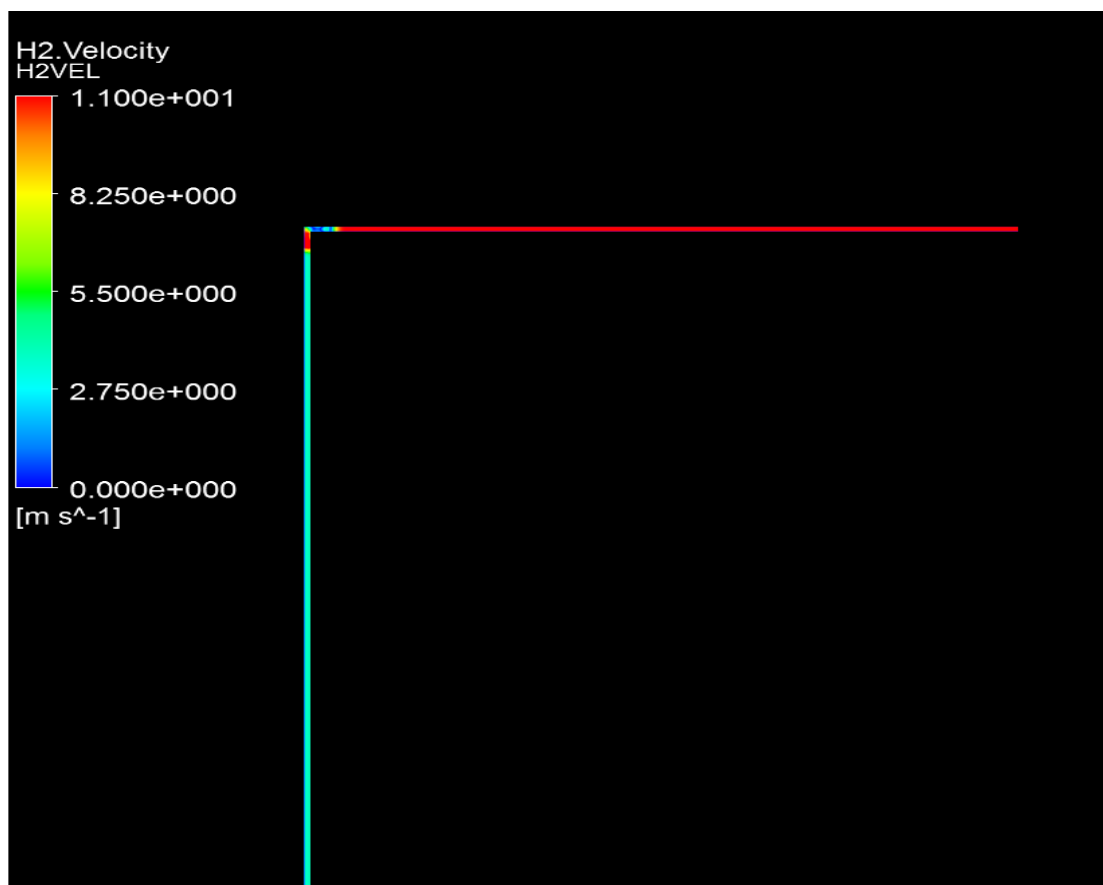
Appendice 33: Hydrogen velocity at inlet



Appendice 34: Hydrogen velocity at 1st pitch



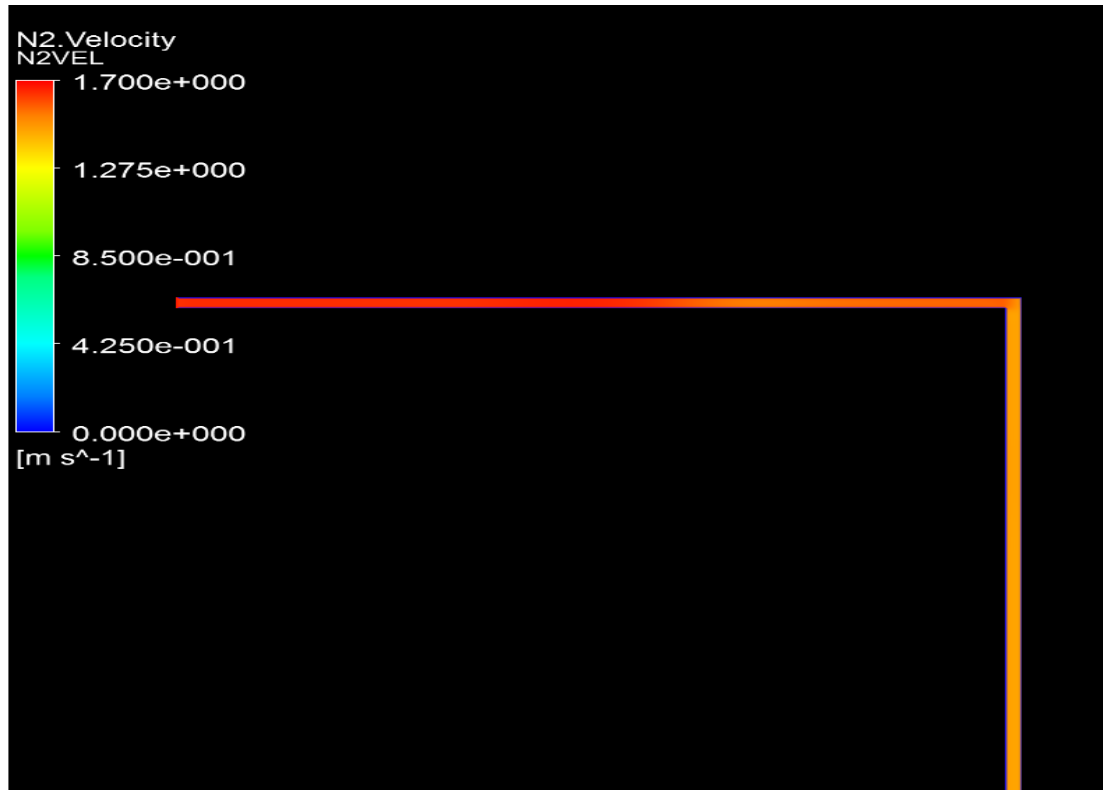
Appendice 35: Hydrogen velocity at 2nd pitch



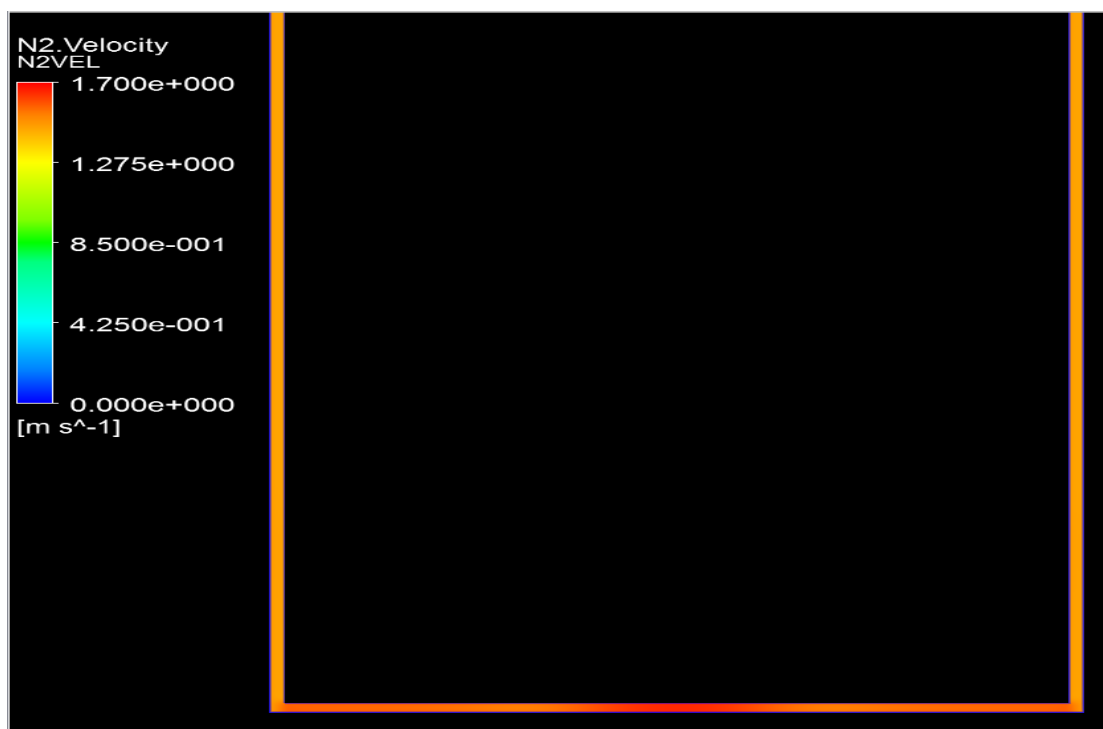
Appendice 36: Hydrogen velocity at outlet

APPENDIX II: Velocity Contours For Nitrogen Component

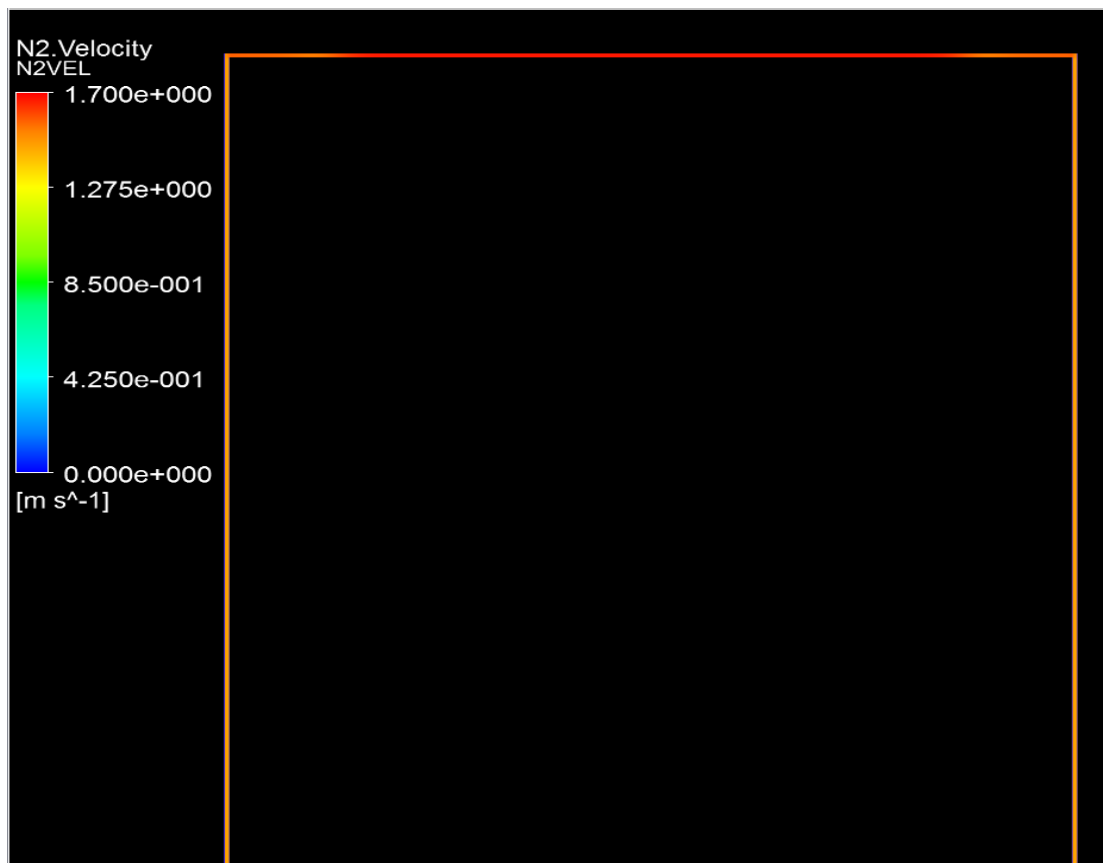
Model A at 1.67 m/s Inlet Velocity



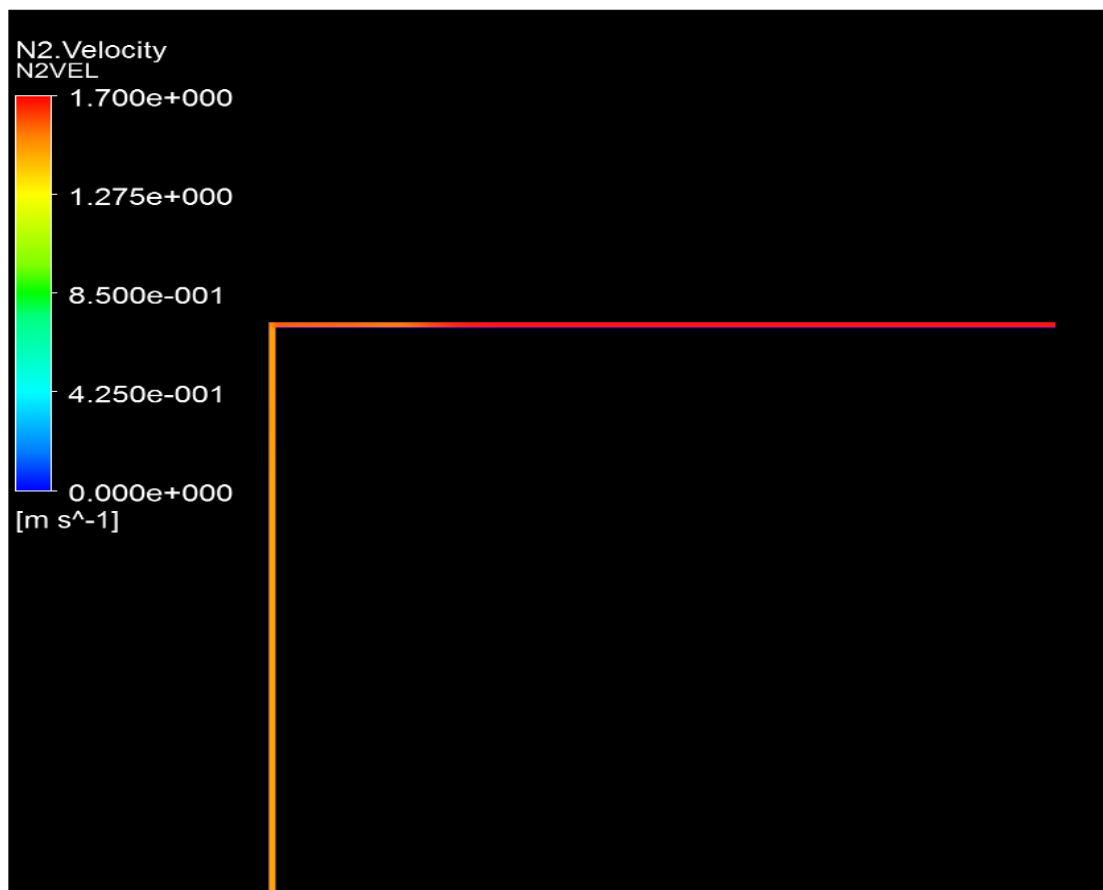
Appendice 37: Nitrogen velocity at inlet



Appendice 38: Nitrogen velocity at 1st Pitch

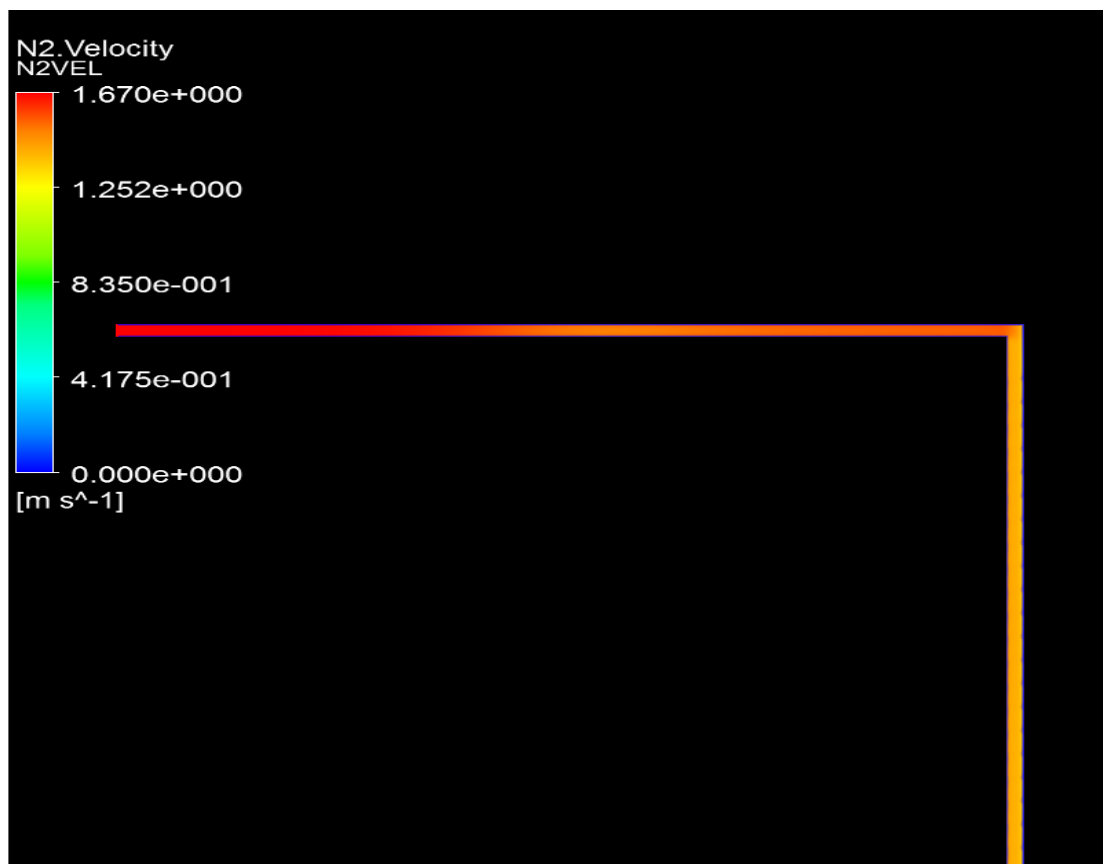


Appendice 39: Nitrogen velocity at 2nd pitch

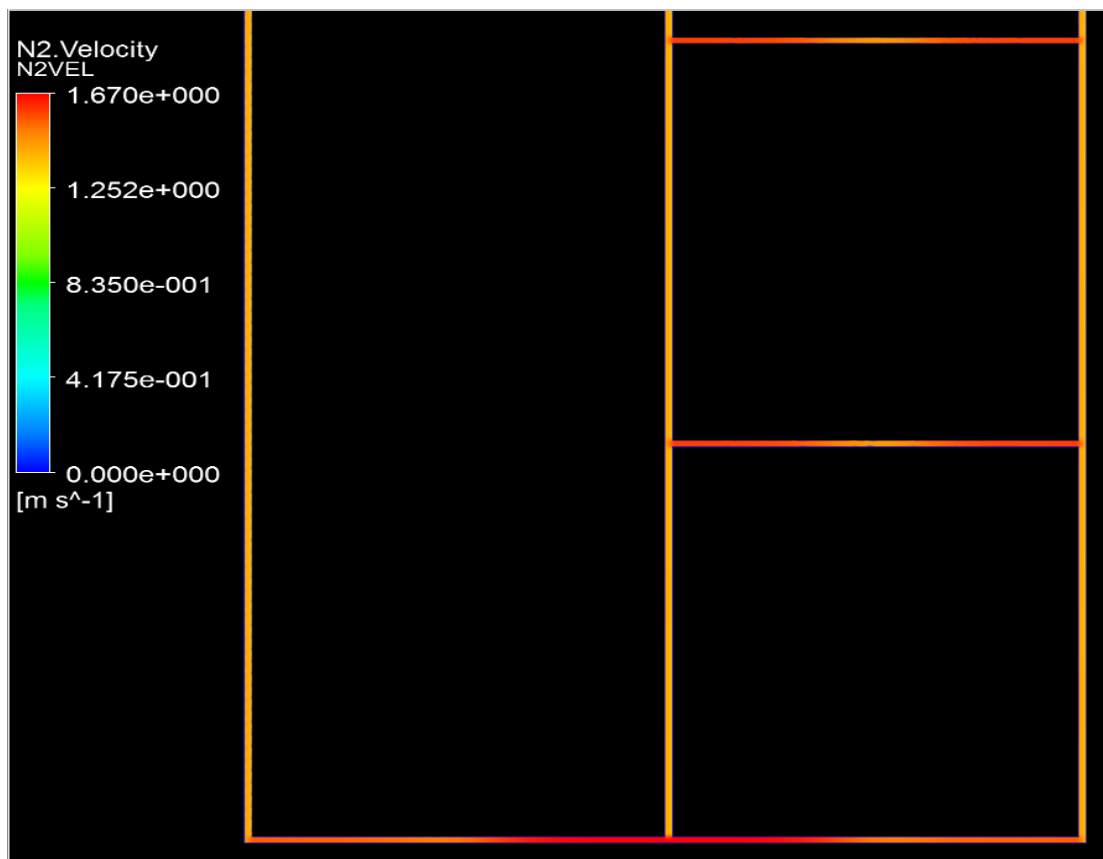


Appendice 40: Nitrogen velocity at outlet

Model B at 1.67 m/s Inlet Velocity



Appendice 41: Nitrogen velocity at inlet



Appendice 42: Nitrogen velocity at 1st Pitch

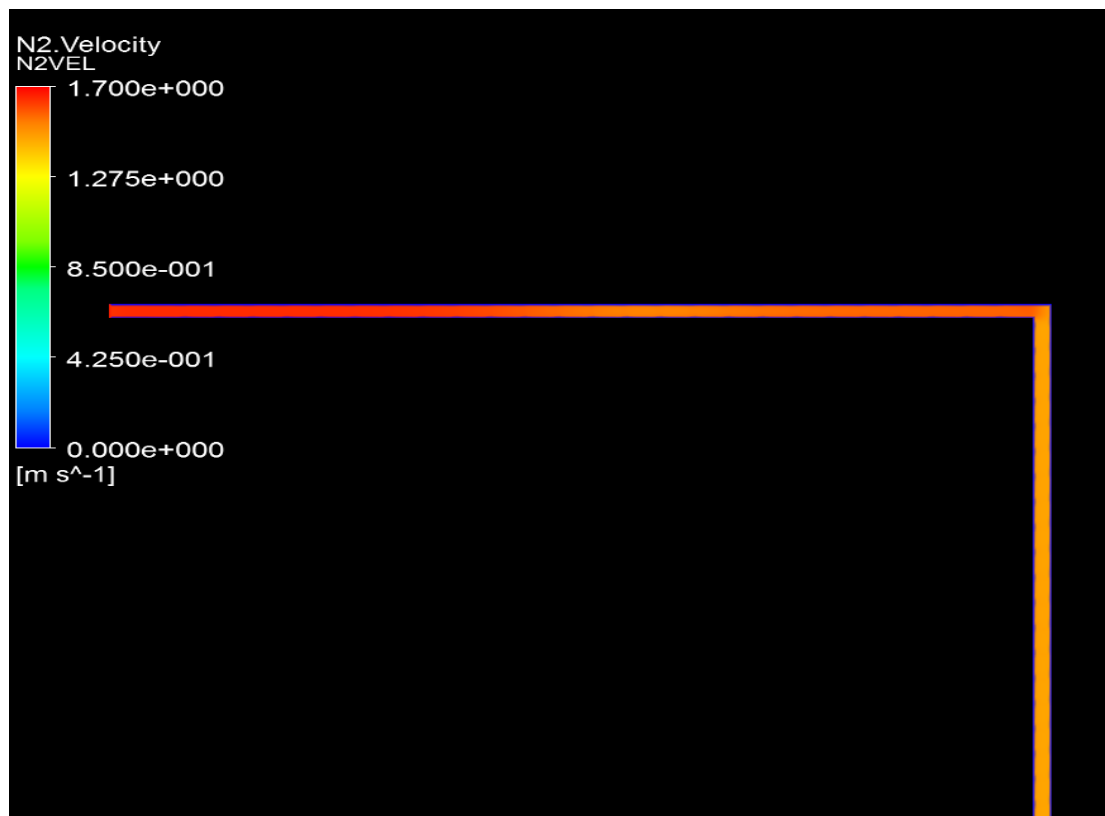


Appendice 43: Nitrogen velocity at 2nd pitch

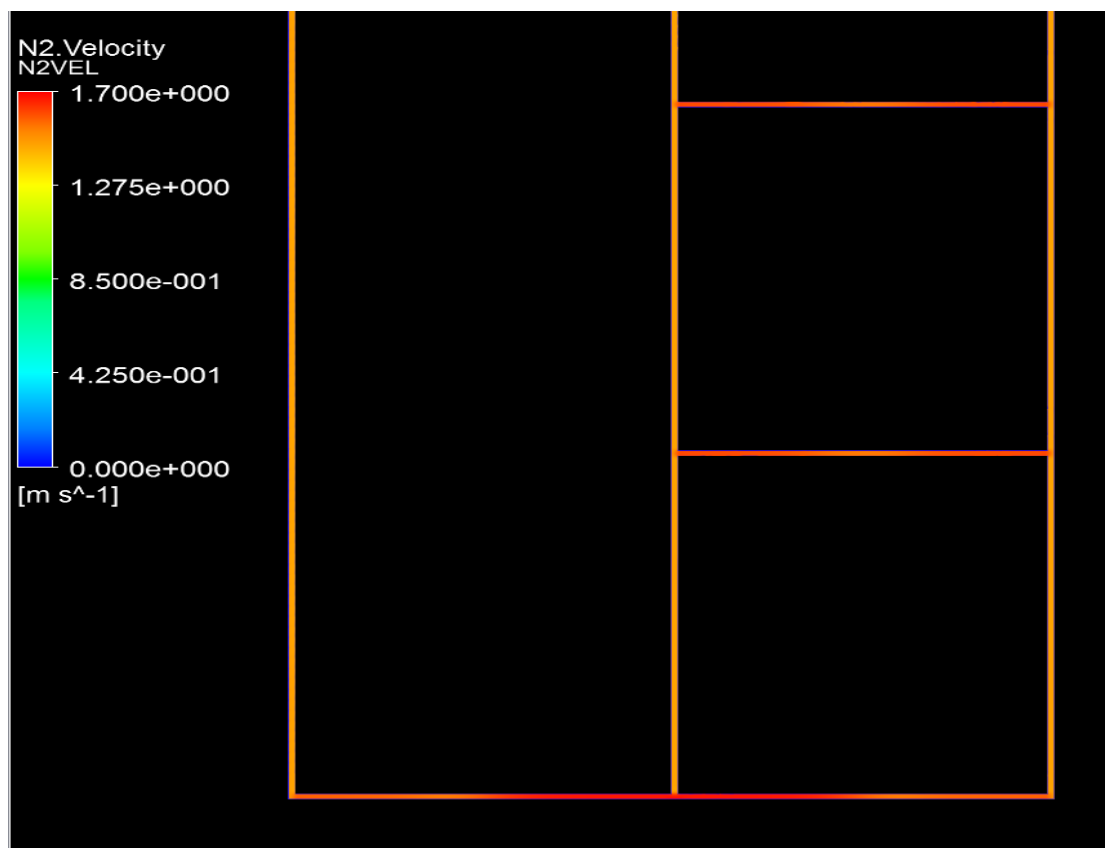


Appendice 44: Nitrogen velocity at outlet

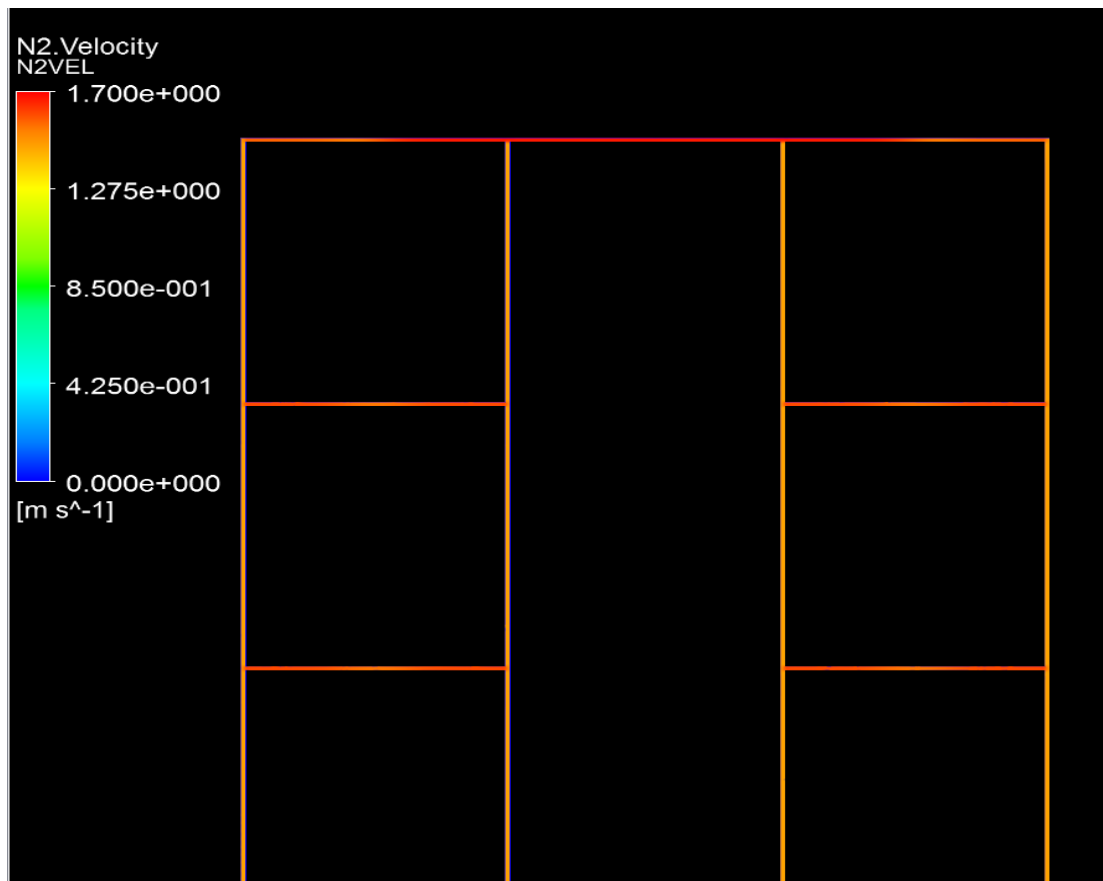
Model C at 1.67 m/s Inlet Velocity



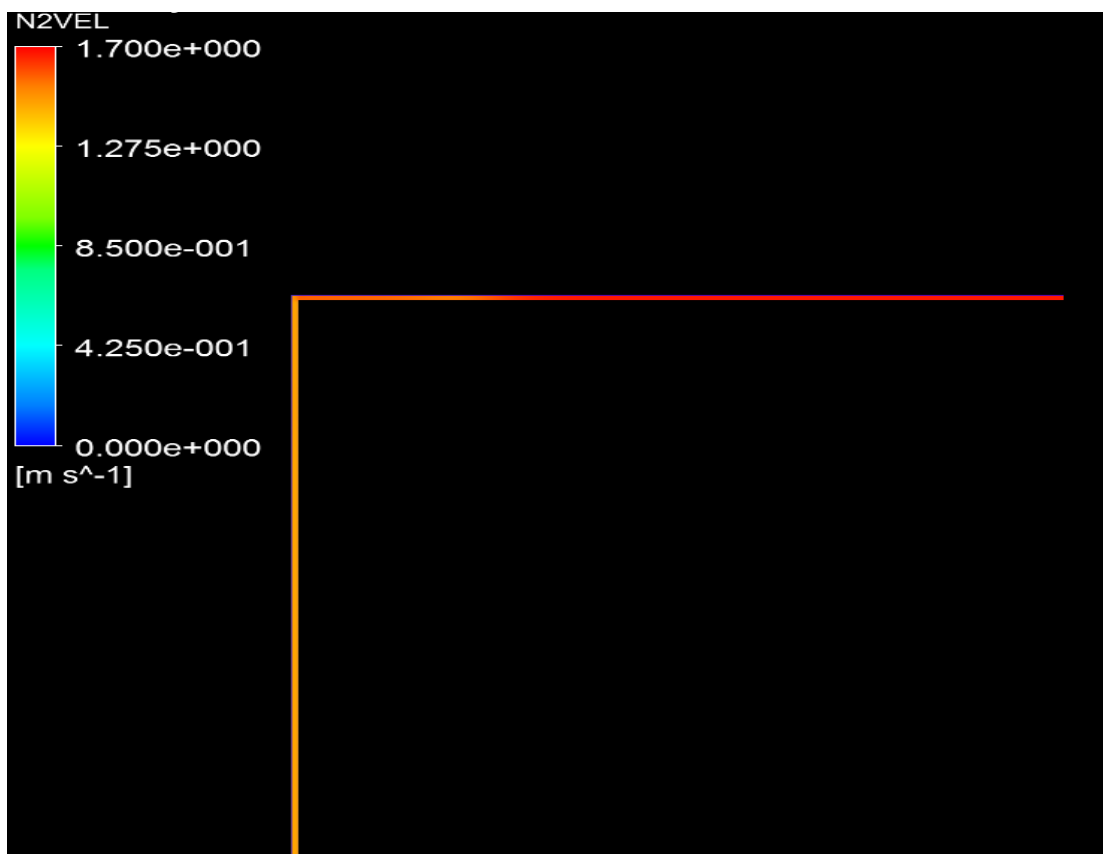
Appendice 45: Nitrogen velocity at inlet



Appendice 46: Nitrogen velocity at first pitch

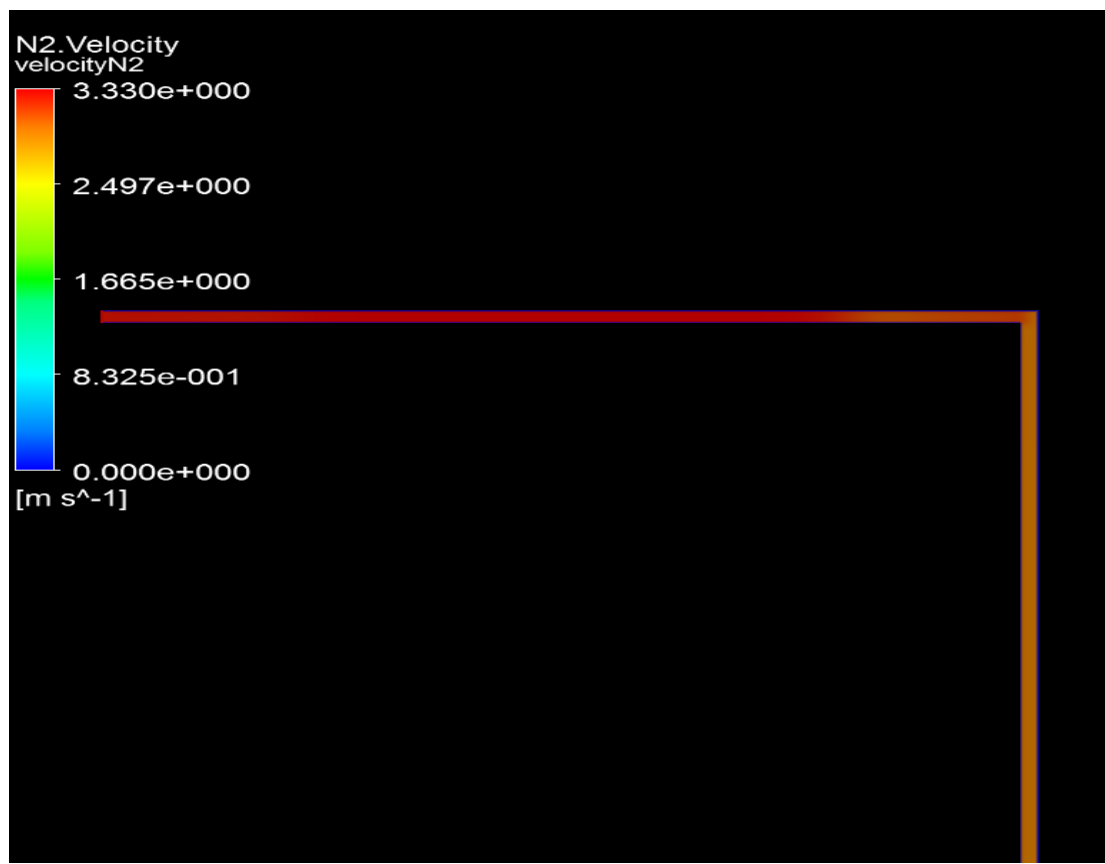


Appendice 47: Nitrogen velocity at 2nd pitch

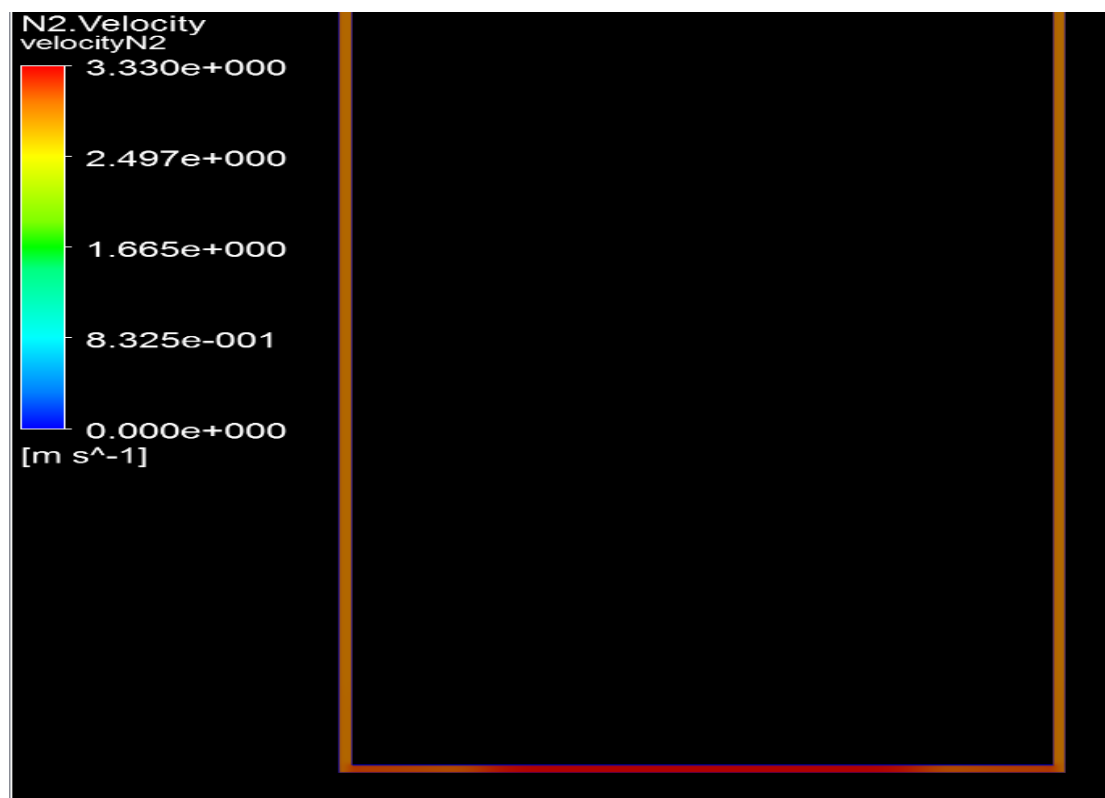


Appendice 48: Nitrogen velocity at outlet

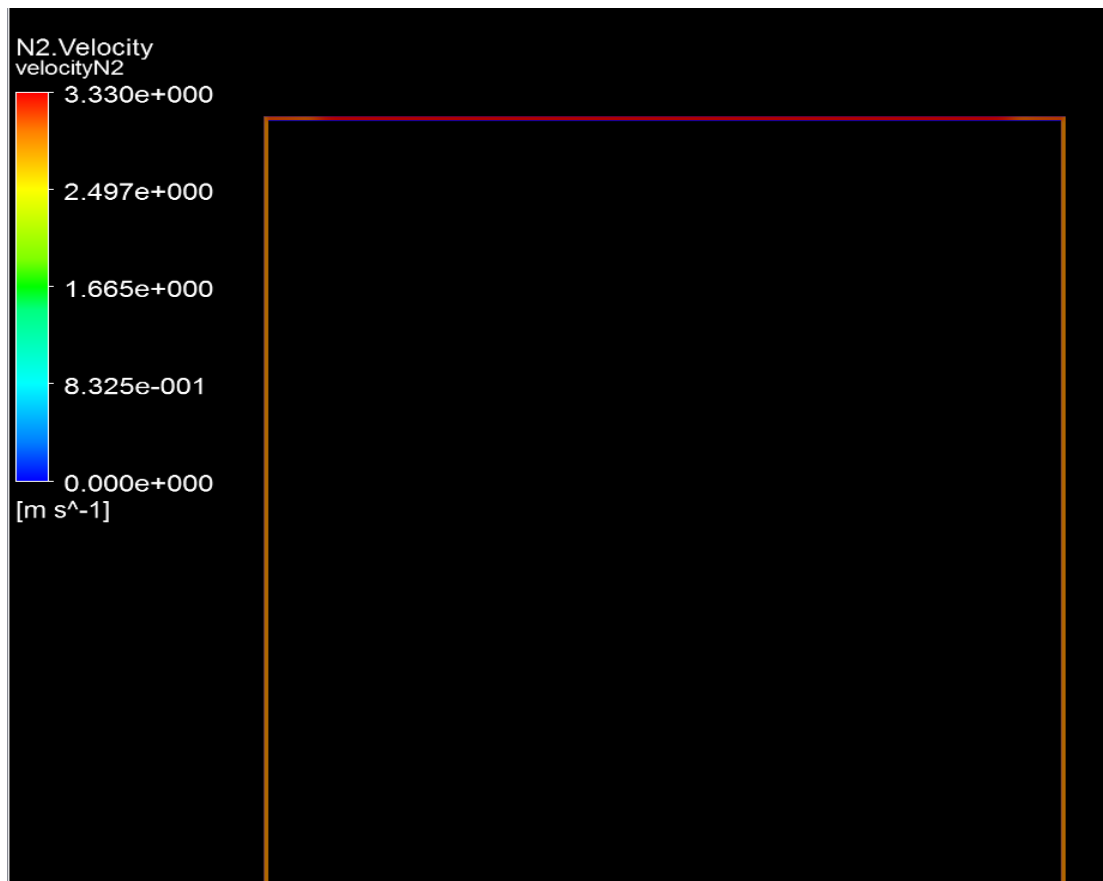
Model A at 3.33 m/s Inlet Velocity



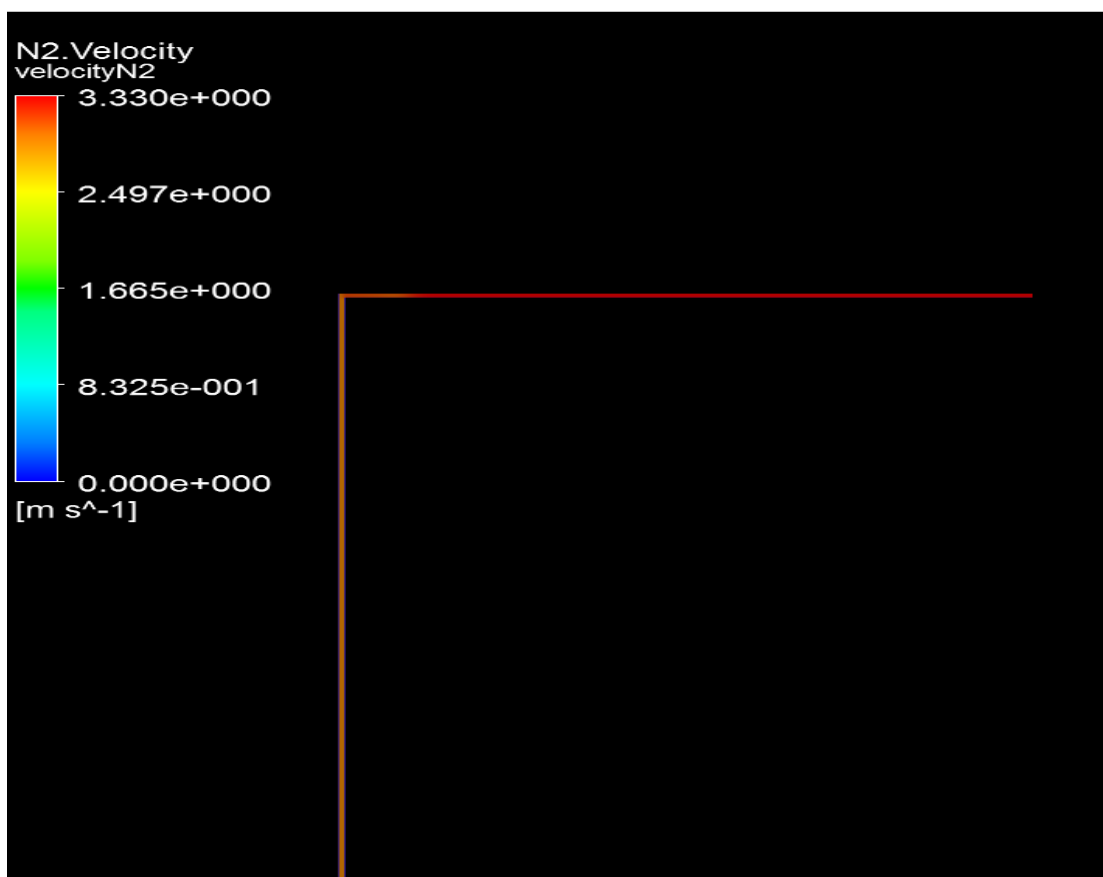
Appendice 49: Nitrogen velocity at inlet



Appendice 50: Nitrogen velocity at 1st pitch

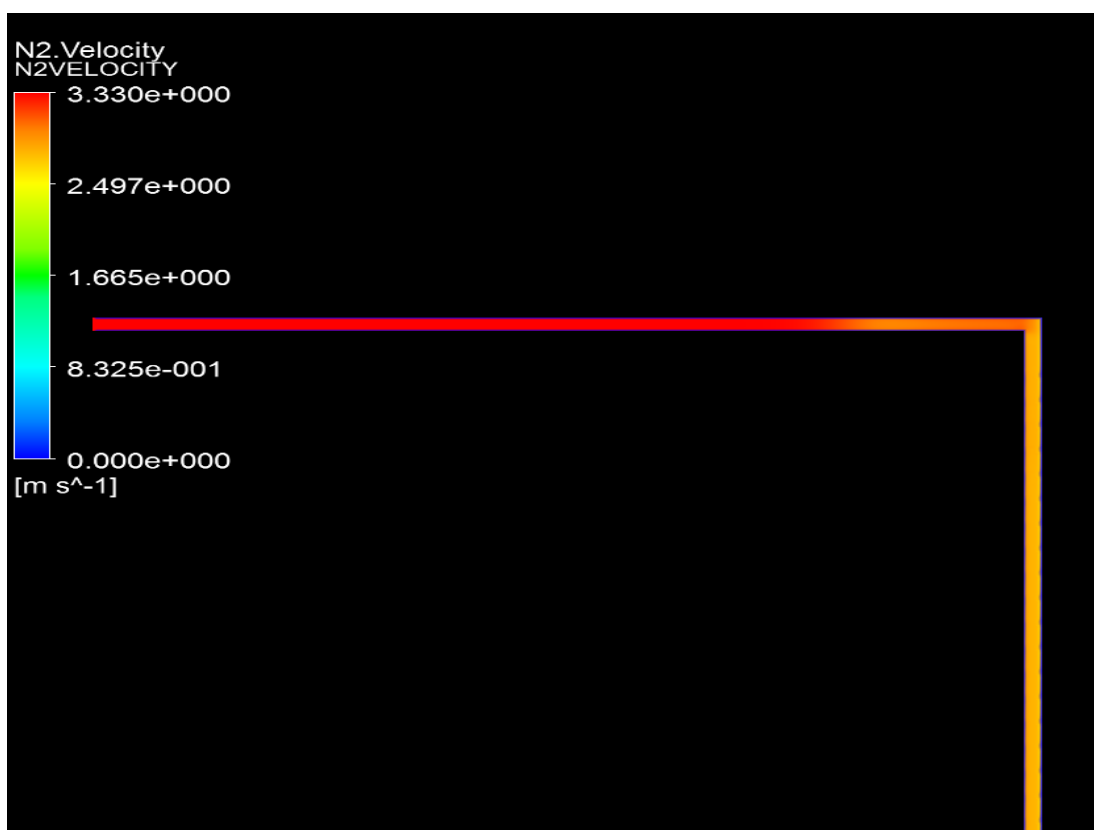


Appendice 51: Nitrogen velocity at 2nd pitch

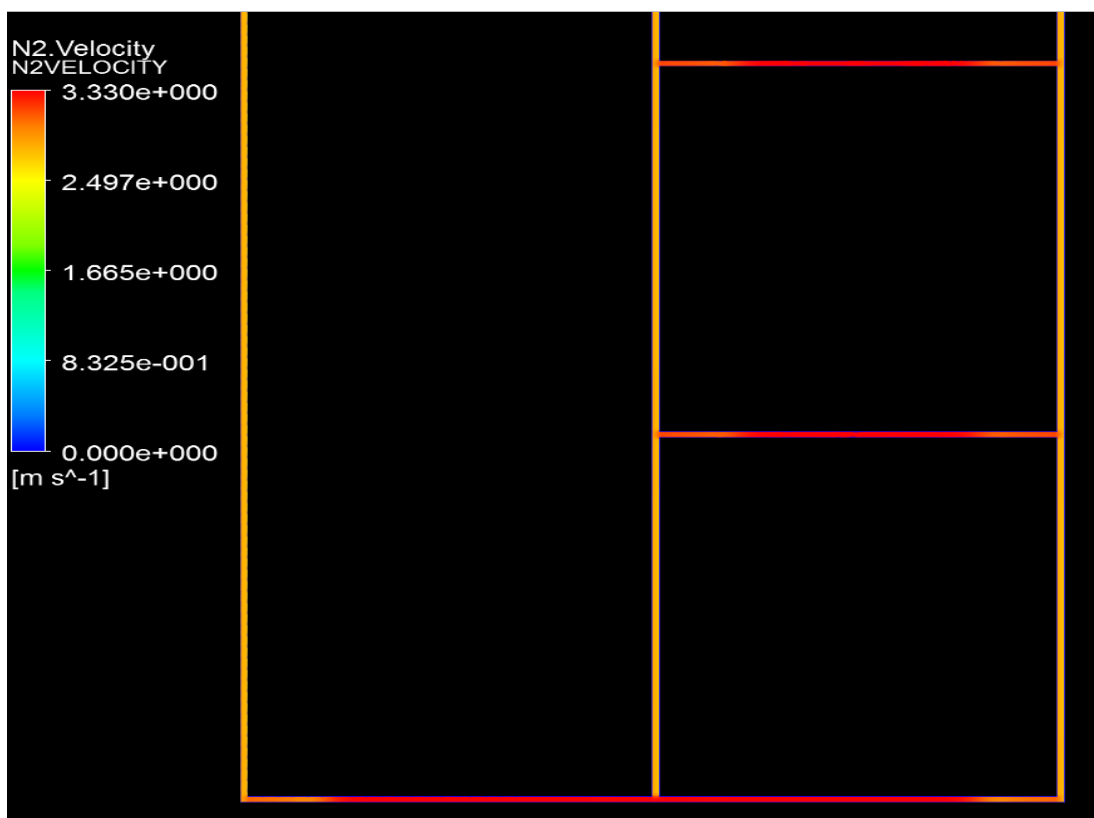


Appendice 52: Nitrogen velocity at outlet

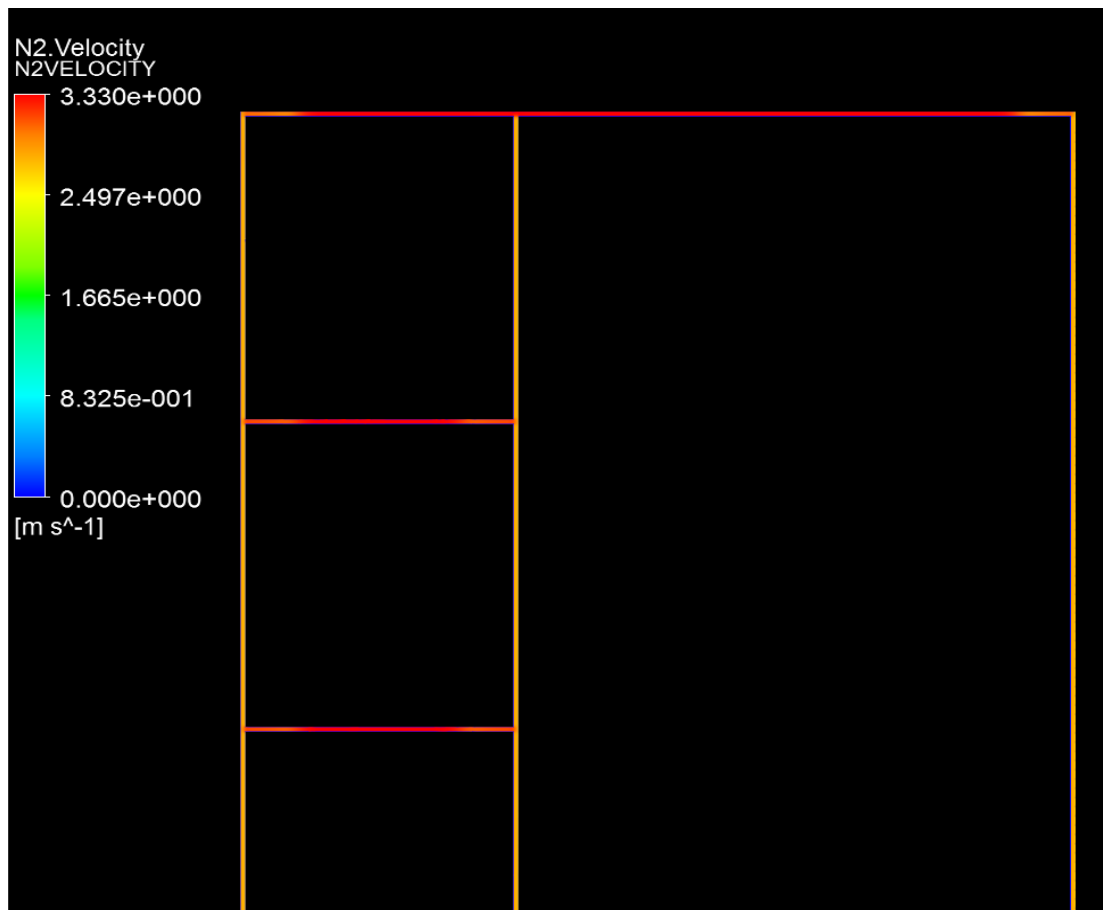
Model B at 3.33 m/s Inlet Velocity



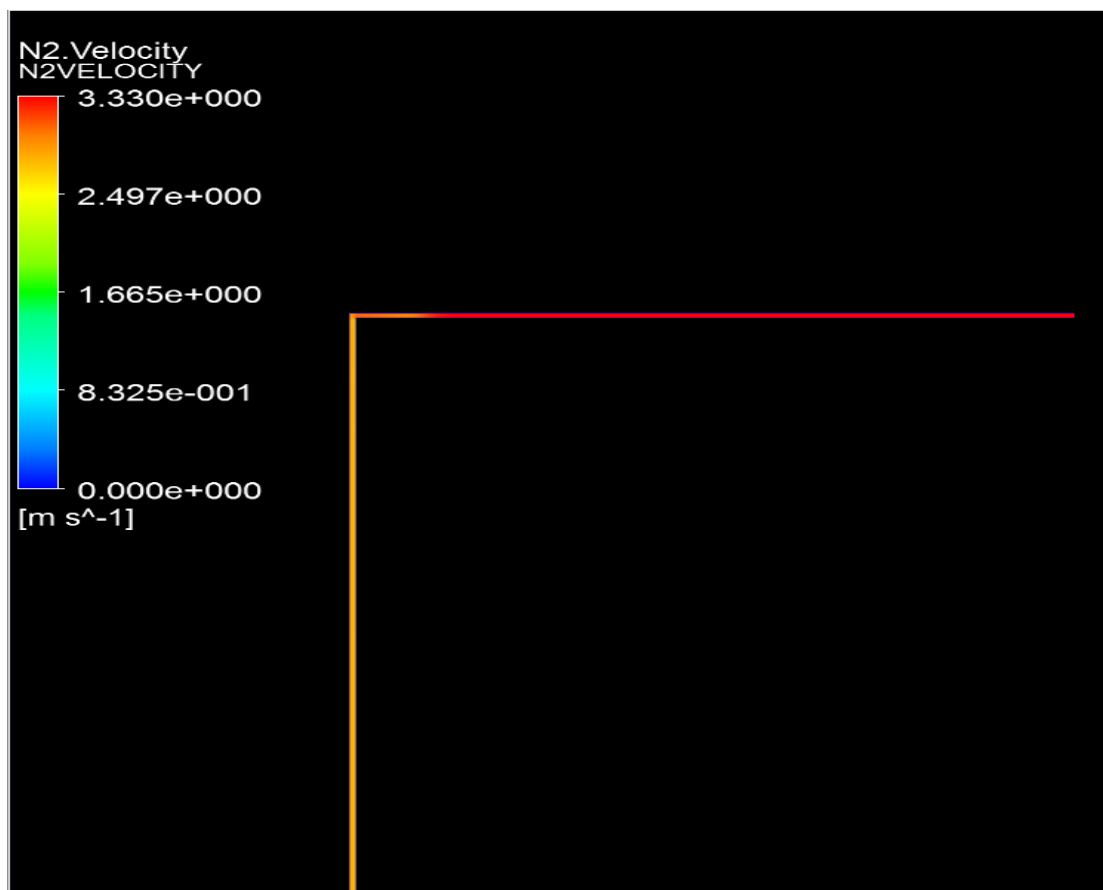
Appendice 53: Nitrogen velocity at inlet



Appendice 54: Nitrogen velocity at 1st pitch

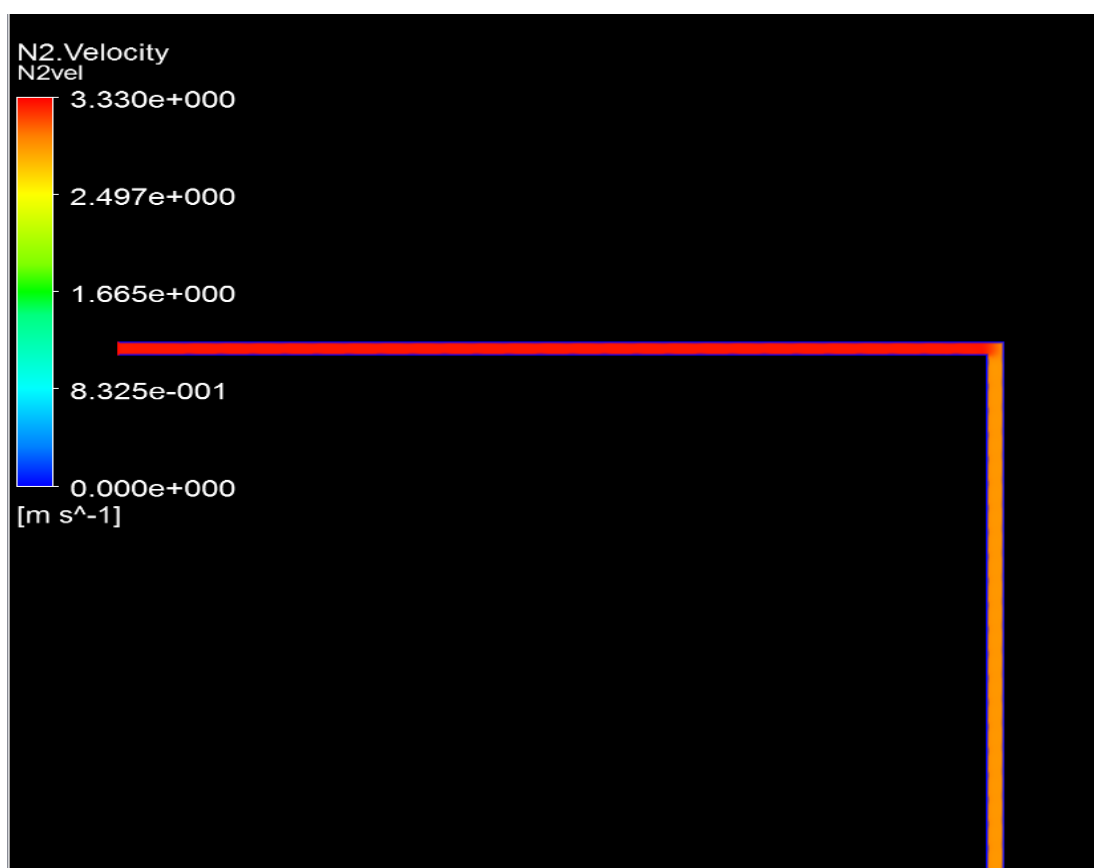


Appendice 55: Nitrogen velocity at 2nd pitch

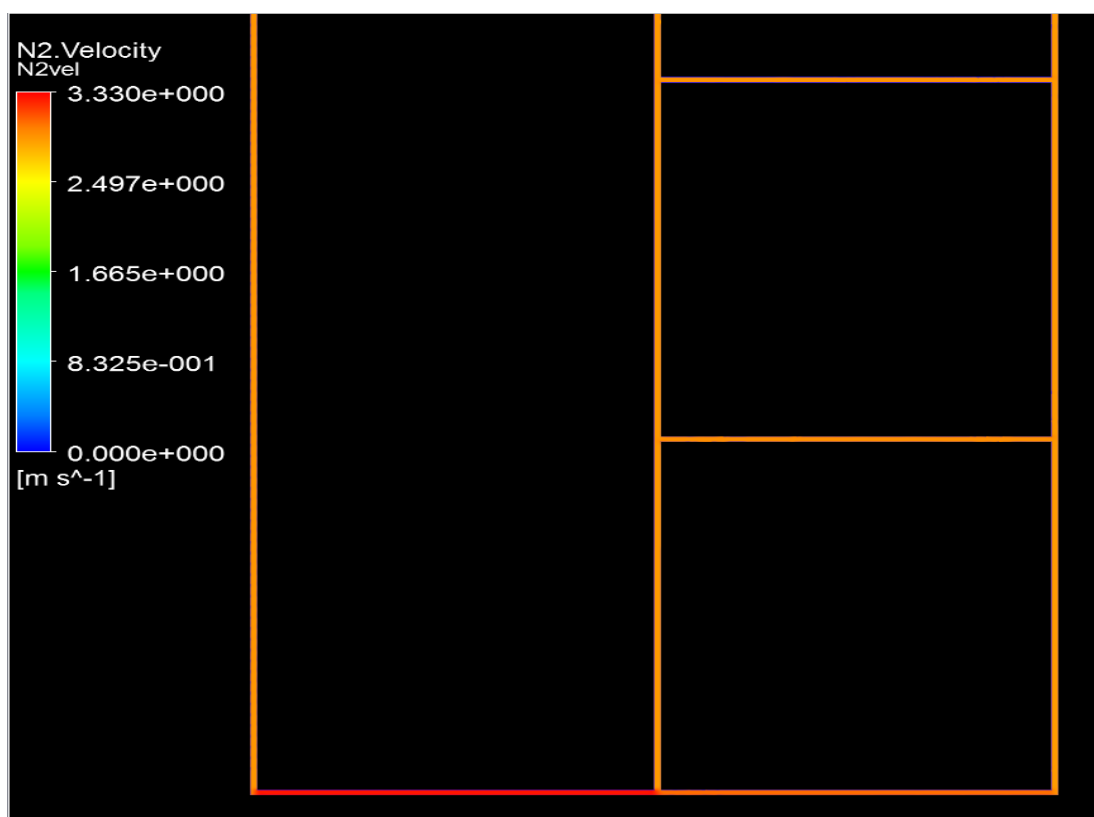


Appendice 56: Nitrogen velocity at outlet

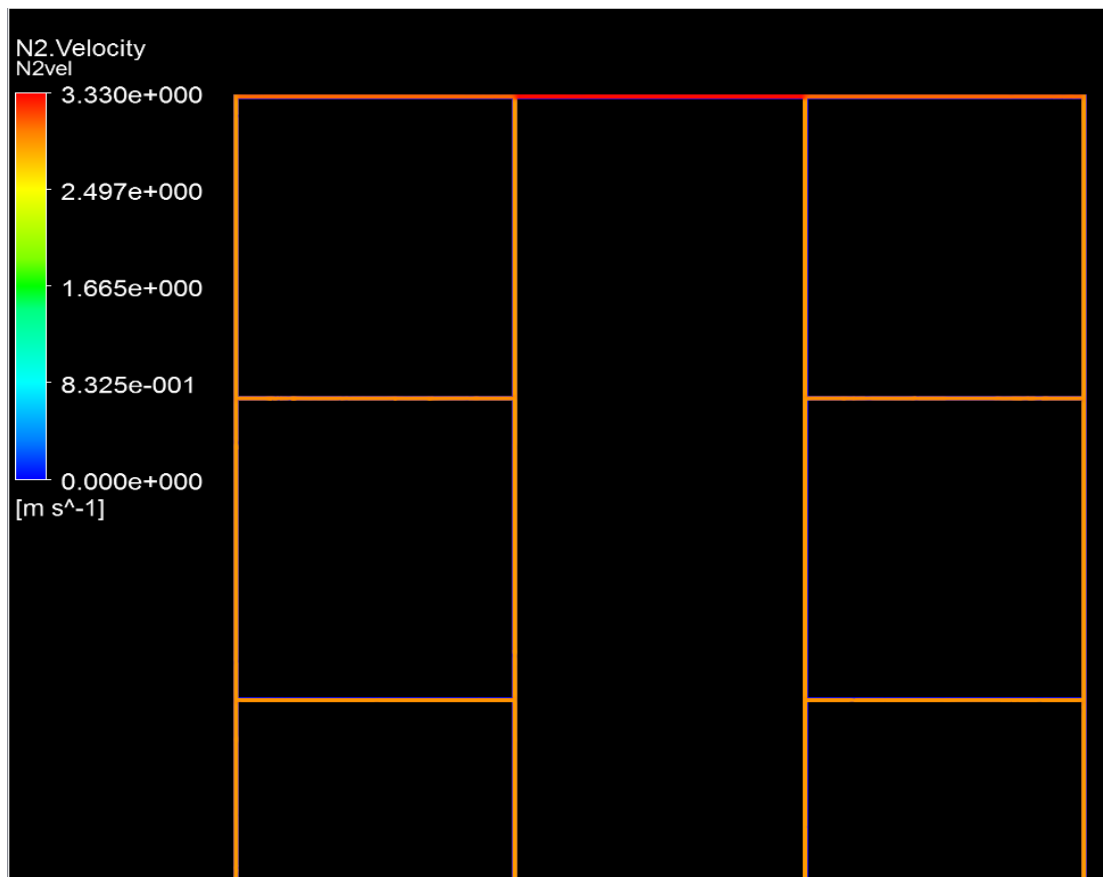
Model C at 3.33 m/s Inlet Velocity



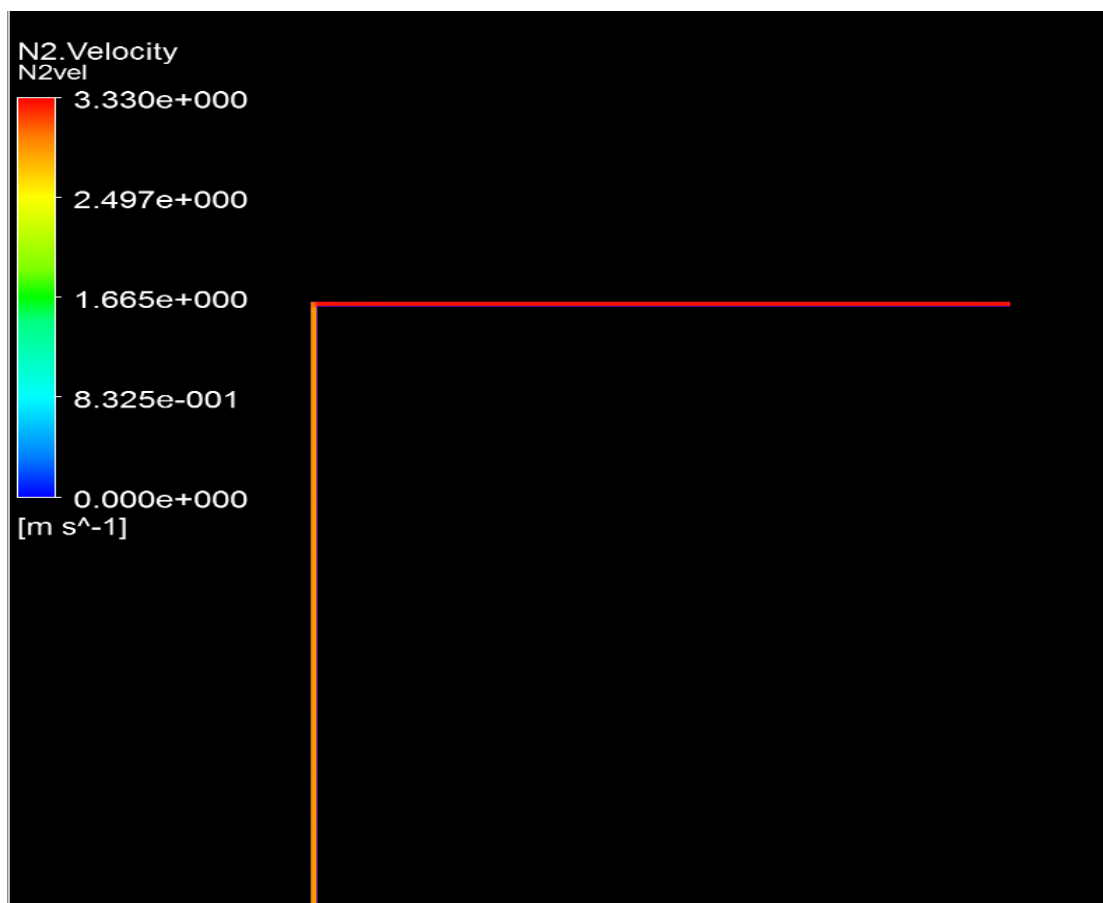
Appendice 57: Nitrogen velocity at inlet



Appendice 58: Nitrogen velocity at 1st pitch

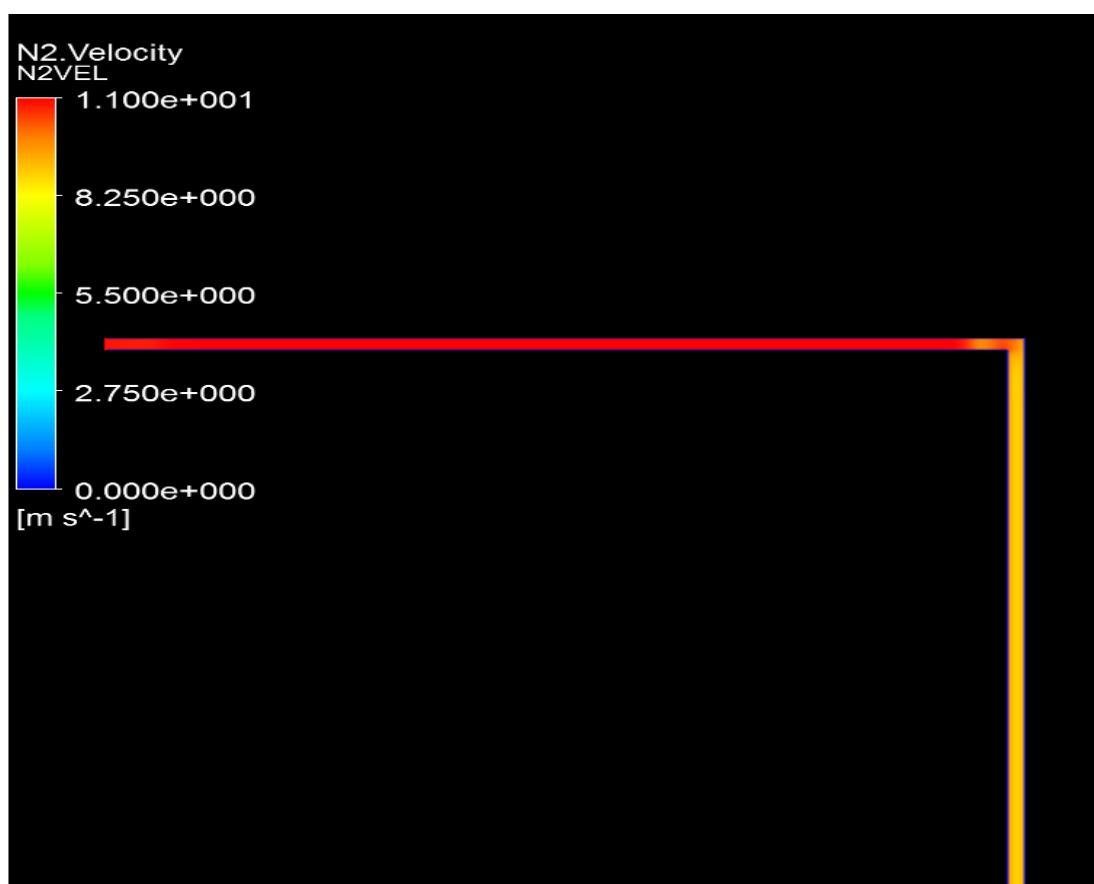


Appendice 59: Nitrogen velocity at 2nd pitch

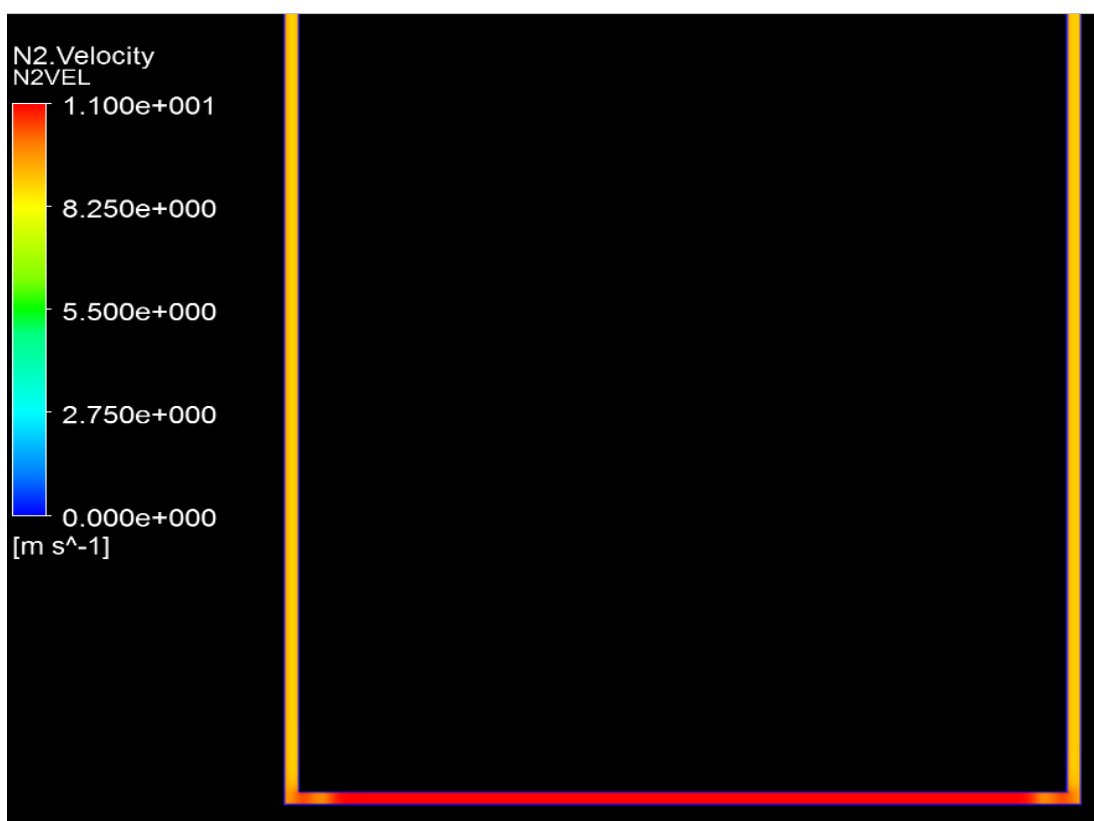


Appendice 60: Nitrogen velocity at outlet

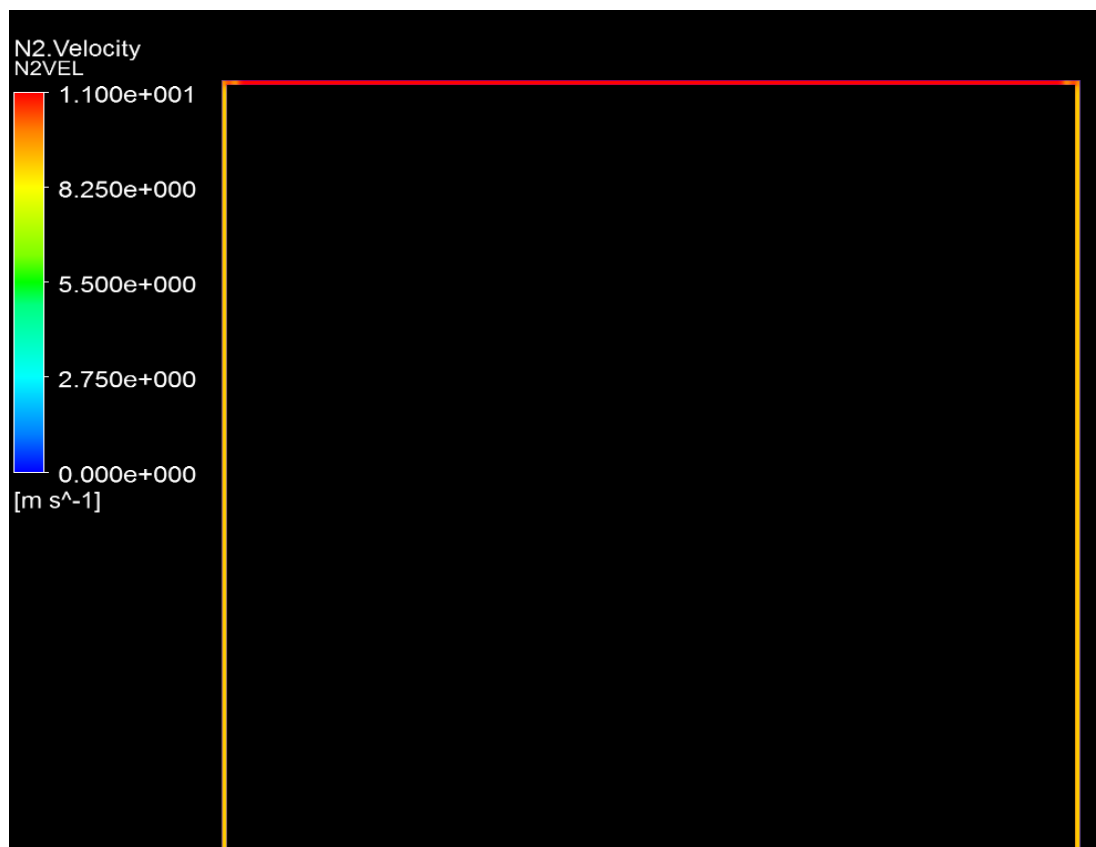
Model A at 10.99 m/s Inlet Velocity



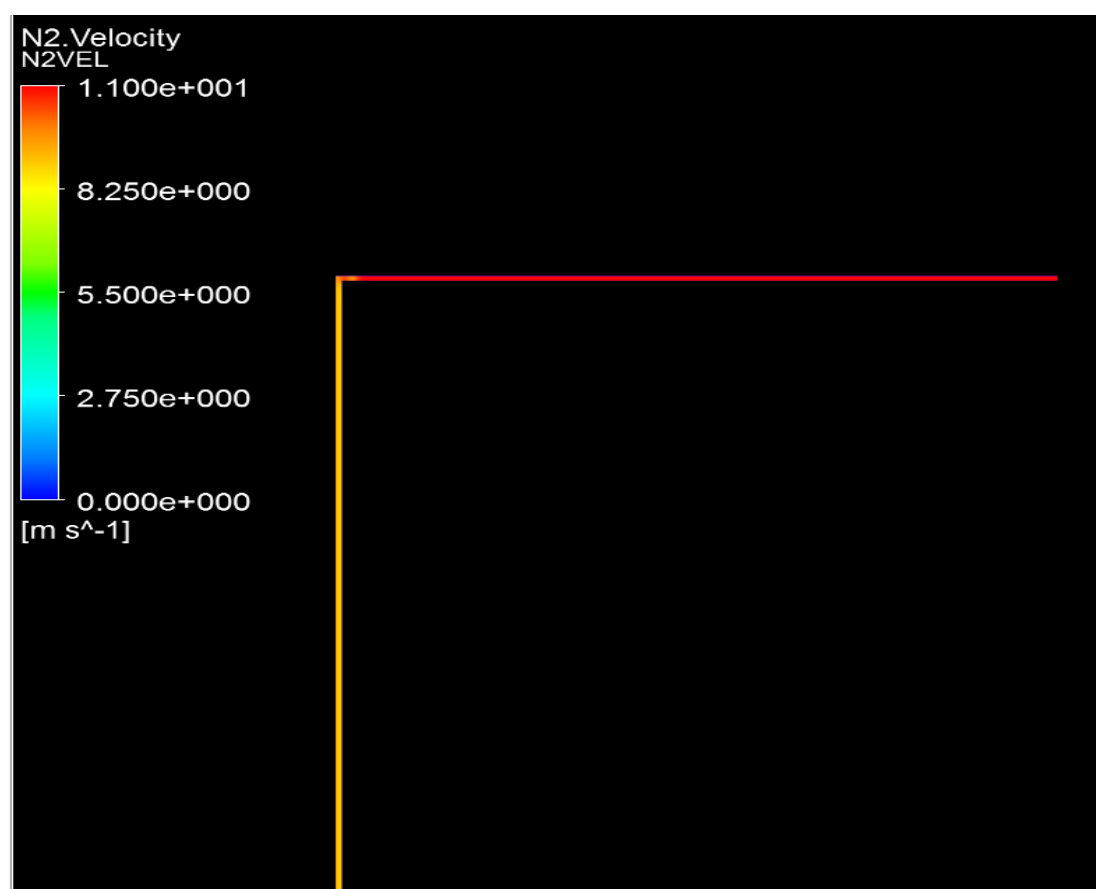
Appendice 61: Nitrogen velocity at inlet



Appendice 62: Nitrogen velocity at 1st pitch

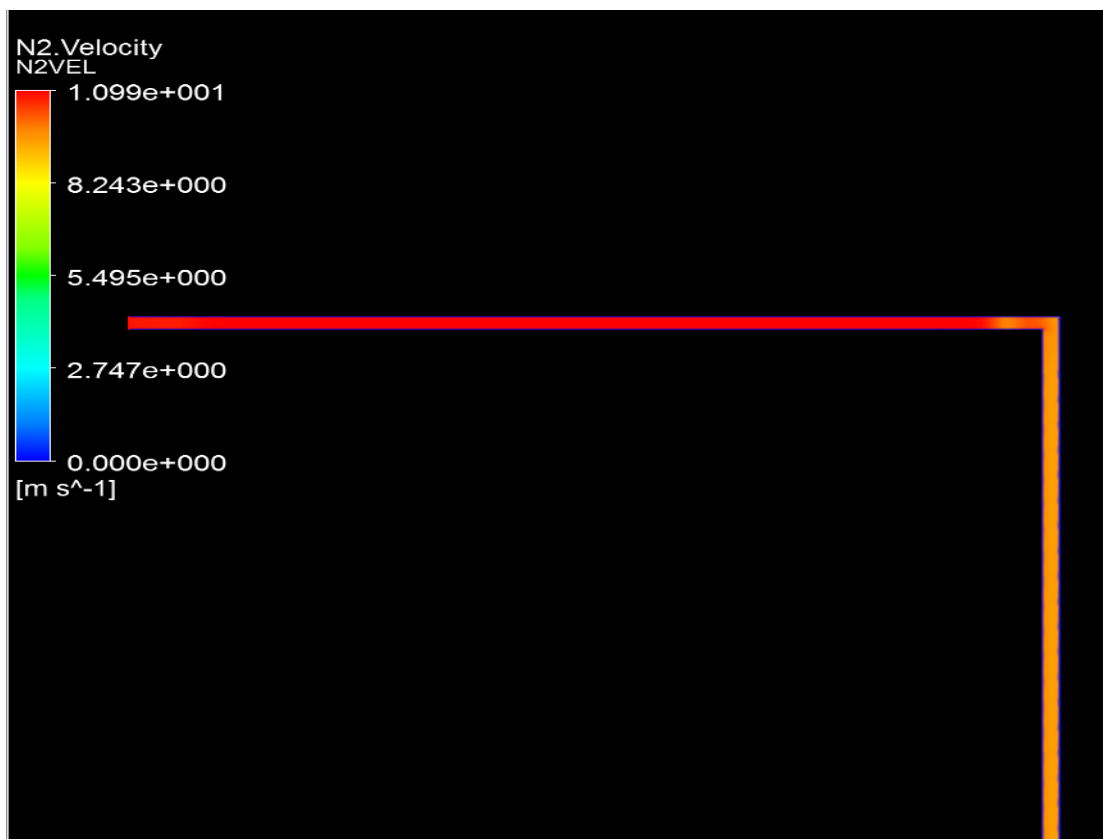


Appendice 63: Nitrogen velocity at 2nd pitch

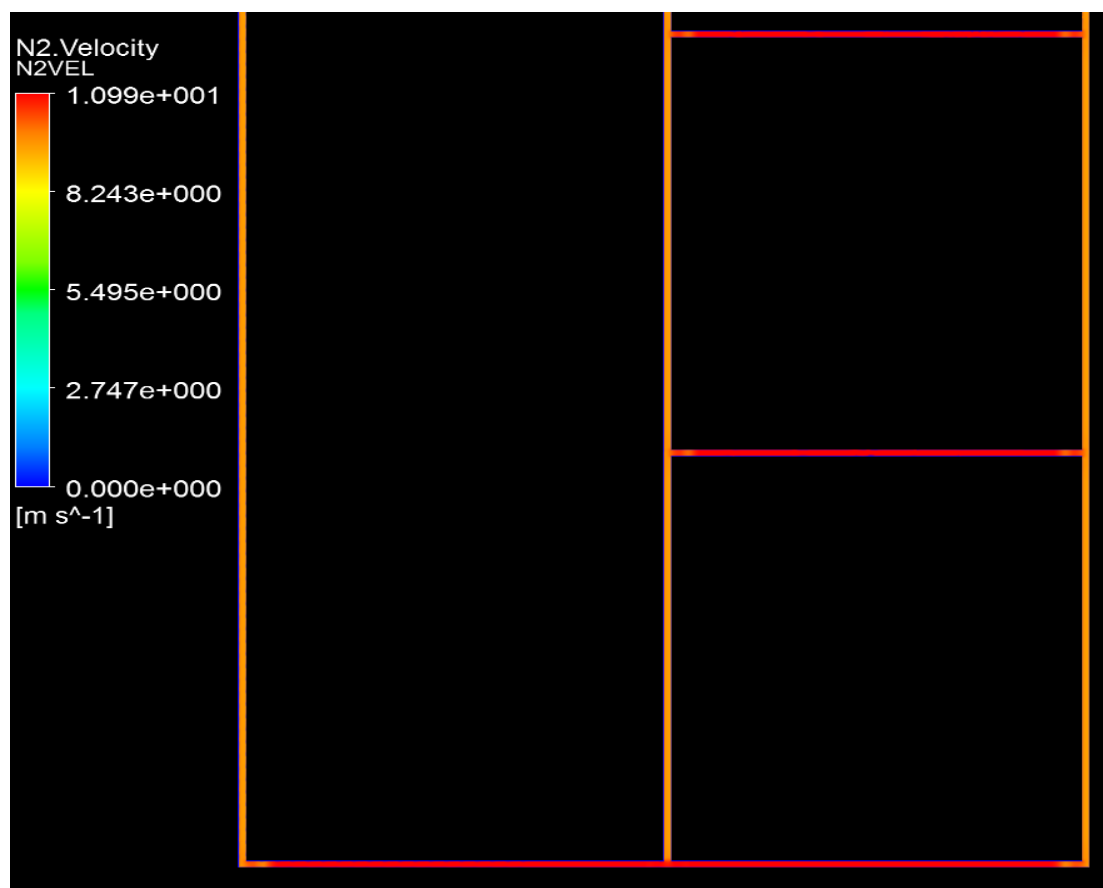


Appendice 64: Nitrogen velocity at outlet

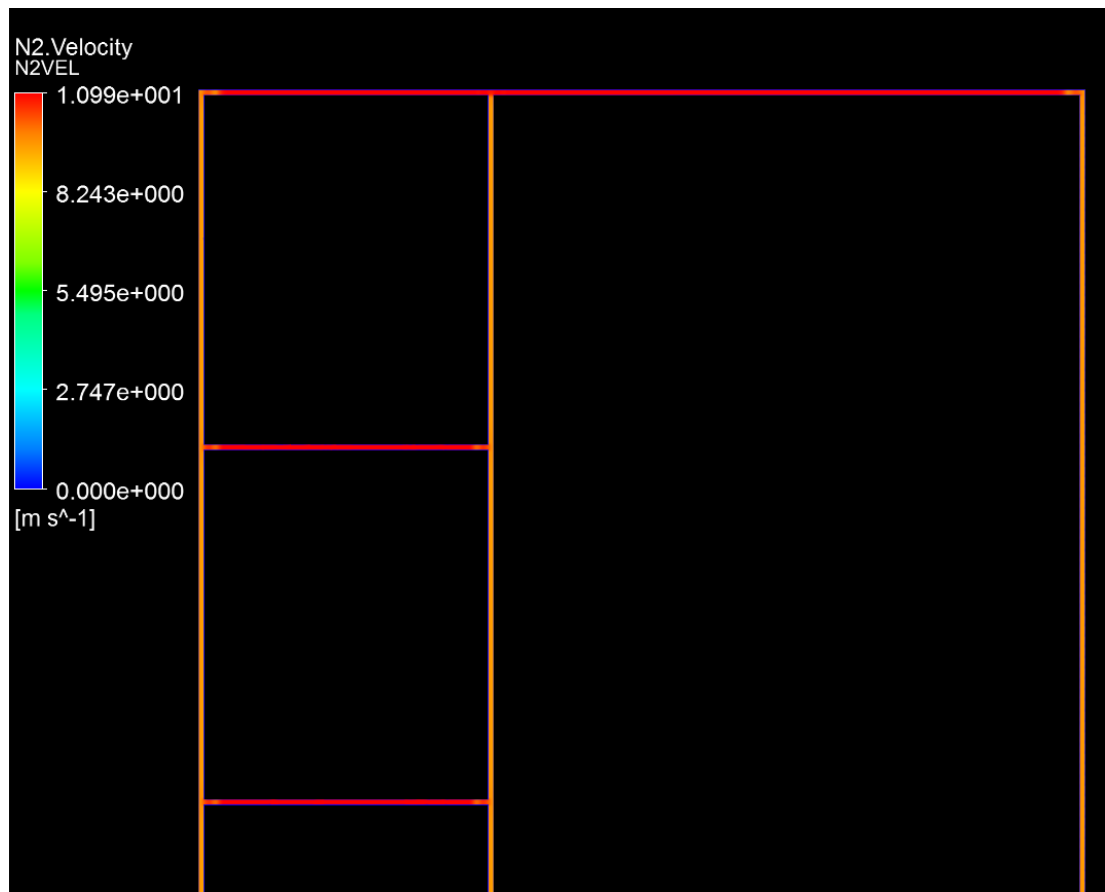
Model B at 10.99 m/s Inlet Velocity



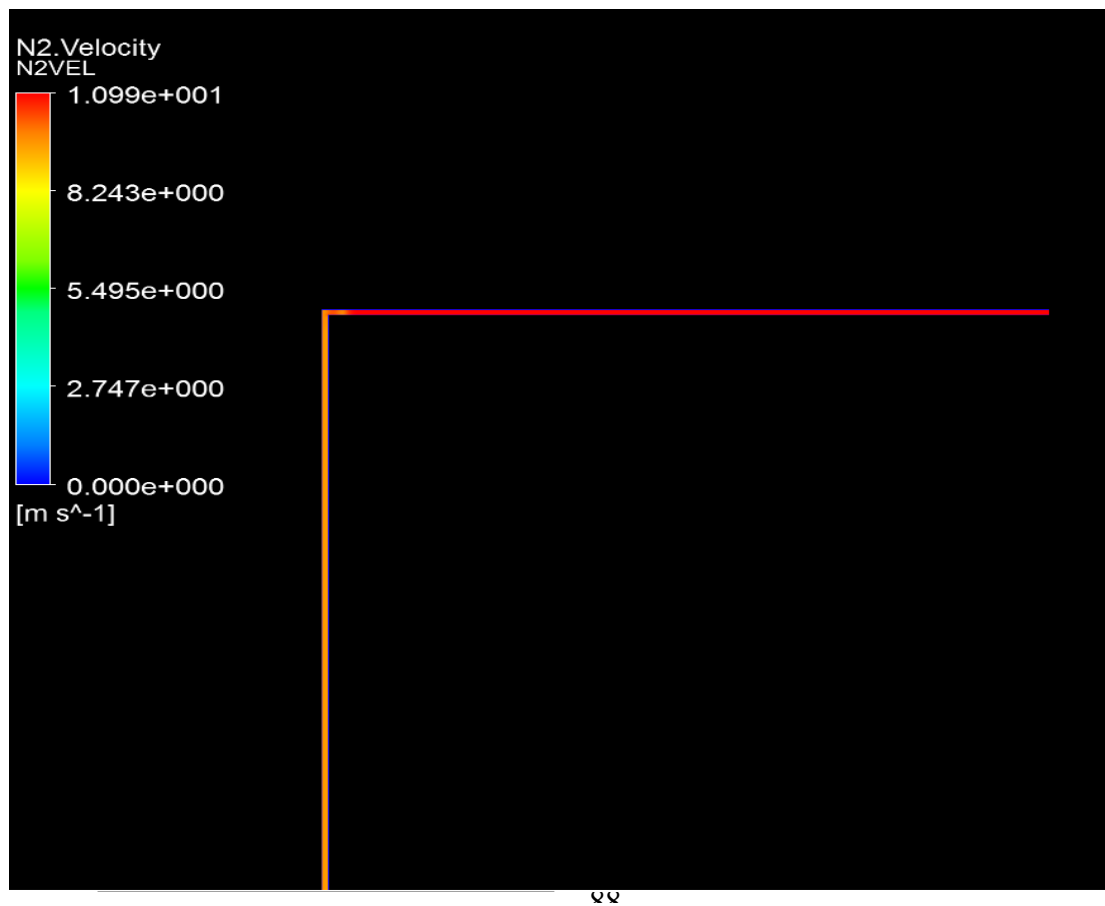
Appendice 65: Nitrogen velocity at inlet



Appendice 66: Nitrogen velocity at 1st pitch

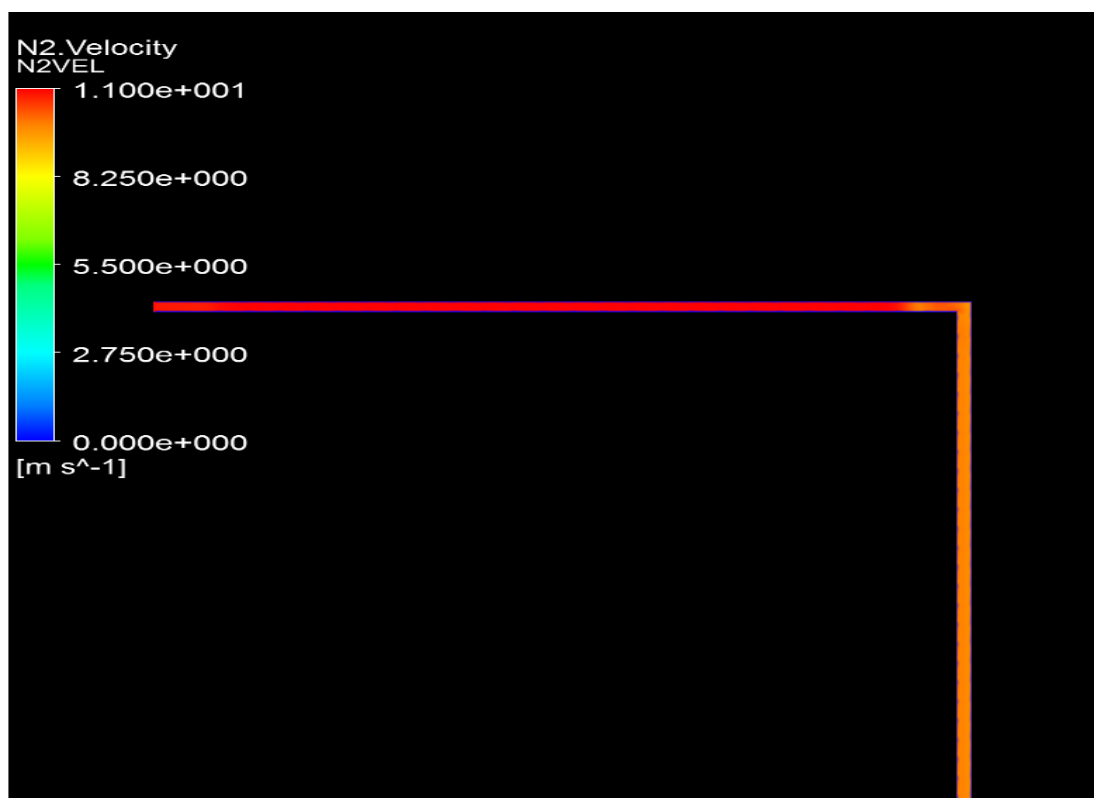


Appendice 67: Nitrogen velocity at 2nd pitch

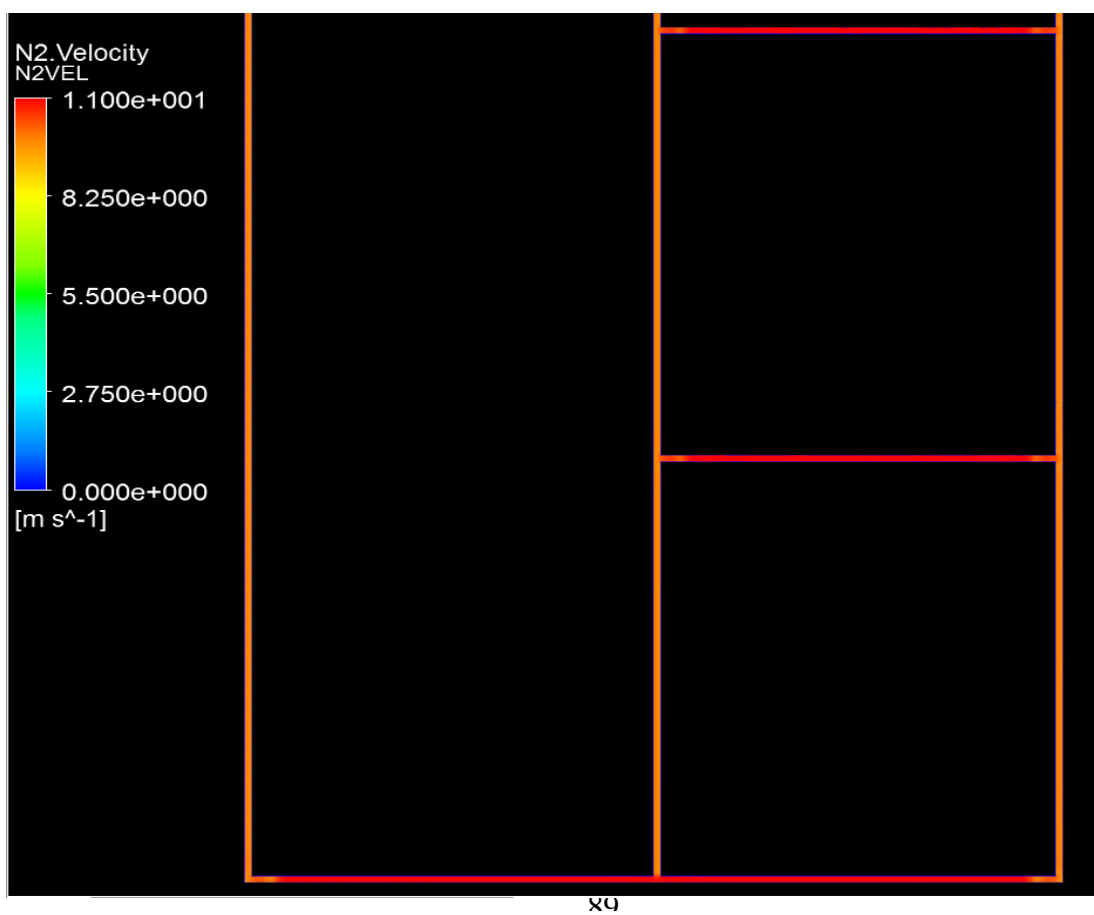


Appendice 68: Nitrogen velocity at outlet

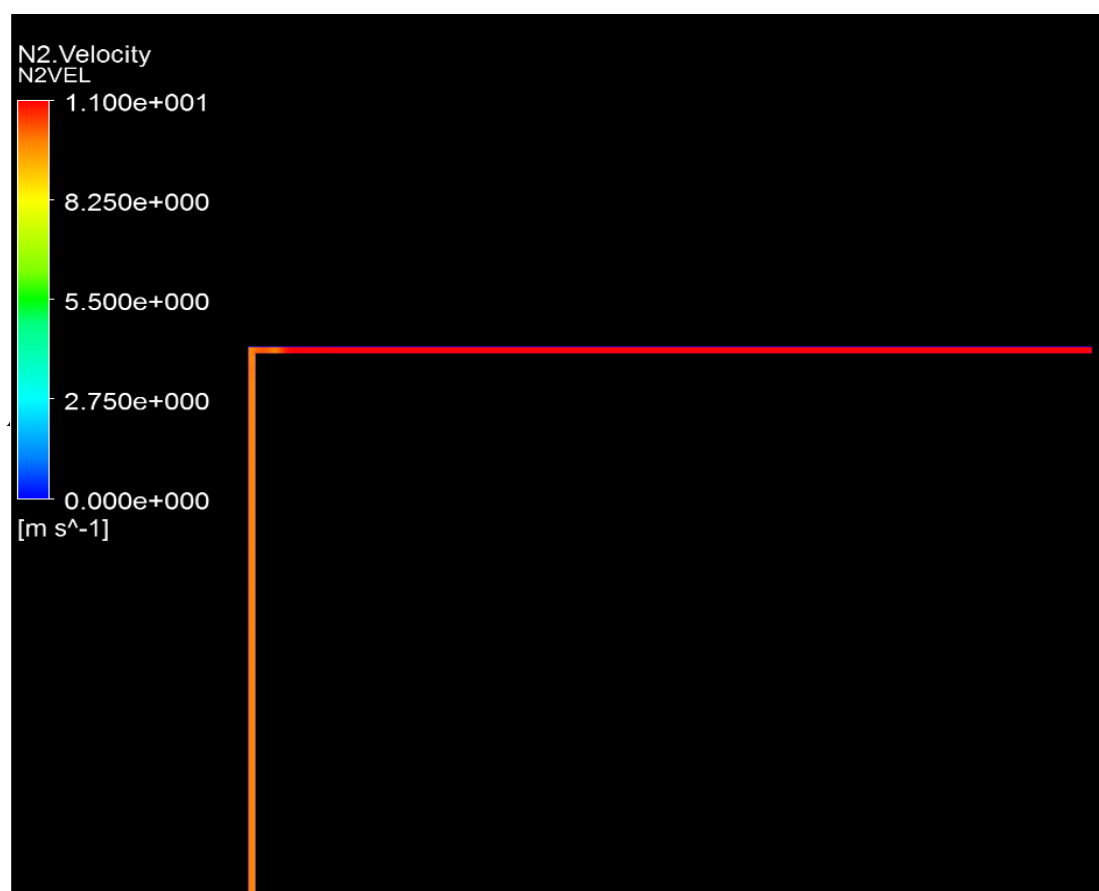
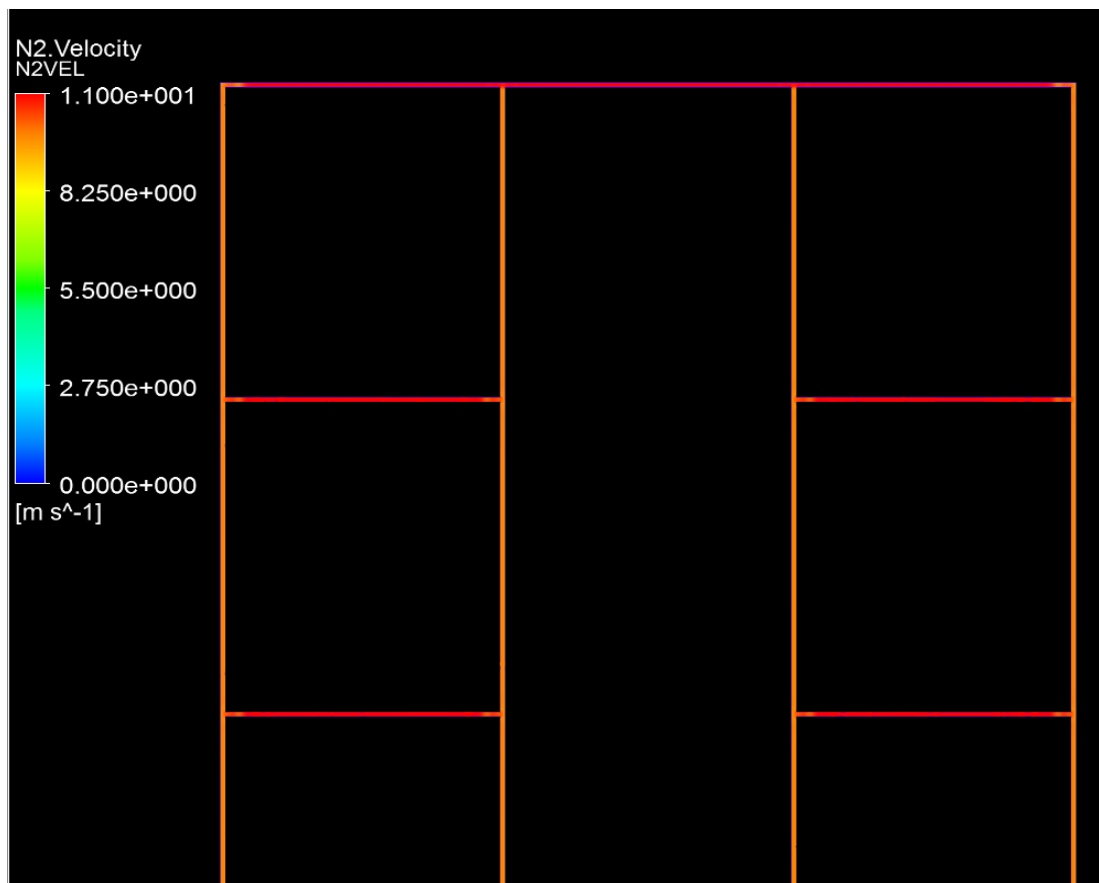
Model C at 10.99 m/s Inlet Velocity



Appendice 69: Nitrogen velocity at inlet



Appendice 70: Nitrogen velocity at 1st pitch



Appendice 72: Nitrogen velocity at outlet

APPENDIX III: Gantt Chart Of Project Work And Milestones

Week / Project Management	Week 1-2	Week 3-4	Week 5-6	Week 7-8	Week 9-10	Week 11-12	Week 13-14	Week 15-16	Week 17-18	Week 19-20	Week 21-22	Week 23-24	Week 25-26	Week 27-28	Week / Project Activities
Confirmation of Project topic															
Preliminary research work on literature review.															Complete Introduction of project
Submission of extended proposals															Complete Literature reviews for basis of project proposals
Proposal defence presentation															
ANSYS CFX software training															Familiarization of ANSYS CFX
Submission of Interim Draft Report															
Submission of Interim Report															
															Creation of geometry Designs
															Creation of meshing (quality studies)
															Run simulation and collect data flow 1 and 2 for each effects
															Analyse and interpret results obtained.
															Thesis write up
Presentations															